Master's thesis

NTNU
Norwegian University of Science and Technology
Faculty of Natural Sciences
Department of Physics

Hans Gløckner Giil

Spin Accumulation and Effective Models for Odd-Frequency Superconductivity

Master's thesis in Applied Physics and Mathematics
Supervisor: Jacob Linder
June 2022

NTNU
Norwegian University of
Science and Technology

Hans Gløckner Giil

Spin Accumulation and Effective Models for Odd-Frequency Superconductivity

Master's thesis in Applied Physics and Mathematics
Supervisor: Jacob Linder
June 2022

Norwegian University of Science and Technology
Faculty of Natural Sciences
Department of Physics

NTNU
Norwegian University of
Science and Technology

Abstract

We derive criteria for the quasiclassical Green functions in odd-frequency superconducting systems in the dirty limit and use these criteria to make three ansatzes for models that give physically reasonable behavior. The density of states, the renormalization of the spin-flip and spin-orbit scattering lengths, and the Meissner response of these models are calculated and compared to the properties of conventional superconductors. Depending on the model used, the density of states can be either peaked or gapped at the Fermi energy. A general result is derived, stating that odd-frequency superconductors display the same robustness towards spin-flip scattering as a normal metal, while the effects of spin-orbit scattering are renormalized in energy domains where the anomalous Green function has a real part. The Meissner response is conventional, zero, or unconventional, depending on the model. Finally, we solve numerically a realistic proximity system in which odd-frequency superconductivity naturally arises and compare it with the analytic models. The Meissner effect in this system is unconventional, and the density of states is peaked, consistent with results for one of the analytic models. We apply a spin-voltage to this system to study the non-equilibrium spin mode and find that the spin-orbit scattering length is renormalized, while the spin-flip scattering length is unchanged from the normal state, consistent with our analytical results. The spin accumulation is enhanced compared with a conventional superconductor. Moreover, for low temperatures and spin-voltages, the spin accumulation is enhanced even compared to the normal state.

Sammendrag

Vi utleder kriterier for den kvasiklassiske Green-funksjonen i superledende odde-frekvens systemer hvor urenhets-spredning er dominerende, og bruker disse kriteriene til å lage tre ansatser for modeller som gir fysisk rimelig oppførsel. Tilstandstettheten, renormaliseringen av spinn-flipp- og spinn-bane-spredningslengdene og Meissner-responsen til disse modellene blir så beregnet og sammenlignet med egenskaper hos en konvensjonell superleder. Tilstandstettheten kan ha et gap eller en topp rundt Fermi-energien, avhengig av modellen som blir brukt. Vi utleder et generelt resultat, som sier at odde-frekvens-superledning viser samme robusthet mot spinn-flipp-spredning som et normalmetall, mens effekten av spinn-bane-spredning blir renormalisert for energidomenet der den abnormale Green-funksjonen har en realdel. Meissner-responsen er konvensjonell, null eller ukonvensjonell, avhengig av modellen. Til slutt løser vi numerisk et realistisk system hvor odde-frekvens-superledning oppstår naturlig, og sammenligner med de analytiske modellene. Meissner-effekten i dette systemet er ukonvensjonell, og tilstandstettheten har en topp på Fermienergien, noe som er tilsvarende oppførsel som vi fant i en av de analytiske modellene. Vi påsetter en spinn-spenning til dette systemet for a undersøke hvordan ikke-likevekts-spinn-moden oppfører seg i et slikt system, og finner at spinn-bane-spredningslengden blir renormalisert, mens spinn-flipp-spredningslengden er uforandret fra normaltilstanden, noe som er konsistent med de analytiske resultatene. For lave temperaturer og spinn-spenninger, så er spinn-akkumulasjonen forhøyet sammenlignet med et normalmetall eller en konvensjonell superleder.

Preface

This master's thesis was written during the spring semester of 2022, as a part of a five-year "Sivilingeniør" degree at the Norwegian University of Science and Technology. It amounts to 30 ECTS credits and concludes my degree. The thesis builds upon the work of a 15 ECTS credits specialization thesis, which was written in the autumn semester of 2021. In the specialization thesis, emphasis was put on understanding the field theory of many-body systems and approximations relevant for studying the interplay between ferromagnetism and superconductivity. This resulted in a detailed derivation of the Usadel equation. In this thesis, emphasis was put on applying this theory to odd-frequency superconducting systems. For this reason, much of the background theory in this thesis is based on last year's work. This includes parts of Chapter 1 and Chapter 3, which have been adapted, as well as Section 2.4 and Section 2.5, which have been taken directly from the specialization thesis.

During this semester, I have experienced the exciting unpredictability of studying physics. The topics tackled in the thesis have changed a lot from what I initially thought they would be, as difficulties and opportunities arose during the semester. Much effort was spent writing Python code for a numerical solver of the Usadel equation, but during the last months of the semester, the emphasis of the thesis was shifted toward more analytical work. In the end, both the analytical part and the numerical part of the thesis were used, approaching the elusive subject of odd-frequency superconductivity from different angles. The results of this thesis will be submitted as a paper to the journal *Physical Review B*.

I want to thank my supervisor Jacob Linder, for not only introducing me to the exciting world of superconductivity, ferromagnetism, and their interplay but also for being patient and always taking the time to answer my questions and help me overcome obstacles. Our weekly meetings have something I have looked forward to, as I always came away from them with new knowledge and motivation. I would also like to thank everyone at QuSpin, for welcoming me and for making me feel at home during the two semesters I have spent here. Finally, I want to thank my girlfriend Amalie, who has supported and motivated me during my studies.

Notation and conventions

The unit system used in this thesis is natural units, with Planck's reduced constant, the speed of light in vacuum, and the Boltzmann constant set to unity. We set the vacuum permeability and vacuum permittivity to unity well. In the usual symbols this is written $\hbar = c = k_B = \mu_0 = \epsilon_0 = 1$. We denote by $e = -|e|$ the electron charge, and the electron mass is denoted m. Partial derivatives will be written as $\partial_t \equiv \partial/\partial t$. Vectors will be typeset as $\boldsymbol{k}$, and four-vectors as k. Similarly, we write $\boldsymbol{\nabla}$ and ∇ for a 3-gradients and 4-gradients, respectively. $d\boldsymbol{r}$ and d^4x will be used to denote the integration measures in three- and four-dimensional space. We use the symbols $\equiv$ for definitions, $\approx$ for approximations, and $\propto$ for proportionality. When considering matrices, we will use the shorthand notations

$$\mathrm{diag}(A, B) \equiv \begin{pmatrix} A & 0 \\ 0 & B \end{pmatrix} \qquad \mathrm{antidiag}(A, B) \equiv \begin{pmatrix} 0 & A \\ B & 0 \end{pmatrix},$$

where A and B can be scalars or square matrices of equal dimensions. For a clear notation we denote a 2×2 matrix as $\underline{F}$, a 4×4 matrix as $\hat{F}$, and a 8×8 matrix as $\check{F}$. Matrices will generalize to higher dimensions as a Kronecker (direct) product with a unit matrix where it is needed, so that e.g.

$$\underline{F}\hat{G} = \begin{pmatrix} \underline{F} & 0 \\ 0 & \underline{F} \end{pmatrix} \hat{G}.$$

Commutators and anticommutators are denoted in the usual way as $[A, B]$ and $\{A, B\}$, respectively. The Pauli matrices in spin space will be denoted by $\underline{\sigma}_1, \underline{\sigma}_2$ and $\underline{\sigma}_3$. When used in particle-hole (Nambu) space, we use the symbols $\underline{\tau}_1$, $\underline{\tau}_2$ and $\underline{\tau}_3$. The identity matrices will be denoted $\underline{\tau}_0$, $\underline{\sigma}_0$, and $\underline{1}$. We gather these matrices in vectors,

$$\underline{\boldsymbol{\sigma}} \equiv (\underline{\sigma}_1, \underline{\sigma}_2, \underline{\sigma}_3)^{Tr} \qquad \underline{\boldsymbol{\tau}} \equiv (\underline{\tau}_1, \underline{\tau}_2, \underline{\tau}_3)^{Tr},$$

where Tr denotes the matrix transpose. For matrices in Nambu-spin space we will use the generalizations of the Pauli matrices,

$$\begin{aligned}\hat{\tau}_1 &\equiv \underline{\tau}_1 \otimes \underline{\sigma}_0 \\ \hat{\tau}_2 &\equiv \underline{\tau}_2 \otimes \underline{\sigma}_0 \\ \hat{\tau}_3 &\equiv \underline{\tau}_3 \otimes \underline{\sigma}_0,\end{aligned}$$

and

$$\begin{aligned}\hat{\sigma}_1 &\equiv \mathrm{diag}(\sigma_1, \sigma_1^*) \\ \hat{\sigma}_2 &\equiv \mathrm{diag}(\sigma_2, \sigma_2^*) \\ \hat{\sigma}_3 &\equiv \mathrm{diag}(\sigma_3, \sigma_3^*)\,,\end{aligned}$$

where "$\otimes$" denotes the tensor product. The unit matrix in Nambu-spin space will be denoted as $\hat{1}$. We gather the Nambu spin-matrices in 3-vectors as well,

$$\hat{\boldsymbol{\sigma}} \equiv (\hat{\sigma}_1, \hat{\sigma}_2, \hat{\sigma}_3)^{Tr} \qquad\qquad \hat{\boldsymbol{\tau}} \equiv (\hat{\tau}_1, \hat{\tau}_2, \hat{\tau}_3)^{Tr}.$$

For the numerical calculations, it is convenient to introduce additional matrices,

$$\begin{array}{llll}\hat{\rho}_0 \equiv \hat{\tau}_0\hat{\sigma}_0 & \hat{\rho}_1 \equiv \hat{\tau}_0\hat{\sigma}_1 & \hat{\rho}_2 \equiv \hat{\tau}_0\hat{\sigma}_2 & \hat{\rho}_3 \equiv \hat{\tau}_0\hat{\sigma}_3 \\ \hat{\rho}_4 \equiv \hat{\tau}_3\hat{\sigma}_0 & \hat{\rho}_5 \equiv \hat{\tau}_3\hat{\sigma}_1 & \hat{\rho}_6 \equiv \hat{\tau}_3\hat{\sigma}_2 & \hat{\rho}_7 \equiv \hat{\tau}_3\hat{\sigma}_3\end{array}$$

The antidiagonal unit matrices, sometimes called the exchange matrices, will be denoted by J_1, so that we have e.g. $\underline{J}_1 \equiv \underline{\sigma}_1 = \mathrm{antidiag}(1,1)$ and $\hat{J}_1 \equiv \underline{\sigma}_1 \otimes \underline{\sigma}_1 = \mathrm{antidiag}(1,1,1,1)$. Finally, we define the antidiagonal version of the third Pauli matrix as $\underline{J}_3 \equiv \mathrm{i}\sigma_2 = \mathrm{antidiag}(1,-1)$, and $\hat{J}_3 \equiv \mathrm{i}\underline{\sigma}_2 \otimes \sigma_1 = \mathrm{antidiag}(1,1,-1,-1)$.

Contents

Chapter 1

Introduction

In this chapter, we introduce the concepts of ferromagnetism and superconductivity, and how they can be applied to the field of spintronics. We also explain the organization of the chapters in this thesis.

1.1 Superconducting spintronics

Ferromagnets have fascinated man for at least 2000 years, and they have been used in a wide range of different applications such as navigation, electrical generators, and computer hard drives [1, 2]. The ferromagnetic state is characterized by the spins of a material aligning to form a macroscopic magnetization, something that cannot be explained by classical physics. Ferromagnets can also be used to make currents spin-polarized, which is used in spintronics, where the spin of a particle is used in solid-state devices. Spintronics has, through the giant magnetoresistance effect [3, 4], which resulted in the Nobel Prize in physics in 2007 [5], already found applications within read heads in hard drives [6], and shows further promise in applications within energy-efficient and faster logic devices [7]. Superconductivity is, together with ferromagnetism, the most dramatic manifestation of quantum effects on macroscopic scales. A conventional superconductor is characterized by the fact that magnetic fields are completely expelled from the interior, as well as the zero-resistance electrical current that gives the effect its name. The fundamental constituent of the superconductor is the Cooper pair, after Cooper [8], which consists of two electrons forming a bound singlet spin-state, avoiding the scattering of the ion lattice of the material. Superconductivity is used today in medical magnetic imaging devices and sensitive imaging devices, due to their ability to energy-efficiently carry large currents, as well as for magnetic levitation in e.g. trains [9] due to the magnetic properties of superconductors [10].

In a world increasingly dependent on computers, the question arises whether it

is possible to obtain synergies between the zero-resistance conductivity of the superconductor and the spin-alignment of a ferromagnet. By placing superconductors and ferromagnets in proximity to each other, properties tend to mix close to the material interface [11], and such systems have been the subject of intense research in the last years, showing promise to be used to produce supercurrents carrying a net spin [6]. Interestingly, in many physically relevant systems, the Cooper pairing becomes non-local and antisymmetric in time, a paring which was first described by Berezinskii [12]. This pairing is usually denoted as *odd-frequency pairing*. Such an exotic pairing is not only exhilarating from a fundamental physics point of view, but it also gives rise to new properties, which differ greatly from the properties of conventional superconductors, as was reviewed in a recent paper by Linder and Balatsky [13]. This includes an altered local density of states [14, 15, 16, 17], and robustness against spin-flip impurity scattering [18, 14]. The Meissner effect in odd-frequency superconductors has been debated in the literature, and it has been argued for both a paramagnetic [19, 20] and diamagnetic Meissner effect [21]. Superconducting systems that are odd in frequency have the advantage of being able to carry net spin while also being robust against impurity scattering [22]. This opens a possible avenue for obtaining long-range spin-polarized supercurrents, which are currents that flow without resistance while simultaneously carrying a net spin [23]. Moreover, in a recent article by [24], it was shown that the spin current was strongly enhanced in a proximity structure compared to what one would expect for a conventional singlet superconductor, indicating that the proximity had induced odd-frequency pairing in the superconductors. For the reasons mentioned above, further understanding the nature of odd-frequency pairing in superconductors could be an important step on the road to realizing energy-efficient superconducting spintronics.

1.2 Structure of the thesis

In this thesis, we study odd-frequency superconductivity using quasiclassical theory. The thesis consists of six chapters, including this introductory chapter. In Chapter 2, we start by discussing some fundamental concepts of ferromagnetism, superconductivity, and quantum theory, which are used extensively in the rest of the thesis. We then proceed in Chapter 3 by introducing the field theory of superconductors, ferromagnets, and metals, deriving equations of motions for the Green functions in such materials. The quasiclassical approximation is introduced, essentially assuming that the energies in the systems are small compared to the Fermi energy. Finally, we consider so-called dirty systems, where impurity scattering dominates other energies in the system, and simplify the equations of motion by averaging over all possible impurity configurations, thus making our approximate

result valid for any system with randomly distributed impurities. Much of Chapter 3 will build upon the specialization thesis, which was written during the fall semester as an introduction to this master's thesis. Most of the specialization thesis is spent deriving the Usadel equation in detail. This derivation is also available in both textbooks and other theses, such as the master theses of Morten [25] or Amundsen [26], or the textbook by Rammer [27]. In this thesis, we will instead give an overview and sketch the methods used to derive the equations and refer the reader to the specialization thesis or the other sources cited above for some of the detailed calculations. The specialization thesis is not readily available but will be handed out upon request. In Chapter 4, we propose physically reasonable criteria that the quasiclassical Green functions of odd-frequency superconductors are expected to satisfy and use these to propose analytical models for the Green functions in odd-frequency superconductors. These models are then studied in detail to investigate the physics they describe. In Chapter 5, we solve numerically a realistic proximity system naturally displaying pure odd-frequency superconductivity and use this system to study properties relevant to spin transport such as spin accumulation, spin-flip and spin-orbit scattering, and the density of states. The Meissner response of the system is also calculated. These properties are compared to properties of conventional superconductors, as well as our analytical models from Chapter 4. The Python program that was written to solve for the equilibrium and non-equilibrium quasiclassical Green function is available upon request. Finally, we summarize and discuss the prospects of the thesis in Chapter 6.

Chapter 2

Fundamental Concepts

In this chapter, we introduce the fundamentals of ferromagnetism, superconductivity, and their interplay. We also explain some fundamental concepts from quantum theory, which is used extensively throughout the thesis.

2.1 Ferromagnetism and superconductivity

We give brief historical introductions to ferromagnetism and superconductivity, two of the most dramatic manifestations of quantum effects on the macroscopic scale, as well as the coexistence of these phases. This will illuminate some of the incredible implications of quantum theory for material properties.

2.1.1 Introduction to ferromagnetism

During the 19th century, the classical theory of electromagnetism was developed, and when James Clerk Maxwell formulated his eponymous equations at the end of the century, one could be led to believe that the theory of electromagnetism was set in stone: static and moving electric charges produced electric and magnetic fields, respectively, and the fields determined the movement of other charged particles [28]. It was then natural to try to apply this theory to ferromagnets, which are materials with a net magnetization even in the absence of external fields. The magnetization was believed to simply be a product of bound currents in the material. However, using statistical mechanics, Niels Bohr derived in his doctorate thesis [29] what is now called the Bohr-van Leeuwen theorem, which states that the net magnetization must be zero for a classical material in equilibrium, if the magnetization comes from currents alone [2]. This was devastating for the hope of using classical electromagnetism to explain the phenomenon of ferromagnetism.

With the invention of quantum mechanics and the discovery of the intrinsic

angular momentum, or quantum spin, of fundamental particles, the situation changed. It is the electrons that carry the magnetization and by thinking of a ferromagnet as a lattice of spin-1/2 particles, it seems natural to consider an analogy to bar magnets placed on a lattice. These magnets try to align their neighbors in the same direction as themselves, through the dipole-dipole-interaction. It can, however, be shown, as done in a note by Timm [2], that the typical energies of such interactions are on the scale of $T \sim 0.3\,\mathrm{K}$, suggesting that the dipole-dipole interaction is too weak to be the dominant mechanism behind ferromagnetism, which is present even at ambient temperatures.

The interaction responsible for the ferromagnetic order is the exchange interaction, which arises due to the Pauli principle, which states that two fermions cannot be in the same quantum mechanical state. Electrons in the same spin state will experience a repulsive *Pauli exchange force*[1]. It can be shown that for a many-body system of localized electrons at half-filling, the Pauli principle results in an exchange interaction, which takes the same form as a Zeeman interaction, and lowers the energy of the system by aligning the spins of the electrons [26]. This produces a ferromagnetic ground state, where spins align to form a macroscopic magnetization.

2.1.2 Introduction to superconductivity

For temperatures in the ambient regime, the conductivity of a metal increases with decreasing temperature. A physical interpretation of this is that the conductivity is due to moving electrons, and resistance is due to scattering with the ion cores in the metal; with increased temperature, the ions move around more, creating more resistance. On the other hand, it was for a long time also unknown whether the conducting electrons would be able to move at a temperature of absolute zero [30], and it was, therefore, an open question what would happen to the resistivity of a conductor at zero temperature. This was the situation in physics in the early 20th century before 1911 when Heike Kamerlingh Onnes observed that the resistivity of liquid mercury dropped abruptly to zero at a critical temperature T_c of a few Kelvin [31], as presented in e.g. [27, 30]. The behavior of the resistivity in such a material is illustrated in Fig. 2.1. This had no explanation within classical physics, and almost 50 years passed before a complete explanation of this phenomenon of *superconductivity* was put forth.

Nevertheless, progress was made during the 1930s. Although the perfect conductivity was the first property of conventional superconductivity to be discovered, it soon became clear that it was not the most fundamental property of such mater-

[1]Of course, in the fundamental physics definition of a force involving the exchange of a force-carrying particle, the Pauli exchange "force" is not an actual force.

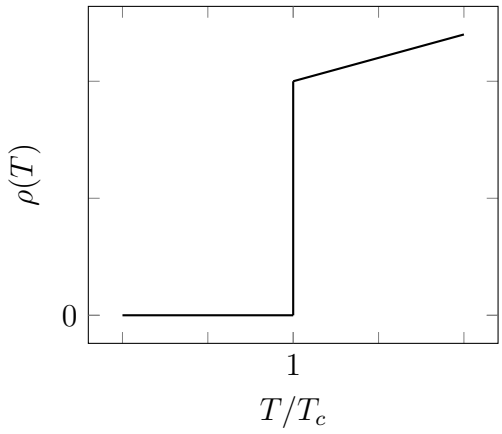

Figure 2.1: The temperature dependence of the resistivity ρ drops abruptly to zero at the critical temperature T_c of a superconductor. For low temperatures above the critical temperature, the resistivity increases approximately linearly.

ials. In 1933, Meissner and Ochsenfeld [32] found that magnetic fields are expelled from the bulk of a superconductor below the critical temperature, meaning that superconductors display perfect diamagnetism in addition to perfect conductance. This effect was called the Meissner effect after its discoverer. It can be shown using Maxwell's equations, as is done e.g. by Tinkham [33], that a perfect conductor will in general resist changes in the magnetic field, but this effect differs from the perfect diamagnetism that superconductors display. If one places a superconductor above the critical temperature in a magnetic field and then cools it down, the magnetic field is expelled from the bulk of the superconductor, while in a perfect conductor the field inside could in general remain constant when cooling it down below the critical temperature, and then resisting changes in this magnetic field. In other words, the Meissner effect does not follow from the property of perfect conductance. It can, however, be shown that the opposite is true, perfect conductivity follows from the Meissner effect [13]. The discovery of the Meissner effect was also important for the development of the theory of superconductivity because it showed for the first time that superconductivity was a thermodynamic phase [34].

An important clue for the origin of the superconductivity came in the year 1950 when it was discovered that the critical temperature of mercury superconductors depends on the mass of the ions constituting the lattice [34]. This so-called isotope effect indicated that the electron-phonon interactions between the electrons and the lattice played an important role in explaining the superconducting state. Such an interaction gives rise to an attractive interaction, which at low frequencies is attractive and, in some cases, can even overcome the Coulomb repulsion between electrons [33]. In a monumental paper in 1956, Cooper [8] showed that even a

weak attraction between electrons would lead to an instability in the Fermi sea, suggesting that a phase transition would occur for materials displaying attractive forces between electrons. Cooper showed that for such materials, pairs of electrons would form at least one bound state in the form of spin-singlets, which are today called Cooper pairs, which could move through the lattice without resistance. This was due to the pairs having lower energy than the Fermi sea background, meaning that it would take a finite excitation energy Δ for each electron to break up the Cooper pair. This instability depends on the existence of a Fermi sea, as well as being a consequence of the Fermi statistics [33]. The formation of such a pair is often explained using a classical analogy of two point-charge electrons moving in a rigid lattice, as shown in Fig. 2.2. The rapid electrons displace the positively charged lattice in their wake, creating a temporary increased charge density. This increased charge density will in turn attract other electrons, in effect providing an attractive force between electrons.

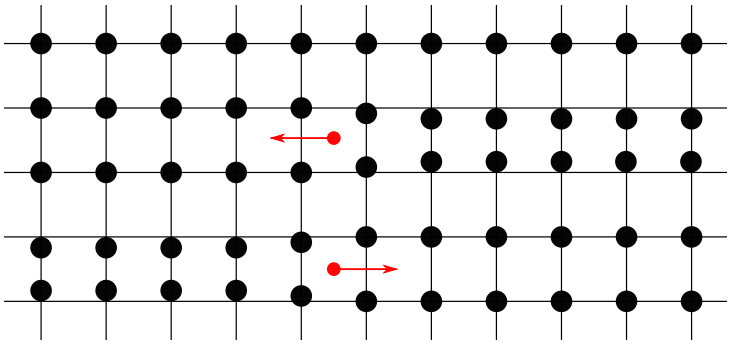

Figure 2.2: The classical analogy of the mechanism behind BCS superconductivity. The ion cores (black), are pulled towards the rapidly moving electrons (red) and create a temporary increased charge density which pulls on other electrons. This results in a net attraction between the electrons. The figure is adapted from [26].

Finally, with the BCS theory of superconductivity in 1957, Bardeen, Cooper, and Schrieffer [35] generalized the results to a condensate of many electrons. The condensation was in essence due to the excitation of quasiparticles from this condensate requiring a finite excitation energy above the condensate ground state energy. The density of states for a superconductor can be found from BCS theory, and is plotted in the left pane in Fig. 2.3. In BCS theory, the temperature dependence of the gap can be approximated by an interpolation formula, as presented e.g. in [36],

$$\Delta(T) = \Delta_0 \tanh\left(1.74\sqrt{\frac{T_c}{T} - 1}\right), \tag{2.1}$$

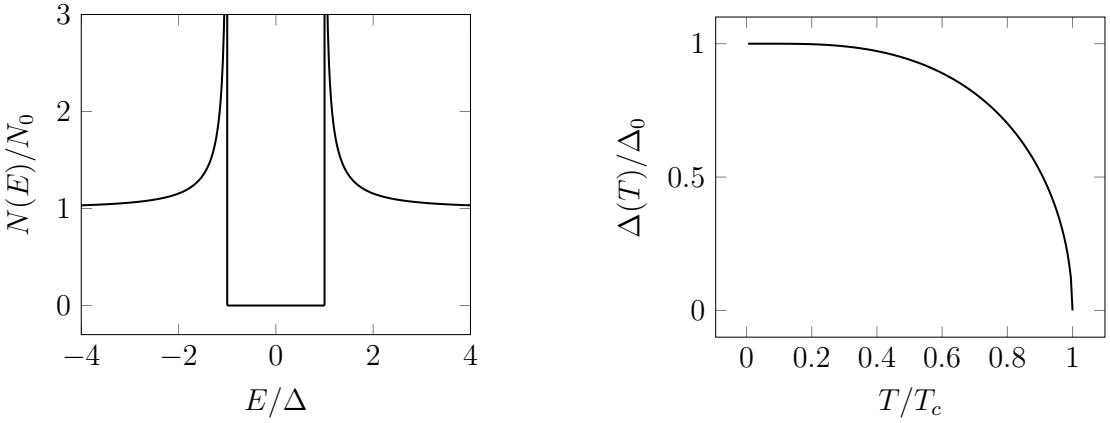

Figure 2.3: In the left pane, the normalized density of states is plotted for a conventional superconductor. In the right pane, the approximate temperature dependence of the gap $\Delta(T)$ is shown. See the main text for more details.

where Δ_0 is the gap at zero temperature. This temperature dependence is plotted in the right pane in Fig. 2.3. In the original paper, it was predicted that the ratio of this energy gap $\Delta_0 \equiv \Delta(T = 0)$ at zero temperature and the critical temperature T_c should be [35]

$$\frac{2\Delta_0}{T_c} = 3.50, \tag{2.2}$$

which matches well with experimental results performed for superconductors like Al, Nb or Hg [33, 37][2].

2.1.3 Coexistence between ferromagnetism and superconductivity

Ferromagnets and superconductors have properties that are useful for many applications within technology, and the question of combining the two effects naturally arose during the development of the theory of superconductivity. Since the early days of superconductivity it has, however, been known that for strong magnetic fields, the superconducting state is broken [38, 23]. Taken together with the fact that conventional superconductors display the Meissner effect, it is clear that the ferromagnetic and superconducting states are largely incompatible [11]. The question of coexistence between the two phases was considered by Ginzburg [39], who studied how Cooper pairs were broken up by the orbital interaction that arises when electrons move in a magnetic field. Moreover, in 1958, Matthias *et al.* [40]

[2]In [33], BCS theory is used to arrive at the ratio $\Delta_0/T_c = 1.764$.

suggested also the effect of *paramagnetic pair breaking*, which originates from the exchange interaction in the ferromagnet attempting to align the electrons in the Cooper pair. The same effect is also present for magnetic fields, where the Zeeman interaction tries to align the electrons [11]. This causes the singlet Cooper pairs to be broken apart, but there is also another effect present, where the singlets are transformed into triplets and back [11]. This is called the FFLO or LOFF effect after Fulde and Ferrell [41] and Larkin and Ovchinnikov [42] who discovered this effect independently and is due to the exchange splitting of the energy bands causing the Cooper pair to acquire a nonzero center-of-mass momentum [23]. While there are bulk systems that display both ferromagnetism and superconductivity, the superconducting effects in singlet s-wave superconductors tend to be destroyed in strong ferromagnets [23]. Triplet superconductors do not feel the exchange interactions in a ferromagnet, but due to such superconductors usually exhibiting p-wave symmetry[3], they are, in contrast to s-wave or d-wave superconductors, extremely sensitive to impurity scattering effects, making applications difficult to realize [43, 23].

2.2 Andreev reflection and the proximity effect

Superconductivity is characterized by the existence of an energy gap Δ, which means that there are no one-particle states available for excitation energies below this gap, relative to the Fermi energy. The energy of such a quasiparticle is in a BCS superconductor given as

$$E_k = \sqrt{\Delta^2 + \xi_k^2}, \tag{2.3}$$

where $\xi_k = k^2/2m - \mu$ is the kinetic energy relative to the Fermi energy μ of a particle with momentum k in the normal state, and m is the mass of the particle. When placing a conductor in proximity to a superconductor, electrons with energies below the gap can still move across the boundary from the normal metal into the superconductor, by the mechanism known as Andreev reflection [44]. In this effect, the incident electron is reflected as a *hole*, while a Cooper pair is created on the superconducting side, meaning a charge transfer of $2e$ has occurred in the process. This is illustrated in Fig. 2.4. Thinking of this process as one particle being transformed into two electrons and a hole shows that the total charge is conserved in the system. The reflected hole has the opposite momentum and spin compared to the incident electron[4], causing conservation of momentum and spin as well.

[3]This is explained in more detail in Section 2.3

[4]Due to the hole being a missing electron, the physical spin of a hole is the opposite of the spin of the missing electron.

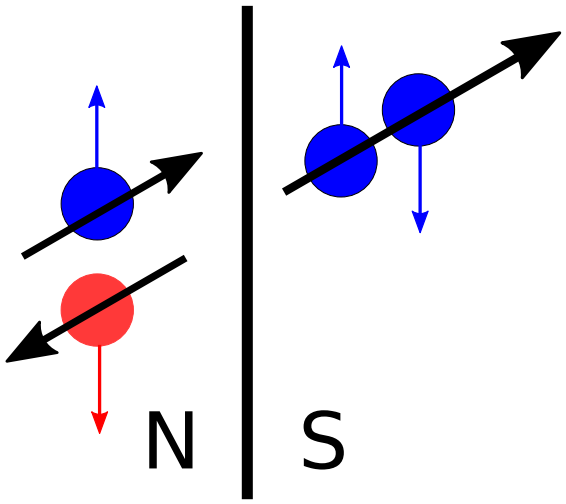

Figure 2.4: Illustration of Andreev reflection between a normal metal (N) and a superconductor (S). The electrons are shown in blue and the holes in red. The black arrows show the velocity direction of the velocities of the particles, and the blue arrows show the spin of the electrons. The red arrow shows the spin of the missing electron.

An important feature of this process is that the reflected hole in the normal metal will be phase-coherent with the transmitted Cooper pair, meaning that the normal metal will become, to some extent, coherent with the superconductor [45]. It has been known since the 1960s that placing superconductors and metals in the normal state together in so-called superconductor-normal metal (SN) heterostructures, dramatically charges material properties; superconducting properties can be induced in the metal, and the superconducting properties in the superconductor is weakened [46, 47]. Such phase-coherence is due to the mechanism of Andreev reflection, causing the superconducting properties to persist for lengths much longer than the microscopic scale into the normal metal [48], an effect known as the proximity effect. Another type of proximity effect arises when placing a superconductor together with a ferromagnet in a so-called superconductor-ferromagnet (SF) heterostructure. In the ferromagnet, the FFLO effect causes the singlet amplitude to oscillate into a triplet amplitude. For homogeneous magnetization, these components both decay quickly inside the ferromagnet, but by utilizing a ferromagnet with an inhomogeneous magnetization, it is possible to make these triplets long-ranged [49, 50]. In Section 5.2, we will use the Python program that was written to study SN and SF structures with both homogeneous and inhomogeneous magnetization, and the reader is directed to this section for a further discussion about the proximity effect.

2.3 Odd-frequency superconductivity

The concept of odd-frequency pairing was introduced by Berezinskii [12] as an explanation for the superfluid phase of Helium-3. It was later found that the superfluid Helium-3 did not display odd-frequency pairing, but rather a different spatial pairing [21]. Nevertheless, the idea of a pairing that is odd in time, was almost 20 years later applied to superconducting systems by Balatsky and Abrahams [51]. In a recent paper, Linder and Balatsky [13] argued that the odd-frequency paring was ubiquitous in superconducting systems and that it appeared not only in heterostructures but also in bulk materials and dynamically driven superconducting states. In this section, we follow this paper and review the fundamental properties of odd-frequency superconductivity.

It can be shown in general that the pairing amplitude $f_{\sigma\sigma'}(\boldsymbol{r}_1, t_1; \boldsymbol{r}_2, t_2)$, which describes superconducting correlations, must be odd under the application of the parity operator P, the spin-interchange operator S, and the time-reversing operator T[5][6]. This motivates the previous statement that was made about triplet superconductors usually displaying p-wave pairing. In this thesis, we will focus on systems where impurity scattering dominates over all other energy terms, which in essence makes the pairing amplitude isotropic in space, thus becoming invariant under P. An odd-frequency superconductor is characterized by a two-electron pairing amplitude which is odd under the application of T [13]. When we Fourier transform this causes the Fourier transformed pairing amplitude to be odd in the relative frequency[7]. This leaves us with two possibilities for such systems: singlet even-frequency or triplet odd-frequency. This classification is summarized in Table 2.1.

Table 2.1: The different symmetry possibilities for the pairing function in a dirty superconductor.

Pairing type	P	S	T
Singlet even-frequency	+	-	+
Triplet odd-frequency	+	+	-

The discussion above reveals that in SF heterostructures, the triplet component that is induced must be odd in frequency. Other possibilities for inducing an odd-frequency pairing in a heterostructure include systems with spin-orbit coupling [52]

[5]Actually, P and T inverts only the relative positions and time coordinates, but we will not discuss this distinction here. See [13] for a more rigorous introduction of these operators.

[6]In general, one could also have orbital indices, in which case we would also have to include the orbital interchange operator. In this thesis, we work only with single-orbit systems.

[7]Energy and frequency have the same units in coordinates where we set $\hbar = 1$.

and SN systems with unconventional superconductors [53, 54]. The amplitudes of the odd-frequency pairing amplitude can in some systems, such as in systems with inhomogeneous magnetization[8] or spin-orbit coupling [52], persist for long distances into the heterostructures.

Odd-frequency pairing alters the local density of states, and it seems that both densities of states that are peaked and gapped at the Fermi energy are possible [14, 13, 13]. Another signature of odd-frequency superconductivity is that they are expected to be less robust to spin-orbit impurity scattering than conventional superconductors, and more robust to spin-flip scattering on magnetic impurities [14]. Finally, there has been some disagreement about the Meissner effect in odd-frequency superconducting systems. The Meissner effect in a conventional superconductor is diamagnetic, meaning that currents arise to cancel external magnetic fields. It has been argued, e.g. in [19, 20] that the Meissner effect in s-wave superconductors should exhibit a paramagnetic Meissner effect, and that this causes an instability in bulk odd-frequency systems, effectively arguing odd-frequency superconductivity to exist in the ground state in uniform systems. In a later article, Solenov *et al.* [21] argued that these conclusions were incorrect due to the erroneous assumption of the existence of a mean-field Hamiltonian. It was argued that the retardation effect, that is the time delay in the interaction between electrons, could not be ignored in the same way as it is in the BCS theory of conventional superconductivity when one approximates the two-body interaction as a mean-field term in the Hamiltonian. It was found, using a path-integral approach, that the Meissner effect was diamagnetic, and a stable ground state in a uniform system was possible. Note that even though the Meissner effect of a bulk system is expected to be diamagnetic for the matter to be stable, it is possible to find a paramagnetic Meissner effect, e.g. in superconductor-ferromagnet heterostructures [13, 16]. The Meissner effect in odd-frequency superconductors will be further explored in Section 4.5 and Section 5.3.2.

2.4 Second quantization

In this section, we introduce the notion of second quantization in quantum mechanics. This section will be based on the condensed matter field theory textbook by Altland and Simons [55].

In quantum mechanics, one can describe a system of many particles through a many-particle wave function, which can be constructed from the single-particle wave functions. For the simple case of non-interacting particles, this is done by (tensor) multiplying the single-particle wave functions, as well as symmetrizing or antisymmetrizing the resulting wave function, following the spin-statistics theorem [56].

[8] Such a system is considered in Chapter 5.

The procedure of applying the correct symmetries is simple for a two-particle system, but as the number of particles increases, the procedure becomes cumbersome. Using Dirac's bra-ket notation, the N-particle wave function can be written as

$$|\lambda_1, \lambda_2 ... \lambda_N\rangle = \frac{1}{\sqrt{N! \prod_{k=0}^{\infty}(n_{\lambda_k}!)}} \sum_{\mathcal{S}} \xi^{1-\mathrm{sgn}(\mathcal{S})} |\lambda_{S_1}\rangle \otimes \cdots \otimes |\lambda_{S_N}\rangle . \tag{2.4}$$

Here, $|\lambda_i\rangle$ is the one-particle wave function, "$\otimes$" denotes the tensor product, $\mathcal{S}$ is the permutation of order N, $\mathrm{sgn}(\mathcal{S})$ is the sign function which is 1 (-1) for even (odd) permutations, n_{λ_k} is the number of particles in the state λ_k and $\xi = 1$ for bosons and $\xi = -1$ for fermions. It is the fact that we need to symmetrize or anti-symmetrize the functions that lead to the complicated form of this many-particle wave function. In addition to being complicated, this formalism has another disadvantage; the wave functions only exist for a fixed particle number. From statistical mechanics in classical physics, we know that it can often be convenient to use the grand canonical ensemble, where the number of particles is allowed to fluctuate. When the number of particles is large enough, the particle fluctuation will make no difference, but many calculations can be made easier this way. Additionally, in the theory of superconductivity, it is useful to have basis functions that contain superpositions of states with different particle numbers.

Motivated by the arguments above, we instead introduce the formalism of *second quantization*, which is sometimes also called the occupation number formalism. In this formalism, instead of writing a ket on the form $|\lambda_1, \lambda_2 ...\rangle$, where λ_i is the state that particle i is in, we write the state as $|n_1, n_2 ...\rangle$, where n_i is the number of particles that occupy state number i. We also introduce the *vacuum state* $|0\rangle$ as the state with no particles.

We now introduce the creation and annihilation operators as the operators that raise or lower the number of particles in a given state. For simplicity, this is done for fermionic particles only in the rest of the thesis, since we will consider mainly electrons, which are fermions[9]. The creation operators $c_\lambda^\dagger$ and the annihilation operators c_λ are defined through their effect on the vacuum state,

$$c_\lambda^\dagger |0\rangle = |\lambda\rangle \qquad\qquad c_\lambda |\lambda\rangle = |0\rangle . \tag{2.5}$$

The operators follow fermionic anticommutation relations

$$\left\{c_\lambda, c_{\lambda'}^\dagger\right\} = \delta_{\lambda,\lambda'} \qquad \left\{c_\lambda, c_{\lambda'}\right\} = 0 \qquad \left\{c_\lambda^\dagger, c_{\lambda'}^\dagger\right\} = 0, \tag{2.6}$$

where $\delta_{\lambda,\lambda'}$ is the Kronecker delta function. In the case of $\lambda = \lambda'$, the last two equations mean that using either operator twice will destroy any state. This can

[9]For a general introduction to the second quantization of bosons, the reader is directed to the book by Altland and Simons [55].

be interpreted as the fact that only one fermionic particle can occupy a given state at the time. This is the well-known Pauli principle, which is responsible for much of the physics behind everyday effects, such as the stability of matter [57].

In the second quantization formalism, a one-particle operator A is given by

$$A = \sum_{\lambda,\lambda'} \langle \lambda' | A_1 | \lambda \rangle c^\dagger_{\lambda'} c_\lambda, \tag{2.7}$$

where A_1 is the first-quantized operator corresponding to A. By multiplying with $|\alpha\rangle$ from the right and $\langle\beta|$ from the left we obtain

$$\langle \beta | A | \alpha \rangle = \sum_{\lambda,\lambda'} \langle \lambda' | A_1 | \lambda \rangle \langle 0 | c_\beta c^\dagger_{\lambda'} c_\lambda c^\dagger_\alpha | 0 \rangle = \langle \beta | A_1 | \alpha \rangle , \tag{2.8}$$

where in the last equation we have used the anticommuatation relations of the creation and annihilation operators. We then see that the two formulations yield the same matrix elements, and thus will give the same results for all physical observable quantities. For N-particle operators, the procedure for constructing the second quantized version is a straightforward generalization of the one-particle operator, with the sum going over $2N$ variables, the first-quantized operator being sandwiched between N bras and N kets, and with N creation operators and N annihilation operators.

So far, the quantum number λ could be any quantum number that labels the states. It is convenient to choose the quantum number and thus the basis in a way that fits the system, in order to make calculations as simple as possible. In this thesis, it will be convenient to choose[10] $\lambda = \boldsymbol{r}$, the position vector. Since $\boldsymbol{r}$ is a continuous quantum number, discrete sums are replaced with integrals, and Kronecker delta functions are replaced with Dirac delta functions. We denote the creation and annihilation operators by

$$\psi(\boldsymbol{r}, t) = \int d\boldsymbol{r} \phi_\lambda(\boldsymbol{r}, t) c_\lambda \qquad \psi^\dagger(\boldsymbol{r}, t) = \int d\boldsymbol{r} \phi^*_\lambda(\boldsymbol{r}, t) c^\dagger_\lambda, \tag{2.9}$$

where $\phi_\lambda(\boldsymbol{r}, t)$ is the wave function of the state characterized by λ. These operators are often called field operators and can be interpreted as the operators that create and annihilate particles at position $\boldsymbol{r}$ and time t, and are sometimes referred to as the *field operators*.

The operators, follow fermionic anticommutation relations at equal times,

$$\left\{ \psi(\boldsymbol{r}, t), \psi^\dagger(\boldsymbol{r}', t) \right\} = \delta(\boldsymbol{r} - \boldsymbol{r}') \tag{2.10a}$$

$$\left\{ \psi(\boldsymbol{r}, t), \psi(\boldsymbol{r}', t) \right\} = 0 \tag{2.10b}$$

$$\left\{ \psi^\dagger(\boldsymbol{r}, t), \psi^\dagger(\boldsymbol{r}', t) \right\} = 0, \tag{2.10c}$$

[10] We will also include the spin quantum number, but here we are discussing the choice of the quantum numbers for spatial degrees of freedom.

where δ is the Dirac delta function. For an introduction to field theory in the context of the Schrödinger equation, the reader is directed to Appendix B.

2.5 Pictures of quantum mechanics

In the formulation of quantum mechanics, one can choose whether to put the time-dependence in the operators or the state vectors. We refer to these different formulations as *pictures* of quantum mechanics. This section will be based on the textbook on introductory quantum mechanics by Sakurai and Napolitano [56].

In the Schrödinger picture, the time evolution is placed only in the state vectors. The time evolution of a state $|\Psi(t)\rangle$ is given by the Schrödinger equation

$$\mathrm{i}\partial_t |\Psi(t)\rangle = H(t) |\Psi(t)\rangle , \tag{2.11}$$

where H is the Hamiltonian operator of the system, and where we have suppressed the dependence on all variables except for time. We define the unitary time-translation operator as

$$\mathcal{U}(t, t_0) |\Psi(t_0)\rangle = |\Psi(t)\rangle . \tag{2.12}$$

We can then rewrite the Schrödinger equation in terms of this operator as

$$\mathrm{i}\partial_t \mathcal{U}(t, t_0) = H(t)\mathcal{U}(t, t_0). \tag{2.13}$$

It is worth noting that in the simple case where there is no explicit time dependence in H, the solution of (2.13) is simply

$$\mathcal{U}(t, t_0) = \mathrm{e}^{-\mathrm{i}H(t-t_0)}. \tag{2.14}$$

In the Heisenberg picture, one instead lets the operators carry the time evolution, and the state vectors are independent of time. We consider a general operator A_S in the Schrödinger picture and assume that it has no time dependence, as this will be the case for the field operators we consider in the rest of the thesis. We assume that the state vector and operators coincide at $t = t_0$, and require matrix elements to be the same in the Heisenberg picture as in the Schrödinger picture at all subsequent times. This means that all observable quantities will be the same in the two pictures, which they must be in order for the two pictures to give compatible results. This means that

$$\begin{aligned} \langle\Psi(t)| A_S |\Phi(t)\rangle &= \langle\Psi(t_0)| \mathcal{U}^\dagger(t, t_0) A_S \mathcal{U}^\dagger(t, t_0) |\Phi(t_0)\rangle \\ &= \langle\Psi(t_0)| \mathcal{U}^\dagger(t, t_0) A_H(t_0) \mathcal{U}^\dagger(t, t_0) |\Phi(t_0)\rangle \\ &= \langle\Psi(t_0)| A_H(t) |\Phi(t_0)\rangle , \end{aligned} \tag{2.15}$$

where the subscripts refer to the picture the operator is given in. Since the states Ψ and Φ are arbitrary, the time-evolution of a general Heisenberg operator $A_H(t)$ is given through the operator relation

$$A_H(t) = \mathcal{U}^\dagger(t, t_0) A_H(t_0) \mathcal{U}(t, t_0). \tag{2.16}$$

In order to calculate the time dependence of operators in the Heisenberg picture, one could solve Eq. (2.13) for $\mathcal{U}(t, t_0)$ and then insert into Eq. (2.16). There is, however, a simpler way that involves deriving an equation of motion of the operator $A(t)$ directly. This equation is often called the Heisenberg equation of motion. We start by considering the time derivative of the operator A_H and use the definition of the time evolution in Eq. (2.16). This yields (suppressing the time arguments in $\mathcal{U}$)

$$\begin{aligned}
\partial_t A_H(t) &= \partial_t \left(\mathcal{U}^\dagger A_S \mathcal{U} + \mathcal{U}^\dagger A_S \mathcal{U} \right) \\
&= -\frac{1}{\mathrm{i}} \mathcal{U}^\dagger H \mathcal{U} \mathcal{U}^\dagger A_S \mathcal{U}^\dagger + \frac{1}{\mathrm{i}} \mathcal{U}^\dagger A_S \mathcal{U} \mathcal{U}^\dagger H \mathcal{U} \\
&= \frac{1}{\mathrm{i}} \left[\mathcal{U}^\dagger A_S \mathcal{U}, \mathcal{U}^\dagger H \mathcal{U} \right] \\
&= \frac{1}{\mathrm{i}} \left[A_H(t), H \right] \\
&= \mathrm{i} \left[H, A_H(t) \right],
\end{aligned} \tag{2.17}$$

In the first line, the Schrödinger equation for the time-evolution operator from Eq. (2.13) and its adjoint equation was used. In the fourth line, we used Eq. (2.16) and assumed the Hamiltonian to be time-independent such that it commutes with the time-evolution operator[11]. This equation will be used extensively in Section 3, where the operators in question are the field operators introduced in Section 2.4. From here, we drop subscripts on the operators, with the knowledge that all operators are given in the Heisenberg picture.

[11]This implies that from the definition of Heisenberg operators in Eq. (2.15), the Hamiltonian is the same in both pictures. We can thus refer to the Hamiltonian of a system without specifying which of the two pictures we are considering.

Chapter 3

Theory

In this chapter, we introduce the non-equilibrium field theory of superconductors using Green functions and introduce the quasiclassical approximation to simplify the equations of motion. We take the dirty limit, assuming that the systems we will consider are dominated by impurity scattering. This will result in the derivation of the Usadel equation, valid for a superconductor where the impurity scattering is assumed to be strong compared to other interactions. This equation is a nonlinear differential equation that can be solved for the quasiclassical Green function of the system. Much of this chapter is based on the specialization thesis [58]. Since much of the specialization thesis is spent deriving the Usadel equation, and because this is a derivation that is readily available in other texts, we will in this thesis focus on conveying the concepts behind the derivation. To this end, we will cite other works for some results, in order to keep the derivation short and to the point.

3.1 Field operators and their equations of motion

In this section, we introduce the dynamics of a superconducting system, and derive equations of motion for the field operators.

3.1.1 Hamiltonian

We consider a superconducting system with spin-flip impurity scattering, spin-orbit impurity scattering, and elastic impurity scattering. To be able to describe ferromagnetic effects, we allow for an exchange interaction to be present in the system. We also allow for electromagnetic fields in the material but neglect the effect of spin-orbit coupling. For a thorough introduction to all these interactions and a derivation of their Hamiltonian terms, the reader is directed to the master's thesis of Amundsen [26], where the microscopic theory of superconductivity, ferromagnetism,

and elastic impurity scattering is derived and discussed. We will also include the effects of spin-orbit scattering and spin-flip scattering on impurities, which are discussed in the appendix of an article by Johnsen and Linder [14]. The Hamiltonian of such a system is given by

$$H = H_0 + H_{\text{BCS}} + H_{\text{sc}} + H_{\text{sf}} + H_{\text{ex}} + H_{\text{so}}, \tag{3.1}$$

where we have defined the kinetic term H_0, the BCS mean field term H_{BCS}, the ferromagnetic exchange term H_{ex}, the impurity scattering term H_{sc}, the spin-flip scattering term H_{sf}, the ferromagnetic exchange term H_{ex}, and the spin-orbit impurity scattering term H_{so}, as

$$H_0 = \sum_\sigma \int d\boldsymbol{r} \psi_\sigma^\dagger(\boldsymbol{r},t) \left[-\frac{1}{2m}\tilde{\nabla}^2 - \mu(\boldsymbol{r},t) + e\phi(\boldsymbol{r},t) \right] \psi_\sigma(\boldsymbol{r},t) \tag{3.2a}$$

$$H_{\text{BCS}} = \int d\boldsymbol{r} \left[\Delta^*(\boldsymbol{r},t)\psi_\downarrow(\boldsymbol{r},t)\psi_\uparrow(\boldsymbol{r},t) + \Delta(\boldsymbol{r},t)\psi_\uparrow^\dagger(\boldsymbol{r},t)\psi_\downarrow^\dagger(\boldsymbol{r},t) \right] \tag{3.2b}$$

$$H_{\text{sc}} = \sum_\sigma \int d\boldsymbol{r} \psi_\sigma^\dagger(\boldsymbol{r},t) V_{\text{sc}}(\boldsymbol{r},t) \psi_\sigma(\boldsymbol{r},t) \tag{3.2c}$$

$$H_{\text{sf}} = \sum_{\sigma\sigma'} \int d\boldsymbol{r} \psi_\sigma^\dagger(\boldsymbol{r},t) \left[\underline{\boldsymbol{\sigma}} \cdot \boldsymbol{S}(\boldsymbol{r},t) \right]_{\sigma\sigma'} V_{\text{sf}}(\boldsymbol{r},t) \psi_{\sigma'}(\boldsymbol{r},t) \tag{3.2d}$$

$$H_{\text{ex}} = -\sum_{\sigma\sigma'} \int d\boldsymbol{r} \psi_\sigma^\dagger(\boldsymbol{r},t) \left[\underline{\boldsymbol{\sigma}} \cdot \boldsymbol{h}(\boldsymbol{r},t) \right]_{\sigma\sigma'} \psi_{\sigma'}(\boldsymbol{r},t) \tag{3.2e}$$

$$H_{\text{so}} = \sum_{\sigma\sigma'} \int d\boldsymbol{r} \psi_\sigma^\dagger(\boldsymbol{r},t) \left[V_{\text{so}}(\boldsymbol{r},t) \right]_{\sigma\sigma'} \psi_\sigma(\boldsymbol{r},t), \tag{3.2f}$$

where μ is the chemical potential of the system, $\sigma = \{\uparrow, \downarrow\}$ is the spin of a particle, ϕ is the electrostatic potential, and $\boldsymbol{h}$ is the magnetization. m denotes the electron mass and $e = -|e|$ the electron charge. We have introduced external magnetic effects through the minimal substitution $\boldsymbol{p} \to \boldsymbol{p} - e\boldsymbol{A}(\boldsymbol{r},t)$ in the kinetic Hamiltonian term, where $\boldsymbol{A}$ is the magnetic vector potential. In the position representation of quantum mechanics, this is equivalent to replacing the derivative with the covariant derivative, $\boldsymbol{\nabla} \to \tilde{\boldsymbol{\nabla}} \equiv \boldsymbol{\nabla} - \mathrm{i}e\boldsymbol{A}$. In Appendix D, we justify this substitution as a way of incorporating a magnetic field in the Hamiltonian and also discuss some properties of the vector potential. We have included the time-dependence in all interactions, but will later restrict our discussion to stationary systems. The magnetic spin-flip impurity scattering is described by a potential V_{sf}, describing the magnetic impurities, and $\boldsymbol{S}$ is the spins of the magnetic impurities, which we assumed can be treated as classical vectors. The impurity potential V_{sc} describes the non-magnetic impurities in the system. The spin-orbit scattering is due to the

impurity potential, and can in the position representation be written[1]

$$[V_{\text{so}}(\boldsymbol{r},t)]_{\sigma\sigma'} = \mathrm{i}\alpha\,[\underline{\boldsymbol{\sigma}} \times \boldsymbol{\nabla} V_{\text{sc}}(\boldsymbol{r},t)]_{\sigma\sigma'} \cdot \boldsymbol{\nabla}, \tag{3.3}$$

where α is the spin-orbit scattering parameter.

3.1.2 Field operator equations of motion

Inserting the Hamiltonian in Eq. (3.1) into the Heisenberg equation of motion in Eq. (2.17), one can use the general operator identity

$$\big[A, BC\big] = \big\{A, B\big\}C - B\big\{A, C\big\}, \tag{3.4}$$

and then use the fermionic anticommutation relations of the field operators from Eq. (2.10) in order to simplify the result. After a lengthy but relatively straightforward calculation, the result can be shown to be [25, 58]

$$\begin{aligned}\mathrm{i}\partial_t \psi_\sigma(\boldsymbol{r},t) = &\left(-\frac{\tilde{\boldsymbol{\nabla}}^2}{2m} - \mu(\boldsymbol{r},t) + V_{\text{sc}}(\boldsymbol{r},t) + e\phi(\boldsymbol{r},t)\right)\psi_\sigma(\boldsymbol{r},t) \\ &+ \Delta(\boldsymbol{r},t)\left(\delta_{\sigma\uparrow}\psi^\dagger_\downarrow(\boldsymbol{r},t) - \delta_{\sigma\downarrow}\psi^\dagger_\uparrow(\boldsymbol{r},t)\right) + \sum_{\sigma'}[V_{\text{so}}(\boldsymbol{r},t)]_{\sigma\sigma'}\,\psi_{\sigma'}(\boldsymbol{r},t) \\ &+ \sum_{\sigma'}[\underline{\boldsymbol{\sigma}}\cdot\boldsymbol{S}(\boldsymbol{r},t)]_{\sigma\sigma'}\,V_{\text{sf}}(\boldsymbol{r},t)\psi_{\sigma'}(\boldsymbol{r},t) - \sum_{\sigma'}[\underline{\boldsymbol{\sigma}}\cdot\boldsymbol{h}(\boldsymbol{r},t)]_{\sigma\sigma'}\,\psi_{\sigma'}(\boldsymbol{r},t).\end{aligned} \tag{3.5}$$

In order to obtain a similar equation of motion for the creation operator, we take the Hermitian adjoint of this equation. This is equivalent to taking the complex conjugate, and yields

$$\begin{aligned}-\mathrm{i}\partial_t \psi^\dagger_\sigma(\boldsymbol{r},t) = &\left(-\frac{(\tilde{\boldsymbol{\nabla}}^*)^2}{2m} - \mu(\boldsymbol{r},t) + V_{\text{sc}}(\boldsymbol{r},t) + e\phi(\boldsymbol{r},t)\right)\psi^\dagger_\sigma(\boldsymbol{r},t) \\ &+ \Delta^*(\boldsymbol{r},t)\left(\delta_{\sigma\uparrow}\psi_\downarrow(\boldsymbol{r},t) - \delta_{\sigma\downarrow}\psi_\uparrow(\boldsymbol{r},t)\right) + \sum_{\sigma'}\psi^\dagger_{\sigma'}(\boldsymbol{r},t)\,[V_{\text{so}}(\boldsymbol{r},t)]^*_{\sigma\sigma'} \\ &+ \sum_{\sigma'}\psi^\dagger_{\sigma'}(\boldsymbol{r},t)\,[\underline{\boldsymbol{\sigma}}\cdot\boldsymbol{S}(\boldsymbol{r},t)]^*_{\sigma\sigma'}\,V_{\text{sf}}(\boldsymbol{r},t) - \sum_{\sigma'}\psi^\dagger_{\sigma'}(\boldsymbol{r},t)\,[\underline{\boldsymbol{\sigma}}\cdot\boldsymbol{h}(\boldsymbol{r},t)]^*_{\sigma\sigma'},\end{aligned} \tag{3.6}$$

where $\tilde{\boldsymbol{\nabla}}^* = \boldsymbol{\nabla} + \mathrm{i}e\boldsymbol{A}$.

[1] In the end, we will not consider the situation of both spin-orbit impurity scattering and an external magnetic vector potential, so whether we use the covariant derivative in the last $\boldsymbol{\nabla}$-factor of this potential does not matter. For this reason, we can use the canonical momentum in this expression, which gives the simplest expressions.

3.1.3 Nambu-spin space generalization

It will later prove useful to introduce structure in spin space and in or particle-hole space, often denoted Nambu space [59]. We introduce the Nambu-spin space[2] 4-vector field operators

$$\psi(\boldsymbol{r},t)=\begin{pmatrix}\psi_\uparrow(\boldsymbol{r},t)\\ \psi_\downarrow(\boldsymbol{r},t)\\ \psi_\uparrow^\dagger(\boldsymbol{r},t)\\ \psi_\downarrow^\dagger(\boldsymbol{r},t)\end{pmatrix},\quad \psi^\dagger(\boldsymbol{r},t)=\begin{pmatrix}\psi_\uparrow^\dagger(\boldsymbol{r},t) & \psi_\downarrow^\dagger(\boldsymbol{r},t) & \psi_\uparrow(\boldsymbol{r},t) & \psi_\downarrow(\boldsymbol{r},t)\end{pmatrix}. \tag{3.7}$$

It can be shown that these 4-vector field operators satisfy the equations of motion [25, 26][3]

$$\mathrm{i}\hat{\tau}_3\partial_t\psi(\boldsymbol{r},t)=\hat{H}_1\psi(\boldsymbol{r},t)\qquad -\mathrm{i}\partial_t\psi^\dagger(\boldsymbol{r},t)\hat{\tau}_3=\psi^\dagger(\boldsymbol{r},t)\hat{H}_1^\dagger(\boldsymbol{r},t), \tag{3.8}$$

with

$$\hat{H}_1(\boldsymbol{r},t)=\hat{\xi}(\boldsymbol{r},t)+V_{\mathrm{sc}}(\boldsymbol{r},t)\hat{1}+\hat{S}(\boldsymbol{r},t)+\hat{\Delta}(\boldsymbol{r},t)-\hat{M}(\boldsymbol{r},t) \tag{3.9}$$

$$\hat{H}_1^\dagger(\boldsymbol{r},t)=\hat{\xi}(\boldsymbol{r},t)^*\hat{1}+V_{\mathrm{sc}}(\boldsymbol{r},t)\hat{1}+\hat{S}(\boldsymbol{r},t)-\hat{\Delta}(\boldsymbol{r},t)-\hat{M}(\boldsymbol{r},t), \tag{3.10}$$

where we have defined Nambu-spin generalizations of the Hamiltonian terms,

$$\hat{\xi}(\boldsymbol{r},t)=-\frac{\hat{\tilde{\boldsymbol{\nabla}}}^2}{2m}-\mu(\boldsymbol{r},t)\hat{1}+e\phi(\boldsymbol{r},t)\hat{1} \tag{3.11a}$$

$$\hat{\Delta}(\boldsymbol{r},t)=\mathrm{antidiag}(\Delta(\boldsymbol{r},t),-\Delta(\boldsymbol{r},t),\Delta^*(\boldsymbol{r},t),-\Delta^*(\boldsymbol{r},t)), \tag{3.11b}$$

$$\hat{S}(\boldsymbol{r},t)=V_{\mathrm{sf}}(\boldsymbol{r},t)\hat{\boldsymbol{\sigma}}\cdot\boldsymbol{S}(\boldsymbol{r},t) \tag{3.11c}$$

$$\hat{M}(\boldsymbol{r},t)=\hat{\boldsymbol{\sigma}}\cdot\boldsymbol{h}(\boldsymbol{r},t) \tag{3.11d}$$

$$\hat{V}_{\mathrm{so}}(\boldsymbol{r},t)=\mathrm{i}\alpha\left[\hat{\tau}_3\hat{\boldsymbol{\sigma}}\times\boldsymbol{\nabla}V_{\mathrm{sc}}(\boldsymbol{r},t)\right]\cdot\boldsymbol{\nabla}, \tag{3.11e}$$

where we have defined $\hat{\tilde{\boldsymbol{\nabla}}}=\boldsymbol{\nabla}\hat{1}-\mathrm{i}e\hat{\tau}_3\boldsymbol{A}$, and the derivative in $\hat{\xi}(\boldsymbol{r},t)^*$ must be applied to the operator to the left. Here, we have used the definition $\hat{\boldsymbol{\sigma}}=\mathrm{diag}(\underline{\boldsymbol{\sigma}},\underline{\boldsymbol{\sigma}}^*)$, and $\hat{\tau}_3$ is the Nambu-spin generalization of the third Pauli matrix.

This means that in theory, one could use the Heisenberg equation in Eq. (2.17) together with the Hamiltonian in Eq. (3.1) to solve for the time evolution of the field operators. Observables are given in terms of field operators, and we can determine

[2]This space is a tensor product of Nambu space and spin space, and it is sometimes referred to as "Nambu⊗spin" space.

[3]Note that the notation for the Nambu-spin matrices differ in this thesis and in other theses that derive the Usadel equation, such as [26, 25, 27, 58].

all physical quantities from the equations above. For complicated systems, however, this is an impossible task, and we will in the following chapters explain how one could instead derive equations of motion of Green functions, and express observables from these. This will enable us to make physically relevant approximations allowing us to solve for nontrivial systems, as well as providing a framework that is more suitable for numerical calculations.

3.2 Gauge transformations and physical interpretation of the magnetic vector potential

In this section, we will discuss gauge transformations and argue that we can use the gauge freedom to make the gap Δ a real quantity. This will also cause the gauge field to acquire a physical interpretation, carrying information about the supercurrent. This section is based on the master's thesis by Morten [25] as well as the book by Tinkham [33].

3.2.1 Gauge transformations of the fields

In classical electrodynamics, gauge freedom arises when we define the magnetic vector potential $\boldsymbol{A}$, causing the electromagnetic field to be given through the relation [28] (suppressing coordinates in this section)

$$\boldsymbol{B} = \boldsymbol{\nabla} \times \boldsymbol{A} \tag{3.12}$$

$$\boldsymbol{E} = -\boldsymbol{\nabla}\phi - \partial_t \boldsymbol{A}, \tag{3.13}$$

where $\boldsymbol{B}$ is the magnetic field, $\boldsymbol{E}$ is the electric field and ϕ the electrostatic potential. A standard result from calculus states that for a general function λ,

$$\boldsymbol{\nabla} \times (\boldsymbol{\nabla}\lambda) = 0. \tag{3.14}$$

For this reason, we can add a gradient term $\boldsymbol{\nabla}\lambda$ to $\boldsymbol{A}$, where λ is an arbitrary function, without changing the physical field $\boldsymbol{B}$. To also leave the electrical field invariant, we must transform the two potentials simultaneously as

$$\boldsymbol{A} \to \boldsymbol{A}' = \boldsymbol{A} + \boldsymbol{\nabla}\lambda \tag{3.15}$$

$$\boldsymbol{E} \to \boldsymbol{E}' = \boldsymbol{E} - \partial_t \lambda. \tag{3.16}$$

The gauge transformation should not change any of the physical quantities in the system. When transforming the fields, it can, however, be seen that additional terms will arise in the Hamiltonian in Eq. (3.1). For our observables to be independent of the choice of gauge, we demand that the fields transform in such a way that

they cancel the terms that will have physical implications for our system. It can be shown that this is satisfied for the field transformation

$$\psi_\sigma \to \psi'_\sigma = \psi_\sigma \mathrm{e}^{\mathrm{i}\lambda} \tag{3.17}$$

$$\psi_\sigma \to \psi'^{\dagger}_\sigma = \psi^\dagger_\sigma \mathrm{e}^{-\mathrm{i}\lambda}, \tag{3.18}$$

that must be performed simultaneously as the transformation of the fields. From Eq. (3.1), it is seen that for a complex order parameter $\Delta = |\Delta|\mathrm{e}^{\mathrm{i}\Phi}$, we can choose $\lambda = \Phi/2$ in the gauge transformation, and cancel of the phase factor in the order parameter. The extra terms that arise from this gauge transformation either cancel or can be included in the chemical potential. The result is that we must perform the substitution

$$e\phi \to e\phi - \frac{\partial_t \Phi}{2}, \tag{3.19}$$

and that the magnetic vector potential acquires the physical interpretation of the supercurrent in the system. Making the gap real at all places in this way is not possible if one wants to look at systems with more than one superconductor, such as a Josephson junction. Since we in this thesis will only consider a single superconductor, we assume in the following that we have fixed the gauge such that the order parameter is real.

3.2.2 Physical interpretation of the chosen gauge

In this chapter, we will consider the gauge transformation from another angle, by choosing the London gauge, which completely fixes the magnetic vector potential.

It can be shown that in the second quantized formalism, the electrical current for a particle of spin σ can be written as

$$\boldsymbol{j}_\sigma = -\frac{\mathrm{i}e}{m}\left\langle \psi^\dagger_\sigma \tilde{\boldsymbol{\nabla}} \psi_\sigma \right\rangle. \tag{3.20}$$

We will now follow an argument by London [60], which is discussed also in the textbook by Tinkham [33]. In a superconductor in absence of external fields, the expectation value of the canonical momentum $-\mathrm{i}\boldsymbol{\nabla}$ is expected to be zero[4], meaning that we expect to find

$$\boldsymbol{j}_\sigma = -\frac{e^2}{m}\boldsymbol{A}\left\langle \psi^\dagger_\sigma \psi_\sigma \right\rangle = -\frac{e^2 n_\sigma}{m}\boldsymbol{A}, \tag{3.21}$$

where n_σ is the expectation value of the number operator with spin σ. This equation is sometimes called the London equation, since it can alternatively be obtained by

[4]This is the result of an unpublished theorem by Felix Bloch, which can be found in [60].

combining the two London equations [33]. This means that the current produces a screening effect, as we will justify in Section 4.5.1. Since we expect that the current inside a bulk superconductor is zero, we expect that also $\boldsymbol{A}$ must vanish. Additionally, we have that conservation of charge means that the current, and thus also $\boldsymbol{A}$ must be divergenceless in equilibrium. Finally, it can be shown that if one also demands that no current flows across the boundaries, the gauge uniquely defines the magnetic vector potential. This choice of gauge is called the London gauge in the literature, and is defined by [33]

$$\boldsymbol{\nabla} \cdot \boldsymbol{A} = 0 \qquad \boldsymbol{A} \to 0 \text{ in bulk of superconductor} \qquad \boldsymbol{A} \cdot \boldsymbol{e_n} = 0, \tag{3.22a}$$

where $\boldsymbol{e}_n$ is the normal vector at the surface of the superconductor. In the London gauge, $\boldsymbol{A}$ gets a physical interpretation as being proportional to the supercurrent of the system, because of Eq. (3.21). This is the same result that is obtained by fixing the gauge as we did in Section 3.2.1 [61, 25].

3.3 Green functions and their equations of motion

In many-body quantum field theory, Green functions are defined as correlators between field operators at, in general, different space-time coordinates[5]. Green functions provide a powerful tool in condensed matter field theory, as they allow for a perturbative calculation of physical quantities such as susceptibilities and currents [27]. Moreover, the Green function formalism will be convenient when we later make approximations. In this thesis, we will only consider Green functions involving 2 field operators, so-called 2-point correlators. The Green function for an electron can be thought of as the probability amplitude for an electron to propagate from a given space-time position to another, and these Green functions are thus often referred to as propagators [62]. In this text, Green functions are also used more generally for entities such as electron holes or quasiparticles.

In this section, we will introduce the Keldysh formalism [63], before calculating the equations of motion for the Green function. Because there is some ambiguity about some signs in these equations of motion, with differing results e.g. in [64, 25,

[5]In mathematics, the Green function $G(x)$ of a linear differential operator $\mathcal{L}$ is defined as the function that produces the delta function when acted upon with the operator, $\mathcal{L}G(x) = \delta(x)$. If one views the delta function as the source term, the Green function can be interpreted as the response of an impulse source [27]. Despite the definitions we give in this section bearing little resemblance to the definition from mathematics, it will later become apparent that the many-body Green function is the impulse response of the Schrödinger equation, causing G to be the Green function also in the mathematical sense.

14], the derivation will be done in more detail in this section than in other sections of this thesis.

3.3.1 The Keldysh formalism

Using the Keldysh formalism, which is introduced e.g. in [63, 25, 27], and introducing the shorthand notation $(1,2) \equiv (\boldsymbol{r}_1, t_1; \boldsymbol{r}_2, t_2)$, we define the retarded, advanced, and the Keldysh Green functions as 2×2 matrices in spin space,

$$\underline{G}^R_{\sigma\sigma'}(1,2) = -\mathrm{i}\Theta(t_1 - t_2)\big\langle\big\{\psi_\sigma(1), \psi^\dagger_{\sigma'}(2)\big\}\big\rangle \tag{3.23a}$$

$$\underline{G}^A_{\sigma\sigma'}(1,2) = \mathrm{i}\Theta(t_2 - t_1)\big\langle\big\{\psi_\sigma(1), \psi^\dagger_{\sigma'}(2)\big\}\big\rangle \tag{3.23b}$$

$$\underline{G}^K_{\sigma\sigma'}(1,2) = -\mathrm{i}\big\langle\big[\psi_\sigma(1), \psi^\dagger_{\sigma'}(2)\big]\big\rangle, \tag{3.23c}$$

where Θ is the Heaviside step function, and $\langle A \rangle$ denotes the thermal expectation value of an arbitrary operator A,

$$\langle A \rangle = \mathrm{Tr}\{\rho A\}\,, \tag{3.24}$$

where ρ is the density matrix. These Green functions can be interpreted as the probability that a particle that was created at space-time coordinate 2 is found at space-time coordinate 1. The retarded Green function is nonzero only for times $t_1 > t_2$, which means that it describes propagation forward in time. The advanced Green function is nonzero only for times $t_2 > t_1$, thus describing propagation backward in time. The Keldysh Green function will contain contributions from both forward and backward propagation.

In a superconductor, electrons form Cooper pairs, meaning that there is a correlation between the positions of electrons [27, 65]. In other words, if the position of an electron is known at a certain time, we have some information about where another particle will be at later times. Motivated by this, we define the *anomalous* Green functions[6], which involve expressions of two annihilation operators, and are defined as [63]

$$\underline{F}^R_{\sigma\sigma'}(1,2) = -\mathrm{i}\Theta(t_1 - t_2)\left\langle\left\{\psi_\sigma(1), \psi_{\sigma'}(2)\right\}\right\rangle \tag{3.25a}$$

$$\underline{F}^A_{\sigma\sigma'}(1,2) = \mathrm{i}\Theta(t_2 - t_1)\left\langle\left\{\psi_\sigma(1), \psi_{\sigma'}(2)\right\}\right\rangle \tag{3.25b}$$

$$\underline{F}^K_{\sigma\sigma'}(1,2) = -\mathrm{i}\left\langle\left[\psi_\sigma(1), \psi_{\sigma'}(2)\right]\right\rangle. \tag{3.25c}$$

These functions can be interpreted as the probability of a particle being at space-time coordinate 1, given that we have found a particle at 2, thus describing

[6]We will refer to the Green functions in Eq. (3.23), as well as their generalizations, as the *normal* Green functions.

correlations in the system. Similar to the case for the normal Green functions, the retarded component of the anomalous Green function describes correlation forward in time, the advanced component describes correlations backward in time, and the Keldysh component contains contributions from both forward and backward propagation.

It is convenient to gather the normal and anomalous Green functions in 4×4 Green function matrices,

$$\hat{G}^R(1,2) = \begin{pmatrix} \underline{G}^R(1,2) & \underline{F}^R(1,2) \\ \underline{F}^R(1,2)^* & \underline{G}^R(1,2)^* \end{pmatrix} \tag{3.26a}$$

$$\hat{G}^A(1,2) = \begin{pmatrix} \underline{G}^A(1,2) & \underline{F}^A(1,2) \\ \underline{F}^A(1,2)^* & \underline{G}^A(1,2)^* \end{pmatrix} \tag{3.26b}$$

$$\hat{G}^K(1,2) = \begin{pmatrix} \underline{G}^K(1,2) & \underline{F}^K(1,2) \\ -\underline{F}^K(1,2)^* & -\underline{G}^K(1,2)^* \end{pmatrix}. \tag{3.26c}$$

From the form of the 4-vector field operators, it can then be seen that Eq. (3.26a) can be written in terms of 4-vectors as

$$\hat{G}^R(1,2) = -\mathrm{i}\hat{\tau}_3\Theta(t_1 - t_2)\big\langle\big\{\psi(1), \psi^\dagger(2)\big\}\big\rangle, \tag{3.27}$$

where the $\hat{\tau}_3$-matrix can be thought of as a way of including the negative sign arising when doing the complex conjugation of $\underline{F}^R$ and $\underline{G}^R$ in Eq. (3.26a). In Eq. (3.27), and the rest of this thesis, we have implicitly assumed matrix transposing where it is needed in order to make the matrix product between the Nambu-spin field operators have the right dimension. As an example, the anticommuator is Eq. (3.27) can be written in component form as

$$\big\{\psi(1), \psi^\dagger(2)\big\}_{ij} = [\psi(1)]_i[\psi^\dagger(2)]_j + [\psi^\dagger(2)]_i[\psi(1)]_j. \tag{3.28}$$

Similar relations to Eq. (3.27) hold also for the advanced and the Keldysh components [25],

$$\hat{G}^A(1,2) = \mathrm{i}\hat{\tau}_3\Theta(t_2 - t_1)\left\langle\big\{\psi(1), \psi^\dagger(2)\big\}\right\rangle \tag{3.29}$$

$$\hat{G}^K(1,2) = -\mathrm{i}\hat{\tau}_3\left\langle\big[\psi(1), \psi^\dagger(2)\big]\right\rangle. \tag{3.30}$$

Finally, we gather the three matrices in a 8×8 Green function matrix in Keldysh-Nambu-spin space,

$$\check{G}(1,2) = \begin{pmatrix} \hat{G}^R(1,2) & \hat{G}^K(1,2) \\ 0 & \hat{G}^A(1,2) \end{pmatrix}, \tag{3.31}$$

which will later enable us to write the equation of motion for the three Green functions compactly.

3.3.2 Green function equations of motion

We proceed by using the results for the equations of motion for the field operators in Eq. (3.5) and Eq. (3.6) to obtain equations of motion for the Green functions defined in Section 3.3.1. We start by calculating

$$\begin{aligned}
\mathrm{i}\partial_{t_1}\hat{G}^R(1,2) &= \mathrm{i}\partial_{t_1}\left(-\mathrm{i}\hat{\tau}_3\Theta(t_1-t_2)\left\langle\left\{\psi(1),\psi^\dagger(2)\right\}\right\rangle\right) \\
&= \hat{\tau}_3\delta(t_1-t_2)\left\langle\left\{\psi(1),\psi^\dagger(2)\right\}\right\rangle - \mathrm{i}\Theta(t_1-t_2)\left\langle\left\{\mathrm{i}\hat{\tau}_3\partial_{t_1}\psi(1),\psi^\dagger(2)\right\}\right\rangle \\
&= \hat{\tau}_3\delta(t_1-t_2)\delta(\boldsymbol{r}_1-\boldsymbol{r}_2)\hat{1} - \mathrm{i}\Theta(t_1-t_2)\left\langle\left\{\hat{H}_1(1)\psi(1),\psi^\dagger(2)\right\}\right\rangle \\
&= \hat{\tau}_3\delta(1-2)\hat{1} - \mathrm{i}\Theta(t_1-t_2)\hat{H}_1(1)\left\langle\left\{\psi(1),\psi^\dagger(2)\right\}\right\rangle \\
&= \hat{\tau}_3\delta(1-2)\hat{1} - \hat{H}_1(1)\hat{\tau}_3\left\langle\left\{\mathrm{i}\hat{\tau}_3\Theta(t_1-t_2)\psi(1),\psi^\dagger(2)\right\}\right\rangle \\
&= \hat{\tau}_3\delta(1-2)\hat{1} + \hat{H}_1(1)\hat{\tau}_3\hat{G}^R(1,2),
\end{aligned} \tag{3.32}$$

where we in the first line used that the derivative of a Heaviside step function is a delta function, and introduced

$$\delta(1-2) \equiv \delta(t_1-t_2)\delta(\boldsymbol{r}_1-\boldsymbol{r}_2). \tag{3.33}$$

In the second line of Eq. (3.32), we have used that

$$\delta(t_1-t_2)\left\langle\left\{\psi(\boldsymbol{r}_1,t_1),\psi^\dagger(\boldsymbol{r}_2,t_2)\right\}\right\rangle = \delta(t_1-t_2)\left\langle\left\{\psi(\boldsymbol{r}_1,t_1),\psi^\dagger(\boldsymbol{r}_2,t_1)\right\}\right\rangle, \tag{3.34}$$

and the anticommutation relation for the 4-vectors. In the third line, we used that we could pull out $\hat{H}_1(1)$, since it works only on $\psi(1)$. Finally, in the fifth line of Eq. (3.32), we inserted a factor of $\hat{1} = \hat{\tau}_3^2$. By multiplying both sides of Eq. (3.32) by $\hat{\tau}_3$ from the left, we get the equation of motion for the retarded Green function,

$$\left(\mathrm{i}\hat{\tau}_3\hat{\partial}_{t_1} - \hat{H}(1)\right)\hat{G}^R(1,2) = \delta(1-2)\hat{1}, \tag{3.35}$$

where we have introduced a new Hamiltonian $\hat{H} = \hat{\tau}_3\hat{H}_1\hat{\tau}_3$ in Nambu-spin space. From the form of $\hat{H}_1$ in Eq. (3.9) we see that $\hat{H}$ is similar, but with a negative sign for the superconducting term $\hat{\Delta}$. Repeating the same steps for the advanced Green function yields the same result, while for the Keldysh component there will not be any delta function terms, due to there not being any step function in the definition of the Keldysh component [25]. In total, this can be written as[7]

$$\left(\mathrm{i}\hat{\tau}_3\partial_{t_1} - \hat{H}(1)\right)\check{G}(1,2) = \delta(1-2)\check{1}. \tag{3.36}$$

[7]This equation justifies the naming of the Green functions, since this is exactly the defining equation for a Green function for a differential operator $(\mathrm{i}\hat{\tau}_3\partial_{t_1} - \hat{H}(1))$, which of course is just a Nambu-spin generalization of the Schrödinger equation.

It will later prove useful to have also derived a "left-handed" version of Eq. (3.36), i.e. an equation where the Hamiltonian works to the left on the Green function. To this end, we first rename the coordinate labels $1 \leftrightarrow 2$, take the Hermitian adjoint of Eq. (3.35), and then multiply with $\hat{\tau}_3$ from both the right and the left. This yields

$$\hat{\tau}_3 \hat{G}^R(2,1)^\dagger \left(\mathrm{i}\hat{\tau}_3 \partial_{t_2} - \hat{H}(2) \right)^\dagger \hat{\tau}_3 = \hat{\tau}_3 \delta(2-1) \hat{\tau}_3 = \delta(1-2)\hat{1}, \tag{3.37}$$

where now the time derivative works on the Green function to the left. The adjoint of the Green function can be rewritten as

$$\begin{aligned} \hat{G}^R(2,1)^\dagger &= \left(-\mathrm{i}\hat{\tau}_3 \Theta(t_2 - t_1) \left\langle \left\{ \psi(2), \psi^\dagger(1) \right\} \right\rangle \right)^\dagger \\ &= \mathrm{i}\Theta(t_2 - t_1) \left\langle \left\{ \psi(1), \psi^\dagger(2) \right\} \right\rangle \hat{\tau}_3 \\ &= \mathrm{i}\big(1 - \Theta(t_1 - t_2)\big) \left\langle \left\{ \psi(1), \psi^\dagger(2) \right\} \right\rangle \hat{\tau}_3 \\ &= \mathrm{i} \left\langle \left\{ \psi(1), \psi^\dagger(2) \right\} \right\rangle \hat{\tau}_3 + \hat{\tau}_3 \hat{G}^R(1,2) \hat{\tau}_3, \end{aligned} \tag{3.38}$$

where we in the third line used a property of the Heaviside step function, $\Theta(x) = 1 - \Theta(-x)$. Consider now the first term in the last line of Eq. (3.38) inserted into the left-hand side of Eq. (3.37),

$$\begin{aligned} &\mathrm{i}\hat{\tau}_3 \left\langle \left\{ \psi(1), \psi^\dagger(2) \right\} \right\rangle \hat{\tau}_3 \big(\mathrm{i}\hat{\tau}_3 \partial_{t_2} - \hat{H}(2) \big)^\dagger \hat{\tau}_3 \\ &= \mathrm{i}\hat{\tau}_3 \left\langle \left\{ \psi(1), \psi^\dagger(2) \right\} \right\rangle \hat{\tau}_3 \big(-i\hat{\tau}_3 \partial_{t_2} - \hat{H}^\dagger(2) \big) \hat{\tau}_3 \\ &= \mathrm{i}\hat{\tau}_3 \left\langle \left\{ \psi(1), \psi^\dagger(2) \right\} \right\rangle \left(-\mathrm{i}\hat{\tau}_3 \partial_{t_2} - \hat{\tau}_3 \hat{H}^\dagger(2) \hat{\tau}_3 \right) \\ &= -\mathrm{i}\hat{\tau}_3 \left\langle \left\{ \psi(1), \psi^\dagger(2) \right\} \right\rangle \left(\mathrm{i}\hat{\tau}_3 \partial_{t_2} + \hat{H}_1(2) \right) \\ &= -\mathrm{i}\hat{\tau}_3 \left\langle \left\{ \psi(1), \psi^\dagger(2) \big(\mathrm{i}\hat{\tau}_3 \partial_{t_2} + \hat{H}_1(2) \big) \right\} \right\rangle \\ &= -\mathrm{i}\hat{\tau}_3 \left\langle \left\{ \psi(1), 0 \right\} \right\rangle = 0, \end{aligned} \tag{3.39}$$

where we in the last line have used the equation of motion for $\psi^\dagger$ from Eq. (3.8). Inserting the second term of Eq. (3.38) into the left-hand side of Eq. (3.37) we find

$$\hat{\tau}_3 \hat{\tau}_3 \check{G}(1,2) \hat{\tau}_3 \left(\mathrm{i}\hat{\tau}_3 \partial_{t_2} - \hat{H}(2) \right)^\dagger \hat{\tau}_3 = \check{G}(1,2) \left(\mathrm{i}\hat{\tau}_3 \partial_{t_2} - \hat{\tau}_3 \hat{H}(2) \hat{\tau}_3 \right)^\dagger. \tag{3.40}$$

Eq. (3.37) can then be written as

$$\hat{G}^R(1,2) \left(\mathrm{i}\hat{\tau}_3 \partial_{t_2} - \hat{\tau}_3 \hat{H}(2) \hat{\tau}_3 \right)^\dagger = \delta(1-2)\hat{1}. \tag{3.41}$$

Performing the same operators on the equations of motion for the advanced component of the Green function, one obtains similar equations. This allows us to write the total left-handed equation of motion for the Green function,

$$\check{G}(1,2) \left(\mathrm{i}\hat{\tau}_3 \partial_{t_2} - \hat{\tau}_3 \hat{H}(2) \hat{\tau}_3 \right)^\dagger = \delta(1-2)\check{1}. \tag{3.42}$$

The reasoning for also calculating the left-handed equation is that we can now subtract it from the right-handed version, canceling the delta function. This will make subsequent calculations easier. The final equation of motion for the 8×8 Green function becomes[8]

$$\left(\mathrm{i}\hat{\tau}_3\partial_{t_1} - \hat{H}(1)\right)\check{G}(1,2) - \check{G}(1,2)\left(\mathrm{i}\hat{\tau}_3\partial_{t_2} - \hat{\tau}_3\hat{H}(2)\hat{\tau}_3\right)^\dagger = 0. \tag{3.43}$$

3.4 Impurity averaging

One of the reasons why the equation of motion for the Green functions in Eq. (3.43) is difficult to solve, is that it contains the terms $\hat{S}$, $\hat{V}_{\mathrm{so}}$ and V_{sc}, which are scattering terms that depend on the specific configuration of the material in consideration. This is not only impractical, in that we have to specify the exact location of all magnetic and non-magnetic impurities of the material, but it also means that the results will only be valid for a specific configuration. Instead, we will in this section average the equations of motion from the last section over all possible impurity configurations, approximating the scattering potentials as self-energies. The result is an approximation for any configuration of impurities that are randomly distributed in space.

3.4.1 Impurity self-energy

We start by separating the Hamiltonian of the system in an impurity potential part and the remaining part H_0[9],

$$\hat{H}(1) = \hat{H}_0(1) + \hat{V}_{\mathrm{imp}}(1), \tag{3.44}$$

where we have defined the total impurity potential,

$$\hat{V}_{\mathrm{imp}}(1) = V_{\mathrm{sc}}(1)\hat{1} + \hat{S}(1) + \hat{V}_{\mathrm{so}}(1). \tag{3.45}$$

The right-handed equation of motion for the Green function from Eq. (3.36) becomes

$$\left[\mathrm{i}\hat{\tau}_3\partial_{t_1} - \hat{H}_0(1) - \hat{V}_{\mathrm{imp}}(1)\right]\check{G}(1,2) = \delta(1-2)\check{1}. \tag{3.46}$$

We define $\check{G}_0$ as the Green function satisfying Eq. (3.46) without the impurity terms. In Appendix E, it is shown that Eq. (3.46) is equivalent to the Dyson equation, which can be written as

$$\check{G}(1,2) = \check{G}_0(1,2) + [\check{G}_0 \bullet \hat{U}_{\mathrm{imp}} \bullet \check{G}](1,2), \tag{3.47}$$

[8]This expression, which is consistent with the result in the appendix in [14], corrects some minor inaccuracies in [25, 26].

[9]In this section, $\hat{H}_0$ is defined to contain all other terms than the impurity scattering terms.

where we have introduced the bullet product,

$$[A \bullet B](1,2) \equiv \int dx_3 A(1,3)B(3,2), \tag{3.48}$$

as well as the quantity $\hat{U}_{\text{imp}}(1,2) = \hat{V}_{\text{imp}}(1)\delta(1-2)$. This equation is an implicit equation for $\check{G}$, and iterating it to second order, we obtain

$$\begin{aligned}\check{G}(1,2) = \check{G}_0(1,2) &+ [\check{G}_0 \bullet \hat{U}_{\text{imp}} \bullet \check{G}_0](1,2) \\ &+ [\check{G}_0 \bullet \hat{U}_{\text{imp}} \bullet \check{G}_0 \bullet \hat{U}_{\text{imp}} \bullet \check{G}](1,2).\end{aligned} \tag{3.49}$$

For shorthand notation, we denote the average over both all spin impurity directions and all impurity positions $\langle ... \rangle_{av}$. Performing impurity averaging on Eq. (3.49) and defining the averaged Green function as $\check{G}_{av}(1,2) \equiv \langle \check{G}(1,2) \rangle_{av}$, we obtain

$$\begin{aligned}\check{G}_{av}(1,2) = \check{G}_0(1,2) &+ [\check{G}_0 \bullet \langle \hat{U}_{\text{imp}} \rangle_{av} \bullet \check{G}_0](1,2) \\ &+ [\check{G}_0 \bullet \langle \hat{U}_{\text{imp}} \bullet \check{G}_0 \bullet U_{\text{imp}} \bullet \check{G} \rangle_{av}](1,2),\end{aligned} \tag{3.50}$$

where we have used that the impurity averaging operator does not work on $\check{G}_0$. In the second term, the averaging works only on a single potential, and thus the result will be a constant in the case of many randomly distributed impurities. From Appendix E we know that this is equivalent to including a constant in the equation of motion for the Green function. This constant can be absorbed into the chemical potential, and the term is ignored in the following. The third term includes averaging over several quantities, and cannot be ignored in the same way. This term can, however, by expanding $\check{G}$ to order $\mathcal{O}(U_{\text{imp}}^0)$ in the impurity potential, be approximated as

$$\begin{aligned}\left\langle [\hat{U}_{\text{imp}} \bullet \check{G}_0 \bullet \hat{U}_{\text{imp}} \bullet \check{G}](1,2) \right\rangle_{av} &= \int dx_3 \left\langle \hat{V}_{\text{imp}}(1)\check{G}_0(1,3)\hat{V}_{\text{imp}}(3)\check{G}(3,2) \right\rangle_{av} \\ &\approx \int dx_3 \left\langle \hat{V}_{\text{imp}}(1)\check{G}_0(1,3)\hat{V}_{\text{imp}}(3) \right\rangle_{av} \check{G}_{av}(3,2) \\ &= \left[\left\langle \hat{U}_{\text{imp}} \bullet \check{G}_0 \bullet \hat{U}_{\text{imp}} \right\rangle_{av} \bullet \check{G}_{av} \right](1,2)\end{aligned} \tag{3.51}$$

That is, we assume that the full Green function is approximately equal to its averaged value. This gives the expression

$$\check{G}_{av}(1,2) = \check{G}_0(1,2) + [\check{G}_0 \bullet \tilde{\Sigma}_{\text{imp}} \bullet \check{G}_{av}](4,2), \tag{3.52}$$

for the impurity averaged Green function, where we have defined

$$\tilde{\Sigma}_{\text{imp}}(1,2) = \langle \hat{U}_{\text{imp}} \bullet \check{G}_0 \bullet \hat{U}_{\text{imp}} \rangle_{av}. \tag{3.53}$$

Additionally, we let $\check{G}_0 \to \check{G}_{av}$ in this definition [66, 14], so that the final expression is obtained by replacing $\tilde{\Sigma}_{\text{imp}} \to \check{\Sigma}_{\text{imp}}$, where

$$\check{\Sigma}_{\text{imp}}(1,2) = \langle \hat{U}_{\text{imp}} \bullet \check{G}_{av} \bullet \hat{U}_{\text{imp}} \rangle_{av} = \langle \hat{V}_{\text{imp}}(1) \check{G}_{av}(1,2) \hat{V}_{\text{imp}}(2) \rangle_{av}. \tag{3.54}$$

This is the *self-consistent Born approximation* [66, 14, 67]. We know from Appendix E that Eq. (3.52) is equivalent to

$$\left[\mathrm{i}\hat{\tau}_3 \partial_{t_1} - \hat{H}_0(1)\right] \check{G}_{av}(1,2) - [\check{\Sigma}_{\text{imp}} \bullet \check{G}_{av}](1,2) = \delta(1-2)\check{1}, \tag{3.55}$$

effectively replacing the impurity potential, which was a function of coordinate 1, by a self-energy, which is a function of coordinates $(1,2)$. Repeating this for the left-handed equation of motion, and then subtracting it from the right-handed equation, causes the equation of motion in Eq. (3.43) to become

$$\left(\mathrm{i}\hat{\tau}_3 \partial_{t_1} - \hat{H}_0(1)\right) \check{G}_{av}(1,2) - \check{G}_{av}(1,2) \left(\mathrm{i}\hat{\tau}_3 \partial_{t_2} - \hat{\tau}_3 \hat{H}_0(2) \hat{\tau}_3\right)^\dagger - \left[\check{\Sigma}_{\text{imp}} \overset{\bullet}{,} \check{G}_{av}\right](1,2) = 0, \tag{3.56}$$

where we have introduced the bullet commutator,

$$[A \overset{\bullet}{,} B](1,2) \equiv [A \bullet B](1,2) - [B \bullet A](1,2) \tag{3.57}$$

and where

$$\hat{H}_0(1) = \hat{\xi}(1) - \hat{\Delta}(1) - \hat{M}(1).(1) \tag{3.58}$$

To simplify notation, we will from this point on be referring to the impurity averaged Green function without the subscript, remembering that we are dealing with a quantity that has been averaged over all impurity configurations.

3.5 The Wigner representation

To derive approximate equations, it will be convenient to introduce new coordinates. The new coordinates will be used to transform Eq. (3.56) into a form more suitable for approximations. Much of this section is based on the master's thesis of Morten [25]

3.5.1 Relative and center-of-mass coordinates

For a system dependent on the coordinates $(\boldsymbol{r}_1, t_1)$ and $(\boldsymbol{r}_2, t_2)$, we introduce the center-of-mass coordinates as

$$\boldsymbol{R} \equiv \frac{\boldsymbol{r}_1 + \boldsymbol{r}_2}{2} \qquad\qquad T \equiv \frac{t_1 + t_2}{2}, \tag{3.59}$$

and the relative coordinates as

$$\boldsymbol{r} \equiv \boldsymbol{r}_1 - \boldsymbol{r}_2 \qquad\qquad t \equiv t_1 - t_2. \tag{3.60}$$

Using the chain rule, the derivatives with respect to the old coordinates can be written in terms of the relative and center-of-mass coordinates,

$$\begin{aligned} \partial_{t_1} &= \partial_{t_1} T(t_1, t_2)\partial_T + \partial_{t_1} t(t_1, t_2)\partial_t = \frac{1}{2}\partial_T + \partial_t \\ \partial_{t_2} &= \partial_{t_2} T(t_1, t_2)\partial_T + \partial_{t_2} t(t_1, t_2)\partial_t = \frac{1}{2}\partial_T - \partial_t, \end{aligned} \tag{3.61}$$

and

$$\begin{aligned} \boldsymbol{\nabla}_1 &= \boldsymbol{\nabla}_1 \boldsymbol{R}(\boldsymbol{r}_1, \boldsymbol{r}_2)\boldsymbol{\nabla}_{\boldsymbol{R}} + \boldsymbol{\nabla}_1 \boldsymbol{r}(\boldsymbol{r}_1, \boldsymbol{r}_2)\boldsymbol{\nabla}_{\boldsymbol{r}} = \frac{1}{2}\boldsymbol{\nabla}_{\boldsymbol{R}} + \boldsymbol{\nabla}_{\boldsymbol{r}} \\ \boldsymbol{\nabla}_2 &= \boldsymbol{\nabla}_2 \boldsymbol{R}(\boldsymbol{r}_1, \boldsymbol{r}_2)\boldsymbol{\nabla}_{\boldsymbol{R}} + \boldsymbol{\nabla}_2 \boldsymbol{r}(\boldsymbol{r}_1, \boldsymbol{r}_2)\boldsymbol{\nabla}_{\boldsymbol{r}} = \frac{1}{2}\boldsymbol{\nabla}_{\boldsymbol{R}} - \boldsymbol{\nabla}_{\boldsymbol{r}}. \end{aligned} \tag{3.62}$$

It can be checked that when transforming from coordinates $(\boldsymbol{r}_1, \boldsymbol{r}_2)$ into $(\boldsymbol{r}, \boldsymbol{R})$, the absolute value of the Jacobi determinant is unity, which means that one can transform an integral into the Wigner representation without any prefactors appearing. We note also that we can write

$$\boldsymbol{\nabla}_1^2 - \boldsymbol{\nabla}_2^2 = \big(\frac{1}{2}\boldsymbol{\nabla}_{\boldsymbol{R}} + \boldsymbol{\nabla}_{\boldsymbol{r}}\big)^2 - \big(\frac{1}{2}\boldsymbol{\nabla}_{\boldsymbol{R}} - \boldsymbol{\nabla}_{\boldsymbol{r}}\big)^2 = \boldsymbol{\nabla}_{\boldsymbol{R}}\cdot\boldsymbol{\nabla}_{\boldsymbol{r}} + \boldsymbol{\nabla}_{\boldsymbol{R}}\cdot\boldsymbol{\nabla}_{\boldsymbol{r}} = 2\boldsymbol{\nabla}_{\boldsymbol{R}}\cdot\boldsymbol{\nabla}_{\boldsymbol{r}}, \tag{3.63}$$

an identity that will prove useful later when transforming the equations of motion for the Green functions into the Wigner representation.

3.5.2 Fourier transformation and Moyal products

In the following, it will be convenient to use 4-vector notation for the space-time and energy-momentum coordinates. These are formulated in the standard way, as

$$x = (t, \boldsymbol{r}) \tag{3.64}$$

$$p = (E, \boldsymbol{p}). \tag{3.65}$$

These are contravariant vectors [68], and we will not introduce the corresponding covariant vectors, but simply note that the inner product between two 4-vectors such as p and x must be interpreted as

$$p \cdot x = -Et + \boldsymbol{p}\cdot\boldsymbol{r} \tag{3.66}$$

where the product sign must be understood to be a 4-vector dot product or a normal 3-vector dot product depending on the quantities involved. The derivatives with respect to 4-vector will be denoted

$$\nabla_x = (\partial_t, \boldsymbol{\nabla r}) \qquad\qquad \nabla_p = (\partial_E, \boldsymbol{\nabla_p}), \tag{3.67}$$

and their inner products are

$$\nabla_p \cdot \nabla_x = -\partial_E \partial_t + \boldsymbol{\nabla_p} \cdot \boldsymbol{\nabla r}. \tag{3.68}$$

Using the 4-vector notation, we can write a function f depending on two space-time coordinates as

$$\begin{aligned} f(\boldsymbol{r}_1, t_1; \boldsymbol{r}_2, t_2) &= f\left(\frac{1}{2}\boldsymbol{r} + \boldsymbol{R}; \frac{1}{2}t + T, -\frac{1}{2}\boldsymbol{r} + \boldsymbol{R}, -\frac{1}{2}t + T\right) \\ &= f\left(X + \frac{x}{2}, X - \frac{x}{2}\right), \end{aligned} \tag{3.69}$$

where $X = (T, \boldsymbol{R})$ is the center-of-mass 4-vecor coordinate. This function is transformed into the Wigner representation by performing a Fourier transform in the relative coordinates,

$$f(X, p) \equiv \int dx \mathrm{e}^{-\mathrm{i}x\cdot p} f\left(X + \frac{x}{2}, X - \frac{x}{2}\right). \tag{3.70}$$

Note that we use the same symbol for functions in real-space and in the Wigner representation, and they are distinguished only by their arguments. This resulting function $f(X, p)$ is a function of the center-of-mass space-time coordinate and the relative energy-momentum. For this reason, the Wigner representation is also called the mixed representation [69, 70].

When we later transform Eq. (3.56) into the Wigner representation, we have to calculate Fourier transformations of bullet products. To this end, we introduce the *Moyal product* as [69]

$$[A \odot B](X, p) \equiv \int dx \mathrm{e}^{-\mathrm{i}x\cdot p} \left[A \bullet B\right](X + \frac{x}{2}, X - \frac{x}{2}) \tag{3.71}$$

$$= \mathrm{e}^{\frac{\mathrm{i}}{2}\left(\nabla_X^A \cdot \nabla_p^B - \nabla_p^A \nabla_X^B\right)} \left[A(X, p) B(X, p)\right], \tag{3.72}$$

where the identity in the last line is shown in the appendix of [25]. Here, we introduced the notation ∇_u^W for a derivative with respect to the four-vector u, working only on a function $W(u)$. As usual, the exponential of the differential operators must be interpreted as a Taylor series in the operators.

It will be relevant to consider the special case where $A(1, 2) = A(1)\delta(1, 2)$, i.e. A is only a function of one coordinate. In this case, the bullet product reduces to

a simple product, and the Fourier transformed quantity becomes a function of the center-of-mass coordinate only. The Moyal product becomes

$$[A \odot B](X,p) = \int dx \mathrm{e}^{-\mathrm{i}x\cdot p} A(x) B(X+\frac{x}{2}, X-\frac{x}{2}) = \mathrm{e}^{\frac{\mathrm{i}}{2}\left(\nabla_X^A \cdot \nabla_p^B\right)} \left[A(X)B(X,p)\right]. \tag{3.73}$$

Similarly, for $B(1,2) = \delta(1-2)B(2)$, we get

$$[A \odot B](X,p) = \mathrm{e}^{-\frac{\mathrm{i}}{2}\left(\nabla_p^A \nabla_X^B\right)} \left[A(X)B(X,p)\right]. \tag{3.74}$$

In the following it will be useful to also introduce the Moyal commutators and Moyal anticommutators,

$$\left[A \stackrel{\odot}{,} B\right] \equiv A \odot B - B \odot A \qquad \left\{A \stackrel{\odot}{,} B\right\} \equiv A \odot B + B \odot A. \tag{3.75}$$

It should be noted that while this allows for compact notation, many rules for (anti)commutators do not generalize to the Moyal (anti)commutators. This includes the possibility of pulling out scalar functions that depend on (X,p). We will still use this notation because it allows us to write the equation of motion for the Green function in a suggestive way, suited for approximations.

3.5.3 Transforming the equations of motion

We proceed with the derivation of the Usadel equation by transforming Eq. (3.56) into the Wigner representation. Writing out Eq. (3.56), we get

$$\mathrm{i}\hat{\tau}_3\partial_{t_1}\check{G}(1,2) + \mathrm{i}\partial_{t_2}\check{G}(1,2)\hat{\tau}_3 - \hat{H}_0(1)\check{G}(1,2) + \check{G}(1,2)\hat{\tau}_3\hat{H}_0^\dagger(2)\hat{\tau}_3 - \left[\check{\Sigma}_{\mathrm{imp}} \stackrel{\bullet}{,} \check{G}\right](1,2) = 0. \tag{3.76}$$

We consider the two terms containing time derivatives and transform them into the Wigner representation using the definition in Eq. (3.70) and the identities in Eq. (3.61). This yields

$$\begin{aligned}
&\int dx \mathrm{e}^{-\mathrm{i}x\cdot p}\left[\mathrm{i}\hat{\tau}_3\partial_{t_1}\check{G}(1,2) + \mathrm{i}\partial_{t_2}\check{G}(1,2)\hat{\tau}_3\right] \\
=&\int dx \mathrm{e}^{-\mathrm{i}x\cdot p}\left[\mathrm{i}\hat{\tau}_3\left(\frac{1}{2}\partial_T + \partial_t\right)\check{G}(1,2) + \mathrm{i}\left(\frac{1}{2}\partial_T - \partial_t\right)\check{G}(1,2)\hat{\tau}_3\right] \\
=&\frac{\mathrm{i}}{2}\partial_T \int dx \mathrm{e}^{-\mathrm{i}x\cdot p}\left[\hat{\tau}_3\check{G}(1,2) + \check{G}(1,2)\hat{\tau}_3\right] + \mathrm{i}\int dx \mathrm{e}^{-\mathrm{i}x\cdot p}\partial_t\left[\hat{\tau}_3\check{G}(1,2) - \check{G}(1,2)\hat{\tau}_3\right] \\
=&\frac{\mathrm{i}}{2}\partial_T\left[\hat{\tau}_3\check{G}(X,p) + \check{G}(X,p)\hat{\tau}_3\right] - \mathrm{i}\int dx \partial_t\left(\mathrm{e}^{-\mathrm{i}x\cdot p}\right)\left[\hat{\tau}_3\check{G}(1,2) - \check{G}(1,2)\hat{\tau}_3\right] \\
=&\frac{\mathrm{i}}{2}\left\{\hat{\tau}_3, \partial_T\check{G}(X,p)\right\} + E\left[\hat{\tau}_3, \check{G}(X,p)\right].
\end{aligned} \tag{3.77}$$

In the third equation, we have pulled out the center-of-mass time derivatives, since the integral and the exponential factor do not depend on this variable. In the fourth equation, we have performed a partial integration, and discarded the surface term. The surface term vanishes since the Green function approaches zero as the relative coordinate approaches infinity, something that is ensured by adding the infinitesimal imaginary part to the energy. The inclusion of this infinitesimal quantity is discussed in detail in Appendix A. From a physical point of view, this corresponds to the fact that the correlation between two space-time points will be zero as the temporal separation approaches infinity, which is physically reasonable. It will be useful to calculate the Moyal products

$$\begin{aligned}[E\hat{\tau}_3 \odot \check{G}](X,p) &= E\hat{\tau}_3\check{G}(X,p) + \frac{\mathrm{i}}{2}\partial_E(E\hat{\tau}_3)\partial_T\check{G}(X,p) \\ &= E\hat{\tau}_3\check{G}(X,p) + \frac{\mathrm{i}}{2}\hat{\tau}_3\partial_T\check{G}(X,p)\end{aligned} \tag{3.78}$$

and

$$\begin{aligned}[\check{G} \odot E\hat{\tau}_3](X,p) &= \check{G}(X,p)E\hat{\tau}_3 - \frac{\mathrm{i}}{2}\partial_T\check{G}(X,p)\partial_E(E\hat{\tau}_3) \\ &= E\hat{\tau}_3\check{G}(X,p) - \frac{\mathrm{i}}{2}\partial_T\check{G}(X,p)\hat{\tau}_3.\end{aligned} \tag{3.79}$$

Here, we have used that all derivatives except the energy derivative will vanish when operating on $E\hat{\tau}_3$. By combining Eq. (3.78) and Eq. (3.79), we write

$$\begin{aligned}\big[E\hat{\tau}_3 \overset{\circ}{,} \check{G}\big](X,p) &= [E\hat{\tau}_3 \odot \check{G}](X,p) - [\check{G} \odot E\hat{\tau}_3](X,p) \\ &= E\hat{\tau}_3\check{G}(X,p) + \frac{\mathrm{i}}{2}\hat{\tau}_3\partial_T\check{G}(X,p) - E\hat{\tau}_3\check{G}(X,p) + \frac{\mathrm{i}}{2}\partial_T\hat{\tau}_3\check{G}(X,p) \\ &= \big[E\hat{\tau}_3, \check{G}(X,p)\big] + \frac{\mathrm{i}}{2}\big\{\partial_T\check{G}(X,p), \hat{\tau}_3\big\},\end{aligned} \tag{3.80}$$

which is exactly the term found in Eq. (3.77). Thus, we can write this result as a single Moyal commutator.

We now proceed to the rest of the terms in Eq. (3.76), which can be written as

$$\begin{aligned}&-\hat{H}_0(1)\check{G}(1,2) + \check{G}(1,2)\hat{\tau}_3\hat{H}_0^\dagger(2)\hat{\tau}_3 - \big[\check{\Sigma}_{\mathrm{imp}} \overset{\bullet}{,} \check{G}\big](1,2) \\ =&-\hat{\xi}(1)\check{G}(1,2) + \check{G}(1,2)\hat{\xi}(2)^* - \big[\check{\Sigma}_{\mathrm{tot}} \overset{\bullet}{,} \check{G}\big](1,2)\end{aligned} \tag{3.81}$$

where we have introduced the total self-energy term[10]

$$\check{\Sigma}_{\mathrm{tot}}(1,2) = -\hat{M}(1)\delta(1-2) - \hat{\Delta}(1)\delta(1-2) + \check{\Sigma}_{\mathrm{imp}}(1,2). \tag{3.82}$$

[10]The inclusion of the delta function is a notational trick that makes it possible to write all terms in the bullet commutator in the last line of Eq. (3.81).

The reason for this separation is that the kinetic term, which contains derivatives, demands a special treatment.

We start with the kinetic term,

$$\begin{aligned}
&\check{G}(1,2)\hat{\xi}(2)^* - \hat{\xi}(1)\check{G}(1,2) \\
&= \check{G}(1,2)\Big[-\frac{(\hat{\tilde{\boldsymbol{\nabla}}}_2^*)^2}{2m} - \mu(2) + e\phi(2)\Big] - \Big[-\frac{\hat{\tilde{\boldsymbol{\nabla}}}_1^2}{2m} - \mu(1) + e\phi(1)\Big]\check{G}(1,2) \\
&= [\mu(1) - \mu(2) + e\phi(1) - e\phi(2)]\check{G}(1,2) + \frac{\hat{\tilde{\boldsymbol{\nabla}}}_1^2}{2m}\check{G}(1,2) - \check{G}(1,2)\frac{(\hat{\tilde{\boldsymbol{\nabla}}}_2^*)^2}{2m}
\end{aligned} \tag{3.83}$$

The chemical potential term and the electrostatic potential terms does not contain derivatives, and can be absorbed into the total self-energy. We consider only the covariant derivative terms from Eq. (3.83) in the following. First, we note that because the derivatives work to the left in the left-handed Green function equation of motion, we have that

$$\begin{aligned}
\check{G}(1,2)\left(\boldsymbol{\nabla}_2 + \mathrm{i}e\hat{\tau}_3\boldsymbol{A}(2)\right)^2 =& \boldsymbol{\nabla}_2^2\check{G}(1,2) + \mathrm{i}e\boldsymbol{\nabla}_2\cdot\big(\check{G}(1,2)\hat{\tau}_3\boldsymbol{A}(2)\big) \\
&+ \mathrm{i}e\boldsymbol{\nabla}_2\check{G}(1,2)\cdot\boldsymbol{A}(2)\hat{\tau}_3 - e^2\check{G}(1,2)\boldsymbol{A}(2)^2.
\end{aligned} \tag{3.84}$$

The last line in Eq. (3.83) becomes

$$\begin{aligned}
&\frac{1}{2m}\left(\boldsymbol{\nabla}_1 - \mathrm{i}e\hat{\tau}_3\boldsymbol{A}(1)\right)^2\check{G}(1,2) - \frac{1}{2m}\check{G}(1,2)\left(\boldsymbol{\nabla}_2 + \mathrm{i}e\hat{\tau}_3\boldsymbol{A}(2)\right)^2 \\
=&\frac{1}{2m}\left(\boldsymbol{\nabla}_1^2 - \boldsymbol{\nabla}_2^2\right)\check{G}(1,2) - \frac{\mathrm{i}e}{2m}\left[\boldsymbol{\nabla}_1\cdot\big(\hat{\tau}_3\boldsymbol{A}(1)\check{G}(1,2)\big) + \boldsymbol{\nabla}_2\cdot\big(\check{G}(1,2)\hat{\tau}_3\boldsymbol{A}(2)\big)\right] \\
&-\frac{\mathrm{i}e}{2m}\left[\hat{\tau}_3\boldsymbol{A}(1)\cdot\boldsymbol{\nabla}_1\check{G}(1,2) + \boldsymbol{\nabla}_2\check{G}(1,2)\cdot\boldsymbol{A}(2)\hat{\tau}_3\right] - \frac{e^2}{2m}\left[\boldsymbol{A}(1)^2 - \boldsymbol{A}(2)^2\right]\check{G}(1,2).
\end{aligned} \tag{3.85}$$

Here, the last term can be absorbed into the total self-energy as well. Fourier transforming with respect to the relative coordinate, and using the identities for the Moyal products in Eq. (3.73) and Eq. (3.74), as well as the identities for the derivative in Eq. (3.63), it can be shown that the three remaining terms in Eq. (3.85) equals [25]

$$\begin{aligned}
&\frac{\mathrm{i}}{m}\boldsymbol{p}\cdot\boldsymbol{\nabla}_{\boldsymbol{R}}\check{G}(X,p) - \mathrm{i}\frac{\boldsymbol{p}}{m}\big[\mathrm{i}e\boldsymbol{A}\hat{\tau}_3 \diamond \check{G}\big](X,p) \\
&\qquad - \frac{1}{2m}\big[\mathrm{i}e\boldsymbol{\nabla}_{\boldsymbol{R}}\cdot\boldsymbol{A}\hat{\tau}_3 \diamond \check{G}\big](X,p) - \frac{1}{2m}\big\{\mathrm{i}e\boldsymbol{A}\hat{\tau}_3 \diamond \boldsymbol{\nabla}_{\boldsymbol{R}}\check{G}\big\}(X,p).
\end{aligned} \tag{3.86}$$

Finally, we consider the self-energy terms, for which we can just use the definition of the Moyal product,

$$\int dx \mathrm{e}^{-\mathrm{i}x\cdot p}\big[\check{\Sigma}_{\mathrm{tot}} \bullet \check{G}\big](1,2) = \big[\check{\Sigma}_{\mathrm{tot}} \diamond \check{G}\big](X,p). \tag{3.87}$$

Having calculated all terms, we can now write Eq. (3.43) in terms of Moyal commutators as

$$\frac{\mathrm{i}}{m}\boldsymbol{p}\cdot\boldsymbol{\nabla}_{\boldsymbol{R}}\check{G}(X,p)+\left[E\hat{\tau}_3-\check{\Sigma}_{\mathrm{tot}}\overset{\circ}{,}\check{G}\right](X,p)-\mathrm{i}\frac{\boldsymbol{p}}{m}\left[\mathrm{i}e\boldsymbol{A}\hat{\tau}_3\overset{\circ}{,}\check{G}\right](X,p)$$
$$-\frac{1}{2m}\left[e^2\boldsymbol{A}^2\overset{\circ}{,}\check{G}\right](X,p)-\frac{1}{2m}\left[\mathrm{i}e\boldsymbol{\nabla}_{\boldsymbol{R}}\cdot\boldsymbol{A}\hat{\tau}_3\overset{\circ}{,}\check{G}\right](X,p)$$
$$-\frac{1}{2m}\left\{\mathrm{i}e\boldsymbol{A}\hat{\tau}_3\overset{\circ}{,}\boldsymbol{\nabla}_{\boldsymbol{R}}\check{G}\right\}(X,p)=0. \quad (3.88)$$

3.6 The quasiclassical approximation

In this section, we introduce the quasiclassical approximation, assuming that all physical quantities vary on a length scale much larger than the Fermi wavelength λ_F. This is equivalent to assuming that the Fermi energy is the dominating energy in the system of interest. We will show that the Green function generally will have the form of short-wavelength oscillations modulated by an envelope function. In the quasiclassical approximation, these short-wavelength oscillations which have wavelengths on the order of the Fermi wavelength are discarded, making the equations of motion at hand much simpler. This is because the derivatives of the Green function will now vary slowly in spatial coordinates, instead of oscillating over distances in the region of the Fermi wavelength. The quasiclassical approximation is expected to hold for superconductors because long-range correlations are present [69], meaning that observables change slowly in space. Moreover, we will consider superconducting systems at temperatures smaller than the critical temperature, which typically is on the order of a few Kelvin. This approximation will allow us to cancel many of the terms in the equation of motion for the Green function in Eq. (3.88).

3.6.1 Neglecting higher-order terms

In the quasiclassical approximation, we have that $|\boldsymbol{p}|\approx p_F\propto\lambda_F^{-1}$, where p_F is the magnitude of the Fermi momentum. The quasiclassical approximation assumes that the Fermi momentum is much larger than the quantity $e\boldsymbol{A}$, which also has units of momentum. Thus, we can ignore the last three terms in Eq. (3.88), and only include the magnetic vector potential through the third term in the first line, since this term involves a factor of $\boldsymbol{p}$, while the others do not.

3.6.2 Truncating the spatial gradients

Because of the slow spatial variation of the Green function, we will truncate the infinite series of derivatives arising in Eq. (3.88) at first order in spatial derivatives.

The Moyal product then reduces to

$$\begin{aligned}
[A \odot B] &= \mathrm{e}^{\frac{\mathrm{i}}{2}\left(\nabla_X^A \cdot \nabla_p^A - \nabla_p^A \nabla_X^B\right)}[AB] \\
&= \mathrm{e}^{-\frac{\mathrm{i}}{2}\left(\partial_T^A \partial_E^B - \partial_E^A \partial_T^B\right)} \mathrm{e}^{\frac{\mathrm{i}}{2}\left(\boldsymbol{\nabla}_{\boldsymbol{R}}^A \cdot \boldsymbol{\nabla}_{\boldsymbol{p}}^B - \boldsymbol{\nabla}_{\boldsymbol{p}}^A \cdot \boldsymbol{\nabla}_{\boldsymbol{R}}^B\right)}[AB] \\
&\approx \mathrm{e}^{-\frac{\mathrm{i}}{2}\left(\partial_T^A \partial_E^B - \partial_E^A \partial_T^B\right)} \left([AB] + \frac{\mathrm{i}}{2}\big[\boldsymbol{\nabla}_{\boldsymbol{R}}^A \cdot \boldsymbol{\nabla}_{\boldsymbol{p}}^B - \boldsymbol{\nabla}_{\boldsymbol{p}}^A \cdot \boldsymbol{\nabla}_{\boldsymbol{R}}^B\big][AB] \right) \\
&= [A \circ B] + \frac{\mathrm{i}}{2}[\boldsymbol{\nabla}_{\boldsymbol{R}} A \circ \boldsymbol{\nabla}_{\boldsymbol{p}} B] - \frac{\mathrm{i}}{2}[\boldsymbol{\nabla}_{\boldsymbol{p}} A \circ \boldsymbol{\nabla}_{\boldsymbol{R}} B],
\end{aligned} \tag{3.89}$$

where the arguments (X, p) of A and B is suppressed here and in the following for simpler notation, and we have introduced the *circle product*,

$$[A \circ B] = \mathrm{e}^{\mathrm{i}\left(\partial_T^A \partial_E^B - \partial_E^A \partial_T^B\right)}[AB]. \tag{3.90}$$

We now also define the circle commutator and circle anticommutator,

$$\big[A \circ B\big] = [A \circ B] - [B \circ A] \qquad \big\{A \circ B\big\} = [A \circ B] + [B \circ A] \tag{3.91}$$

enabling us to write the gradient approximation for the Moyal commutator as

$$\big[A \mathbin{\odot} B\big] \approx \big[A \circ B\big] + \frac{\mathrm{i}}{2}\big\{\boldsymbol{\nabla}_{\boldsymbol{R}} A \circ \boldsymbol{\nabla}_{\boldsymbol{p}} B\big\} - \frac{\mathrm{i}}{2}\big\{\boldsymbol{\nabla}_{\boldsymbol{p}} A \circ \boldsymbol{\nabla}_{\boldsymbol{R}} B\big\} \tag{3.92}$$

This can now be used to simplify the equation of motion in Eq. (3.88), after neglecting terms as discussed in Section 3.6.1. Considering terms separately, we find

$$\big[E\hat{\tau}_3 \mathbin{\odot} \check{G}\big] \approx \big[E\hat{\tau}_3 \circ \check{G}\big] \tag{3.93}$$

$$\big[\check{\Sigma}_{\mathrm{tot}} \mathbin{\odot} G\big] \approx \big[\check{\Sigma}_{\mathrm{tot}} \circ \check{G}\big] + \frac{\mathrm{i}}{2}\big\{\boldsymbol{\nabla}_{\boldsymbol{R}} \check{\Sigma}_{\mathrm{tot}} \circ \boldsymbol{\nabla}_{\boldsymbol{p}} \check{G}\big\} - \frac{\mathrm{i}}{2}\big\{\boldsymbol{\nabla}_{\boldsymbol{p}} \check{\Sigma}_{\mathrm{tot}} \circ \boldsymbol{\nabla}_{\boldsymbol{R}} \check{G}\big\} \tag{3.94}$$

$$\big[\mathrm{i}e\boldsymbol{A}\hat{\tau}_3 \mathbin{\odot} \check{G}\big] \approx \big[\mathrm{i}e\boldsymbol{A}\hat{\tau}_3 \circ \check{G}\big] + \frac{\mathrm{i}}{2}\big\{\mathrm{i}e\boldsymbol{\nabla}_{\boldsymbol{R}} \cdot \boldsymbol{A}\hat{\tau}_3 \circ \boldsymbol{\nabla}_{\boldsymbol{p}} \check{G}\big\}, \tag{3.95}$$

so that the subtracted equation of motion from Eq. (3.88) becomes (restoring arguments)

$$\begin{aligned}
\frac{\mathrm{i}}{m}\boldsymbol{p} \cdot \boldsymbol{\nabla}_{\boldsymbol{R}} \check{G}(X,p) + \frac{e}{m}\big[\boldsymbol{p} \cdot \boldsymbol{A}(X)\hat{\tau}_3 \circ \check{G}(X,p)\big] + \big[E\hat{\tau}_3 - \check{\Sigma}(X,p) \circ \check{G}(X,p)\big] \\
- \frac{\mathrm{i}}{2}\big\{\boldsymbol{\nabla}_{\boldsymbol{R}} \check{\Sigma}_{\mathrm{tot}}(X,p) + \frac{\boldsymbol{p}}{2m}\boldsymbol{\nabla}_{\boldsymbol{R}} \cdot \boldsymbol{A}(X) \circ \boldsymbol{\nabla}_{\boldsymbol{p}} \check{G}(X,p)\big\} \\
+ \frac{\mathrm{i}}{2}\big\{\boldsymbol{\nabla}_{\boldsymbol{p}} \check{\Sigma}_{\mathrm{tot}}(X,p) \circ \boldsymbol{\nabla}_{\boldsymbol{R}} \check{G}(X,p)\big\} = 0,
\end{aligned} \tag{3.96}$$

where we have used that the circle product is distributive, which follows from the distributive property of the derivative.

3.6.3 The quasiclassical Green function

Even with the approximations made in Section 3.6.2, the equation of motion in Eq. (3.96) for the Green function is still very complicated. It can be significantly simplified by introducing the quasiclassical Green function $\check{g}$, in which we have integrated out the dependence on the size of the momentum. We assume that the Green function is strongly peaked at the Fermi surface, and introduce the quasiclassical Green function $\check{g}$ implicitly through [45, 25, 26]

$$\check{G}(X,p) \approx \frac{\pi}{\mathrm{i}}\delta(\xi_{\boldsymbol{p}})\check{g}(X,\boldsymbol{p}_F,E), \tag{3.97}$$

where $\xi_{\boldsymbol{p}} = \boldsymbol{p}^2/2m - \mu$ is the kinetic energy relative to the Fermi surface. Eq. (3.97) is easily isolated for the quasiclassical Green function by integrating over $\xi_{\boldsymbol{p}}$,

$$\check{g}(X,\boldsymbol{p_F},E) \equiv \frac{\mathrm{i}}{\pi}\int_{-\omega_c}^{\omega_c} d\xi_{\boldsymbol{p}}\check{G}(X,\boldsymbol{p},E), \tag{3.98}$$

where ω_c is a cutoff energy assumed smaller than the Fermi energy, but larger than any other energy scale in the problem [66]. The reason why we assume ω_c larger than other energy scales is because we want to integrate over all poles of the exact Green function, to capture all poles of the Green function, and thus all relevant physics as well. The integration limits are discussed in more detail in [64]. By integrating over the energy $\xi_{\boldsymbol{p}}$, we have eliminated the dependence on the magnitude of the momentum, and the quasiclassical Green function depends only on the direction of the momentum at the Fermi surface $\boldsymbol{p}_F$. In order to get a more physically telling form of the quasiclassical approximation, we Fourier transform Eq. (3.97) back into the relative position space,

$$\check{G}(X,\boldsymbol{r},E) \approx \frac{\pi}{\mathrm{i}}\int\frac{d\boldsymbol{p}}{(2\pi)^3}\mathrm{e}^{-\mathrm{i}\boldsymbol{p}\cdot\boldsymbol{r}}\delta(\xi_{\boldsymbol{p}})\check{g}(X,\boldsymbol{p}_F,E) = \frac{\pi N_0}{\mathrm{i}}\int\frac{d\boldsymbol{e_F}}{4\pi}\mathrm{e}^{-\mathrm{i}\boldsymbol{p}\cdot\boldsymbol{r}}\check{g}(X,\boldsymbol{p}_F,E), \tag{3.99}$$

where we have used

$$\int\frac{d\boldsymbol{p}}{(2\pi)^3} \to N_0\int d\xi_{\boldsymbol{p}}\int\frac{d\boldsymbol{e_F}}{4\pi}, \tag{3.100}$$

which holds for systems with particle-hole symmetry [25]. This means that we get a density of states that is symmetric around the Fermi level, which is why we could pull out N_0 from the integral. We now proceed with integrating Eq. (3.96) over the energy $\xi_{\boldsymbol{p}}$, fixing the momentum to have the magnitude of the Fermi momentum. This causes the anticommutator terms in Eq. (3.96) to vanish [25, 64].

The equation of motion for the quasiclassical Green function can then be written

$$\begin{aligned}\frac{\mathrm{i}}{m}\boldsymbol{p}_F\cdot\boldsymbol{\nabla}_{\boldsymbol{R}}\check{g}(X,\boldsymbol{p}_F,E) - \frac{e}{m}\big[\boldsymbol{p}_F\cdot\boldsymbol{A}(X)\hat{\tau}_3 \circ \check{g}(X,\boldsymbol{p}_F,E)\big] \\ + \big[E\hat{\tau}_3 - \check{\sigma}_{\mathrm{tot}}(X,\boldsymbol{p}_F,E) \circ \check{g}(X,\boldsymbol{p}_F,E)\big] = 0,\end{aligned} \tag{3.101}$$

where $\check{\sigma}_{\text{tot}}(X, \boldsymbol{p}_F, E)$ is the quasiclassical approximated version of the self-energy Σ_{tot}, and will be calculated in the next section. In order to simplify further, we introduce the covariant derivative, and use the notation

$$\left[\tilde{\boldsymbol{\nabla}} \circ, \check{g}\right] \equiv \boldsymbol{\nabla}\check{g} - \left[\mathrm{i}e\boldsymbol{A}\hat{\tau}_3 \circ, \check{g}\right]. \tag{3.102}$$

Using this, we write Eq. (3.101) more compactly,

$$\left[\mathrm{i}\boldsymbol{v}_F \cdot \tilde{\boldsymbol{\nabla}} + E\hat{\tau}_3 - \check{\sigma}_{\text{tot}}(X, \boldsymbol{p}_F, E) \circ, \check{g}(X, \boldsymbol{p}_F, E)\right] = 0, \tag{3.103}$$

where we also introduced the Fermi velocity $\boldsymbol{v}_F \equiv \boldsymbol{p}_F/m$.

3.6.4 Normalization of the quasiclassical Green functions

When subtracting the left-handed and right-handed equations of motion for the Green functions in Section 3.3.2, we removed the delta function and obtained a simpler equation of motion, but we also lost the normalization of the Green function. To see this, we consider Eq. (3.88) and note that for all Green functions $\check{G}$ satisfying this equation, the function $\check{G}' = c\check{G}$, with c an arbitrary constant, will also satisfy this equation. This is in contrast to Eq. (3.36), and we will thus need to apply a normalization condition in addition to Eq. (3.103) to uniquely determine the quasiclassical Green function.

In the literature, a normalization often used is [14, 27, 71]

$$\check{g}(X, \boldsymbol{p}_F, E) \circ \check{g}(X, \boldsymbol{p}_F, E) = \check{1} \tag{3.104}$$

For an extensive discussion of the choice of normalization, the reader is directed to the book by Rammer [27]. By writing out the matrix components of Eq. (3.104), it is easily seen that they satisfy (suppressing the arguments for the rest of this section)

$$\hat{g}^R \circ \hat{g}^R = \hat{1} \qquad \hat{g}^A \circ \hat{g}^A = \hat{1} \qquad \hat{g}^R \circ \hat{g}^K + \hat{g}^K \circ \hat{g}^A = 0. \tag{3.105}$$

It can be shown by insertion that

$$\hat{g}^K = \hat{g}^R \circ \hat{h} - \hat{h} \circ \hat{g}^A \tag{3.106}$$

automatically satisfies the third normalization condition, with $\hat{h}$ a general matrix function. As we will see in Section 3.8, $\hat{h}$ has the interpretation of the matrix describing the filling of states. It is thus a very useful quantity for systems out of equilibrium. For this reason, $\hat{h}$ is often denoted the distribution matrix [71, 25].

3.6.5 Symmetries of the quasiclassical Green functions

In Appendix C.1, we show that due to the matrix structure of retarded Green function in Eq. (3.26a), we can in general write the retarded quasiclassical Green function as

$$\hat{g}^R(X, \boldsymbol{p}_F, E) = \begin{pmatrix} \underline{g}^R(X, \boldsymbol{p}_F, E) & \underline{f}^R(X, \boldsymbol{p}_F, E) \\ -\underline{\tilde{f}}^R(X, \boldsymbol{p}_F, E) & -\underline{\tilde{g}}^R(X, \boldsymbol{p}_F, E) \end{pmatrix}, \tag{3.107}$$

where we have introduced the particle-hole tilde conjugation, which is the combined operation of energy-momentum inversion and complex conjugation,

$$\tilde{\lambda}(X, \boldsymbol{p}_F, E) = \lambda(X, -\boldsymbol{p}_F, -E,)^*, \tag{3.108}$$

for a general function λ. A similar relation holds also for the retarded Green function, but will not be needed due to a relation between the advanced and retarded Green function,

$$\hat{g}^A(X, \boldsymbol{p}_F, E) = -\hat{\tau}_3 \left[\hat{g}^R(X, \boldsymbol{p}_F, E)\right]^\dagger \hat{\tau}_3, \tag{3.109}$$

which is shown in Appendix C.1 as well. Since the Keldysh Green function in Eq. (3.26c) has a similar structure to the retarded and advanced function, but with a positive sign in the lower two components, the quasiclassical Keldysh Green function can be parametrized as well,

$$\hat{g}^K(X, \boldsymbol{p}_F, E) = \begin{pmatrix} \underline{g}^K(X, \boldsymbol{p}_F, E) & \underline{f}^K(X, \boldsymbol{p}_F, E) \\ \underline{\tilde{f}}^K(X, \boldsymbol{p}_F, E) & \underline{\tilde{g}}^K(X, \boldsymbol{p}_F, E) \end{pmatrix}. \tag{3.110}$$

This means that if we have solved for $\hat{g}^R$ and $\hat{g}^K$ for positive energies, we can find the negative-energy solution by

$$\hat{g}^R(X, -\boldsymbol{p}_F, -E) = -\hat{\tau}_1 \left[\hat{g}^R(X, \boldsymbol{p}_F, E)\right]^* \hat{\tau}_1 \tag{3.111}$$

$$\hat{g}^K(X, -\boldsymbol{p}_F, -E) = \hat{\tau}_1 \left[\hat{g}^K(X, \boldsymbol{p}_F, E)\right]^* \hat{\tau}_1. \tag{3.112}$$

Thus, to determine all Green functions of a system, we only need to solve for the positive energy solutions of the retarded and the Keldysh component. Equivalently, we could also solve for the distribution matrix instead of the Keldysh component, and use Eq. (3.106) to determine the Keldysh component.

3.7 The Usadel equation and boundary conditions

In this section, we will take the so-called dirty limit, where we assume that the impurity scattering is so strong that the quasiclassical Green function is effectively

averaged over all momentum directions [22]. This will result in the Usadel equation, which is a simpler equation of motion to solve than Eq. (3.103). We will also state a choice for boundary conditions.

3.7.1 The Usadel equation

Assuming that the quasiclassical Green function is close to being isotropic due to strong impurity scattering, we can expand it to first order in a spherical symmetric s-wave component and a small p-wave component that depends on $\boldsymbol{p}_F$. This can be written as [72]

$$\check{g}(X, \boldsymbol{p}_F, E) \simeq \check{g}_s(X, E) + \boldsymbol{e}_F \cdot \check{\boldsymbol{g}}_{\boldsymbol{p}}(X, E), \tag{3.113}$$

where $\boldsymbol{e}_F = \boldsymbol{p}_F/p_F$. In the following, it will be useful to note that we can isolate the s-wave part of the Green function by integrating Eq. (3.113) over all directions of the Fermi momentum. This is because the s-wave part of the quasiclassical Green function is isotropic in $\boldsymbol{p}_F$, while the p-wave part contains a factor $\boldsymbol{e}_F$ that will vanish when averaging over all directions. This can be written as

$$\int \frac{d\boldsymbol{e}_{\boldsymbol{F}}}{4\pi}\check{g} = \int \frac{d\boldsymbol{e}_{\boldsymbol{F}}}{4\pi}\left(\check{g}_s + \boldsymbol{e}_F \cdot \check{\boldsymbol{g}}_{\boldsymbol{p}}\right) = \check{g}_s \int \frac{d\boldsymbol{e}_{\boldsymbol{F}}}{4\pi} = \check{g}_s. \tag{3.114}$$

Similarly, the p-wave part can be isolated by first multiplying with $\boldsymbol{e}_F$ and then performing the averaging. First, we note that we can parametrize the unit vector $\boldsymbol{e}_F$ in spherical coordinates as $\boldsymbol{e}_F = (\sin\theta\cos\phi, \sin\theta\sin\phi, \cos\theta)^{Tr}$, where θ is the polar angle and ϕ the azimuthal angle. Multiplying Eq. (3.113) by $\boldsymbol{e}_F$ and then averaging yields

$$\begin{aligned}
&\int \frac{d\boldsymbol{e}_{\boldsymbol{F}}}{4\pi}\boldsymbol{e}_F\check{g} = \int \frac{d\boldsymbol{e}_{\boldsymbol{F}}}{4\pi}\boldsymbol{e}_F\left(\check{g}_s + \boldsymbol{e}_F \cdot \check{\boldsymbol{g}}_{\boldsymbol{p}}\right) = \int \frac{d\boldsymbol{e}_{\boldsymbol{F}}}{4\pi}\boldsymbol{e}_F\left(\boldsymbol{e}_F \cdot \check{\boldsymbol{g}}_{\boldsymbol{p}}\right) \\
&= \frac{1}{4\pi}\int_0^{2\pi}\int_0^{\pi} d\phi d\theta \sin(\theta) \begin{pmatrix} \sin\theta\cos\phi \\ \sin\theta\sin\phi \\ \cos\theta \end{pmatrix} \left(g_p^x \sin\theta\cos\phi + g_p^y \sin\theta\sin\phi + g_p^z\cos\theta\right) \\
&= \frac{1}{3}\check{\boldsymbol{g}}_{\boldsymbol{p}},
\end{aligned} \tag{3.115}$$

where the integration in the last line was performed using trigonometric identities.

We start by considering the quasiclassical self-energy $\check{\sigma}_{\text{tot}}$. The terms arising from the superconductivity, ferromagnetism, chemical potential, and electrostatic potential are momentum-independent and are thus unchanged by the momentum integration. The self-energy term

$$\check{\Sigma}_{\text{imp}}(X, p) = \langle \hat{V}_{\text{imp}}(X)\check{G}(X, p)\hat{V}_{\text{imp}}(X)\rangle_{av}, \tag{3.116}$$

on the other hand, depends on the quasiclassical Green function. It can be shown that in the quasiclassical approximation, when taking the dirty limit and the quasiclassical approximation, the terms take the form [14, 25, 26]

$$\check{\Sigma}_{\text{imp}}(X, \boldsymbol{p}, E) \to \check{\sigma}_{\text{imp}}(X, E) = -\check{\sigma}_{\text{sf}}(X, E) - \check{\sigma}_{\text{so}}(X, E) - \check{\sigma}_{\text{ec}}(X, E) \tag{3.117}$$

where we have defined

$$\check{\sigma}_{\text{imp}}(X, E) = \frac{\mathrm{i}}{2\tau_{\text{imp}}}\check{g}_s(X, E) \tag{3.118}$$

$$\check{\sigma}_{\text{sf}}(X, E) = \frac{\mathrm{i}}{8\tau_{sf}}\hat{\boldsymbol{\sigma}} \cdot (\check{g}_s(X, E)\hat{\boldsymbol{\sigma}}) \tag{3.119}$$

$$\check{\sigma}_{\text{so}}(X, E) = \frac{\mathrm{i}}{8\tau_{sf}}\hat{\tau}_3\hat{\boldsymbol{\sigma}} \cdot (\check{g}_s(X, E)\hat{\tau}_3\hat{\boldsymbol{\sigma}}), \tag{3.120}$$

and where the scattering lifetimes are given as

$$\frac{1}{\tau_{\text{sc}}} = 2\pi n_i N_0 \langle |v_i(\boldsymbol{p}_F - \boldsymbol{q})|^2 \rangle_{\boldsymbol{p}_f, \boldsymbol{q}_F} \tag{3.121}$$

$$\frac{1}{\tau_{\text{sf}}} = 8\pi n_m N_0 \langle |v_m(\boldsymbol{p}_F - \boldsymbol{q})|^2 \rangle_{\boldsymbol{p}_f, \boldsymbol{q}_F} \tag{3.122}$$

$$\frac{1}{\tau_{\text{so}}} = \frac{1}{\tau_{\text{sc}}}\frac{8\alpha^2 p_F^4}{9} \tag{3.123}$$

where n_i and n_m is the concentration of non-magnetic and magnetic impurities, and v_i and v_m is the potential from a non-magnetic and a magnetic impurity. Inserting these self-energies, the equation of motion in Eq. (3.103) reads

$$\left[\mathrm{i}\boldsymbol{v}_F \cdot \tilde{\boldsymbol{\nabla}} + E\hat{\tau}_3 + \check{\sigma}_{\text{sf}} + \check{\sigma}_{\text{sc}} + \check{\sigma}_{\text{so}} - \mu\check{1} + \hat{M} + \hat{\Delta} \circ,\ \check{g}_s + \boldsymbol{e}_F \cdot \check{\boldsymbol{g}}_{\boldsymbol{p}}\right] = 0. \tag{3.124}$$

We now proceed by splitting Eq. (3.124) into an odd and an even part. Performing the angular average produces

$$\left[E\hat{\tau}_3 + \check{\sigma}_{\text{sf}} + \check{\sigma}_{\text{so}} + \check{\sigma}_{\text{sc}} - \mu\check{1} + \hat{M} + \hat{\Delta} \circ,\ \check{g}_s\right] + \frac{\mathrm{i}}{3}v_F\left[\tilde{\boldsymbol{\nabla}} \circ,\ \check{\boldsymbol{g}}_{\boldsymbol{p}}\right] = 0, \tag{3.125}$$

where we have used that $\check{\sigma}_{\text{sf}}$ and $\check{\sigma}_{\text{sc}}$ are independent of $\boldsymbol{p}_F$, and that $\check{\sigma}_{\text{sc}}$ commutes with $\check{g}_s$. Multiplying Eq. (3.124) by $\boldsymbol{e}_F$ and performing the averaging, we get

$$\frac{\mathrm{i}}{3}v_F\left[\tilde{\boldsymbol{\nabla}} \circ,\ \check{g}_s\right] + \frac{\mathrm{i}}{6\tau_{\text{sc}}}\left[\check{g}_s \circ,\ \check{\boldsymbol{g}}_{\boldsymbol{p}}\right] \approx 0, \tag{3.126}$$

where we have inserted the explicit form of $\check{\sigma}_{\text{sc}}$, and assumed that the impurity scattering dominates, so that we could ignore the spin-flip and spin-orbit scattering

terms in this equation. By now performing the circle product with $\check{g}_s$ from the left, and canceling a common factor $\mathrm{i}/3$, we get

$$v_F \check{g}_s \circ \big[\tilde{\boldsymbol{\nabla}} \circ \check{g}_s\big] + \frac{1}{2\tau_{\mathrm{sc}}}\big[\check{g}_s \circ \check{g}_s \circ \check{\boldsymbol{g}}_{\boldsymbol{p}} - \check{g}_s \circ \check{\boldsymbol{g}}_{\boldsymbol{p}} \circ \check{g}_s\big] = 0, \tag{3.127}$$

To proceed, we will have to consider the normalization of $\check{g}$, as discussed in Section 3.6.4. Inserting the p-wave expansion from Eq. (3.113), the normalization condition becomes

$$\begin{aligned} \check{1} &= (\check{g}_s + \boldsymbol{e}_F \cdot \check{\boldsymbol{g}}_{\boldsymbol{p}}) \circ (\check{g}_s + \boldsymbol{e}_F \cdot \check{\boldsymbol{g}}_{\boldsymbol{p}}) \\ &= \check{g}_s \circ \check{g}_s + \check{g}_s \circ \boldsymbol{e}_F \cdot \check{\boldsymbol{g}}_{\boldsymbol{p}} + \boldsymbol{e}_F \cdot \check{\boldsymbol{g}}_{\boldsymbol{p}} \circ \check{g}_s + \mathcal{O}(\check{\boldsymbol{g}}_{\boldsymbol{p}}{}^2) \\ &\simeq \check{g}_s \circ \check{g}_s + \boldsymbol{e}_F \cdot \big(\check{g}_s \circ \check{\boldsymbol{g}}_{\boldsymbol{p}} + \check{\boldsymbol{g}}_{\boldsymbol{p}} \circ \check{g}_s\big), \end{aligned} \tag{3.128}$$

where we have ignored second-order terms in the p-wave component, and used that we can pull $\boldsymbol{e}_F$ outside the circle product, with the understanding that it works on $\check{\boldsymbol{g}}_{\boldsymbol{p}}$. Performing the angular average and the angular average after multiplication with $\boldsymbol{e}_F$, we get the two normalization conditions

$$\check{g}_s \circ \check{g}_s = \check{1} \qquad\qquad \check{g}_s \circ \check{\boldsymbol{g}}_{\boldsymbol{p}} + \check{\boldsymbol{g}}_{\boldsymbol{p}} \circ \check{g}_s = 0, \tag{3.129}$$

to first order in the expansion. Using these relations, Eq. (3.127) can be written as

$$v_F \check{g}_s \circ \big[\tilde{\boldsymbol{\nabla}} \circ \check{g}_s\big] + \frac{1}{2\tau_{\mathrm{sc}}}\big[\check{\boldsymbol{g}}_{\boldsymbol{p}} + \check{\boldsymbol{g}}_{\boldsymbol{p}}\big] = 0, \tag{3.130}$$

from which we can isolate

$$\check{\boldsymbol{g}}_{\boldsymbol{p}} = -\tau_{\mathrm{sc}} v_F \check{g}_s \circ \big[\tilde{\boldsymbol{\nabla}} \circ \check{g}_s\big]. \tag{3.131}$$

This means that the p-wave part can be found from the s-wave part, and we thus will only need to solve for $\check{g}_s$. Inserting Eq. (3.131) back into Eq. (3.125), we get an equation of motion containing $\check{g}_s$ only. Defining the diffusion constant $D = \tau_{\mathrm{sc}} p_F^2/3m^2$, the resulting equation reads (restoring arguments)

$$\begin{aligned} &D\Big[\tilde{\boldsymbol{\nabla}} \circ \check{g}_s(X,E) \circ \big[\tilde{\boldsymbol{\nabla}} \circ \check{g}_s(X,E)\big]\Big] \\ &\quad + \mathrm{i}\big[E\hat{\tau}_3 + \check{\sigma}_{\mathrm{sf}}(X,E) + \check{\sigma}_{\mathrm{so}}(X,E) - \mu(X)\hat{1} + \hat{M}(X) + \hat{\Delta}(X) \circ \check{g}_s(X,E)\big] = 0, \end{aligned} \tag{3.132}$$

This is the Usadel equation, valid for a dirty system with superconducting, ferromagnetic, and electromagnetic interactions, as well as spin-flip and spin-orbit scattering. Often, we will consider the stationary case, where there is no dependence

on the center-of-mass time, so the circle products reduce simply to matrix products, and the Usadel equation becomes

$$D\Big[\tilde{\boldsymbol{\nabla}}, \check{g}_s(\boldsymbol{R}, E)\big[\tilde{\boldsymbol{\nabla}}, \check{g}_s(\boldsymbol{R}, E)\big]\Big] + \mathrm{i}\big[E\hat{\tau}_3 + \check{\sigma}_{\mathrm{sf}}(\boldsymbol{R}, E) + \check{\sigma}_{\mathrm{so}}(\boldsymbol{R}, E) + \hat{\Delta}(\boldsymbol{R}) + \hat{M}(\boldsymbol{R}), \check{g}_s(\boldsymbol{R}, E)\big] = 0, \quad (3.133)$$

where we have used that the chemical potential, with the absorbed electrostatic and magnetic potentials, cancels in the stationary case, because it commutes with $\check{g}_s$. We have also used the notation

$$\big[\tilde{\boldsymbol{\nabla}}, \check{g}\big] \equiv \boldsymbol{\nabla}\check{g} - \big[\mathrm{i}e\boldsymbol{A}\hat{\tau}_3, \check{g}\big]. \quad (3.134)$$

Usually, we will express all observables in terms of the s-wave part of the quasiclassical Green function. For this reason, we will in the rest of the thesis drop the subscript, remembering that we are dealing with only the isotropic part of the full quasiclassical Green function in Eq. (3.113).

3.7.2 Dimensionless form

The quasiclassical Green function carries no dimension, but the self-energies have units of energy, and the derivatives have units of inverse energies. We simplify the notation by introducing the total self-energy $\check{\sigma}$ as the sum of all self-energy terms in Eq. (3.133). To numerically solve an equation, we want to write it in a dimensionless form, using dimensionless variables. To this end, we divide Eq. (3.133) by Δ_0, the gap at zero temperature, and introduce the so-called superconducting coherence length $\xi = \sqrt{D/\Delta_0}$, which is a natural length scale in dirty superconductors, and physically describes the length scale on which changes occur in superconducting systems. We define the dimensionless self-energy as $\check{\sigma}' = \check{\sigma}/\Delta_0$, and new coordinates as $\boldsymbol{R}' = \boldsymbol{R}/\xi$. Derivatives then become $\boldsymbol{\nabla}' = \xi\boldsymbol{\nabla}$. For later, we note that we can give temperatures in units of the critical temperature, $T' = T/T_c$. In the stationary case, the Usadel equation then reads

$$\Big[\tilde{\boldsymbol{\nabla}}', \check{g}(\boldsymbol{R}', E')\big[\tilde{\boldsymbol{\nabla}}', \check{g}(\boldsymbol{R}', E')\big]\Big] + \mathrm{i}\big[\check{\sigma}'(\boldsymbol{R}', E'), \check{g}(\boldsymbol{R}', E')\big] = 0, \quad (3.135)$$

where all quantities involved are dimensionless.

3.7.3 Boundary conditions

As discussed previously, the quasiclassical approximation assumes that all length scales on which physical quantities vary are much larger than the Fermi wavelength λ_F. This approximation works well for bulk but fails at interfaces, where there

is an abrupt change in many physical quantities. For this reason, we will have to supply boundary conditions for the quasiclassical Green function, which takes into account the rapidly changing nature close to the interfaces. These boundary conditions necessary have to come from non-quasiclassical theory, and they are often found by expressing the current across a boundary through ballistic Green functions, and then comparing with the quasiclassical expression for current [45].

Using this procedure, it can be derived that in the low transparency, non-magnetic limit, the boundary conditions for the quasiclassical Green functions become [73]

$$2L_j\zeta_j\hat{g}_j^R\nabla_n\hat{g}_j^R = [\hat{g}_1, \hat{g}_2], \tag{3.136}$$

where $j = \{1, 2\}$ denotes which side of the interface we are on, and ∇_n is the derivative across material 1 to material 2. This is the so-called Kuprianov-Lukichev (KL) boundary conditions, after Kuprianov and Lukichev [74]. This boundary condition describes how superconducting correlations leak from one material to another but does not capture the effects of magnetic interfaces, which can cause e.g. singlet-triplet mixing [45].

3.8 Distribution matrix and physical observables

In this section, we concentrate on the distribution matrix and show how it is a useful quantity out of equilibrium. The distribution matrix $\hat{h}$ was introduced in Section 3.6.4 as the matrix used to parametrize the Keldysh Green function. This parametrization automatically satisfied the normalization condition. In the stationary case, this parametrization reads

$$\hat{g}^K = \hat{g}^R\hat{h} - \hat{h}\hat{g}^A. \tag{3.137}$$

Here, we will show that the distribution matrix describes the filling of states in the system. This section is based on the Ph.D. thesis of [45], which presents a convenient formalism, writing the distribution matrix as an 8-vector.

We write the distribution matrix in terms of an 8-vector h_j,

$$\hat{h} = \sum_{j=0}^{8} h_j\hat{\rho}_j, \tag{3.138}$$

where we use the following matrices in Nambu-spin space,

$$\begin{array}{llll} \hat{\rho}_0 \equiv \hat{\tau}_0\hat{\sigma}_0 & \hat{\rho}_1 \equiv \hat{\tau}_0\hat{\sigma}_1 & \hat{\rho}_2 \equiv \hat{\tau}_0\hat{\sigma}_2 & \hat{\rho}_3 \equiv \hat{\tau}_0\hat{\sigma}_3 \\ \hat{\rho}_4 \equiv \hat{\tau}_3\hat{\sigma}_0 & \hat{\rho}_5 \equiv \hat{\tau}_3\hat{\sigma}_1 & \hat{\rho}_6 \equiv \hat{\tau}_3\hat{\sigma}_2 & \hat{\rho}_7 \equiv \hat{\tau}_3\hat{\sigma}_3 \end{array} .$$

These eight matrices are block diagonal and linearly independent, meaning that they span the 8-dimensional space of block-diagonal 4-dimensional matrices. It can be shown that one can project a component h_j from

$$h_j = \frac{1}{4}\mathrm{Tr}\Big\{\hat{\rho}_j \hat{h}\Big\}. \tag{3.139}$$

Here, h_0 is the energy mode, which contains equal contribution for spin-up and spin-up electrons and holes, thus describing the average energy of the system. h_1, h_2, and h_3 are the spin-energy modes in the x-, y-, and z-direction, respectively, describing differences in energy between the spin-up band and spin-down band. This is in contrast to h_5, h_6 and h_7, which are the spin modes in the x-, y-, and z-direction, respectively, which contain equal contributions from particles with the same physical spin[11]. Finally, h_4 describes differences in particles and holes and is for that reason called the charge mode of the system.

If we choose the spin quantization axis to be along the z-axis, the only nonzero modes the energy mode h_0, the z-direction spin-energy mode h_3, the charge mode h_4 and the z-direction spin mode h_7 [45]. This causes the distribution matrix to become diagonal, and it can generally be written

$$\hat{h} = \mathrm{diag}\big(h_\uparrow^+, h_\downarrow^+, h_\uparrow^-, h_\downarrow^-\big), \tag{3.140}$$

where $n_\sigma^{+(-)} = (1 - h_\sigma^{+(-)})/2$ is the occupation number of states for an electron (hole) with spin σ[12]. From this, it can easily be seen that the four diagonal modes can be written

$$h_0 = \frac{1}{4}\left(h_\uparrow^+ + h_\downarrow^+ + h_\uparrow^- + h_\downarrow^-\right) \tag{3.141}$$

$$h_3 = \frac{1}{4}\left(h_\uparrow^+ - h_\downarrow^+ + h_\uparrow^- - h_\downarrow^-\right) \tag{3.142}$$

$$h_4 = \frac{1}{4}\left(h_\uparrow^+ + h_\downarrow^+ - h_\uparrow^- - h_\downarrow^-\right) \tag{3.143}$$

$$h_7 = \frac{1}{4}\left(h_\uparrow^+ - h_\downarrow^+ - h_\uparrow^- + h_\downarrow^-\right). \tag{3.144}$$

In analogy with the equilibrium case, one can then introduce temperatures and voltages for each particle type and spin, as the quantities satisfying

$$h_\sigma^\pm(E) = \tanh\left(\frac{E \pm eV_\sigma}{2T_\sigma}\right). \tag{3.145}$$

[11] A hole in the spin-up band has physical spin-down.

[12] When we say a hole has spin σ, we generally mean a missing electron of spin σ, meaning that the *physical* spin is opposite.

We can then define the averaged quantities of *voltage* $V \equiv (V_\uparrow + V_\downarrow)/2$ and *temperature* $T \equiv (T_\uparrow + T_\downarrow)/2$, and the relative quantities of *spin voltage* $V_s \equiv (V_\uparrow - V_\downarrow)/2$ and *spin temperature* $T_s \equiv (T_\uparrow - T_\downarrow)/2$. In equilibrium, the only non-vanishing quantity is the temperature, and we find that [25]

$$\hat{h}(E) = h_0\hat{\rho}_0 = \tanh\left(\frac{E}{2T}\right)\hat{1}. \tag{3.146}$$

We proceed by defining the spectral weight function for a given spin σ as [75],

$$A_\sigma(\boldsymbol{p}, E) = -\frac{1}{\pi}\Im\{G^R_{\sigma\sigma}(\boldsymbol{p}, E)\}. \tag{3.147}$$

Loosely speaking, the spectral function represents the probability density that a particle with momentum in the range $[\boldsymbol{p}, \boldsymbol{p} + d\boldsymbol{p}]$ has an energy in the range $[E, E + dE]$. The density of states for a particle with spin σ, $N_\sigma(E)$, is found by integrating out the momentum dependence [76],

$$N_\sigma(E) = \int \frac{d\boldsymbol{p}}{(2\pi)^3} A_\sigma(\boldsymbol{p}, E) = -\frac{1}{\pi}\int \frac{d\boldsymbol{p}}{(2\pi)^3}\Im\left\{G^R_{\sigma,\sigma}(\boldsymbol{p}, E)\right\}. \tag{3.148}$$

Inserting the quasiclassical expression from Eq. (3.97), we find that the density of states in the quasiclassical approximation becomes

$$\begin{aligned} N_\sigma(E) &= -\frac{1}{\pi}\int \frac{d\boldsymbol{p}}{(2\pi)^3}\Im\left\{G^R_{\sigma\sigma}(\boldsymbol{p}, E)\right\} \\ &= -\frac{1}{\pi}\int \frac{d\boldsymbol{p}}{(2\pi)^3}\Im\left\{\frac{\pi}{\mathrm{i}}\delta(\xi_{\boldsymbol{p}})g_{\sigma\sigma}(X, \boldsymbol{p}_F, E)\right\} \\ &= N_0\int \frac{d\boldsymbol{e}_F}{4\pi}\int d\xi_{\boldsymbol{p}}\Re\left\{\delta(\xi_{\boldsymbol{p}})g_{\sigma\sigma}(X, \boldsymbol{p}_F, E)\right\} \\ &= N_0\Re\left\{g_{\sigma\sigma}(X, \boldsymbol{p}_F, E)\right\} \end{aligned} \tag{3.149}$$

In situations where we do not care about the spin-resolved density of states, the spin-averaged density of states,

$$N(E) \equiv \frac{1}{2}\left(N_\uparrow(E) + N_\downarrow(E)\right), \tag{3.150}$$

is used.

It can be shown that the quasiclassical spin accumulations is given in terms of the Keldysh components of the Green function as [14, 45, 77]

$$\mu_7(x) = -\int dE\,\frac{N(E)}{N_0}h_7(x, E), \tag{3.151}$$

which measures how much spin can be injected into the material. Similar accumulations can also be found for the other modes. Finally, the charge current $\boldsymbol{j}_4$ and the spin current $\boldsymbol{j}_7$ can be found as [14, 45, 77]

$$\boldsymbol{j}_4(\boldsymbol{R}, E) = \frac{N_0 eD}{16} \int_{-\infty}^{\infty} dE \, \mathrm{Tr}\left\{ \hat{\rho}_4 \left(\check{g} \tilde{\boldsymbol{\nabla}} \check{g} \right)^K \right\} \tag{3.152}$$

$$\boldsymbol{j}_7(\boldsymbol{R}, E) = \frac{N_0 eD}{32} \int_{-\infty}^{\infty} dE \, \mathrm{Tr}\left\{ \hat{\rho}_7 \left(\check{g} \tilde{\boldsymbol{\nabla}} \check{g} \right)^K \right\}, \tag{3.153}$$

where the extra factor of $1/2$ in the spin current is due to the electrons and holes having spin-1/2. We will primarily focus on the electrical current in this thesis, and we will for this reason also use the notation $\boldsymbol{j} \equiv \boldsymbol{j}_4$ for the electrical current.

Chapter 4

Models of Odd-Frequency Superconductivity

In this chapter, we start by solving the Usadel equation in a simple system where odd-frequency superconductivity arises naturally. We discuss symmetries and other properties that the quasiclassical Green functions for odd-frequency superconductivity are expected to satisfy in the context of this simple system. This discussion is then used to make ansatzes for criteria that general quasiclassical odd-frequency Green functions should satisfy, and we make three models for odd-frequency superconductivity satisfying these criteria. We then study the shape of the density of states, the renormalization of the spin-orbit scattering length, and the Meissner response of these properties, comparing with the properties of conventional superconductors.

4.1 Weak odd-frequency proximity effect

In this section, we consider a simple heterostructure, in which odd-frequency superconductivity arises naturally through the proximity effect. This will give us an indication of how the quasiclassical Green function of such a superconductor can look, and indicate which symmetries it satisfies. To this end, we consider a one-dimensional system in the x-direction consisting of a BCS bulk superconductor, two misaligned ferromagnets, and a normal metal. The first ferromagnet is denoted F_1 and has its exchange field pointing in the z-direction, while the second ferromagnet is denoted F_2 and has its exchange field pointing in the x-direction. The ferromagnets are assumed to have exchange fields of equal magnitude h. The electromagnetic fields are assumed to be zero in the entire system, and we assume that the spin-flip scattering and spin-orbit scattering can be neglected. The system is illustrated in Fig. 4.1. Since we are interested in the main characteristic features of the

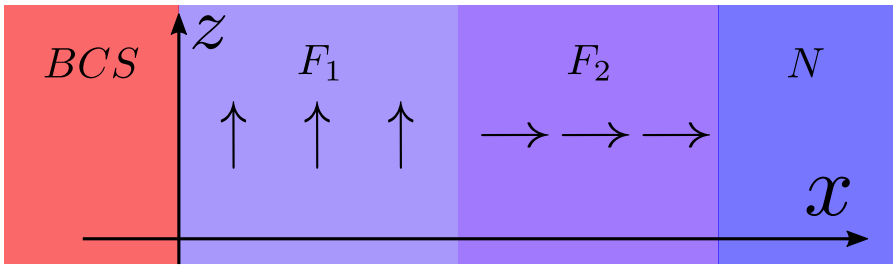

Figure 4.1: The proximity system we solve in the weak proximity regime consists of a superconductor (BCS), two misaligned ferromagnets (F_1 and F_2), and a normal metal (N). The arrows indicate the magnetization direction. The ferromagnets and the normal metal are assumed much longer than the normal metal coherence length.

odd-frequency correlations in this system, such as their energy-symmetry, we will make simplifying assumptions, which will allow for analytical treatment. Firstly, we assume that the boundary between the superconductor and the first ferromagnet allows only for a weak proximity effect. This corresponds to a high resistance interface barrier. This allows us to linearize the Usadel equation, making it a linear differential equation, which can be solved analytically. As another simplifying assumption, we assume that all the materials involved are long compared to the ferromagnetic coherence length $\xi_F = \sqrt{D/h}$ and the normal metal coherence length $\xi_N = \sqrt{D/T}$, such that we can discard exponentially increasing parts of the solutions. We assume that we can solve the Usadel equation in one material, and then use this solution as a boundary condition when solving for the next. These approximations imply that the proximity effect will be extremely weak, but this is tolerable because we are interested in the functional form and the symmetries of the solutions. When we in Chapter 5 study the exact form of the Green functions in a similar proximity structure, a system that produces a stronger proximity effect is chosen. Finally, we assume that the materials are not affected substantially through the inverse proximity effect, such that we can e.g. use the bulk BCS solution as a boundary condition for F_1. The order parameter Δ in the superconductor is assumed to be real, following the discussion in Section 3.2.

4.1.1 Linearization of the Usadel equation and boundary conditions

In the weak proximity effect, the quasiclassical Green functions in the ferromagnets and the normal metal will deviate only slightly from the normal-metal solution $\hat{g}_N^R = \hat{\tau}_3$, which was calculated in Appendix A.2. In the following, we drop the

superscript on the Green functions, keeping in mind that we are solving for the retarded Green functions. We will thus expand the quasiclassical Green function as (dropping arguments of the rest of this section)

$$\hat{g} = \hat{\tau}_3 + \hat{\delta f}, \tag{4.1}$$

where $\hat{\delta f}$ is an off-diagonal matrix. Using the symmetries discussed in Section 3.6.5, we can write this as

$$\hat{\delta f} = \begin{pmatrix} 0 & \underline{\delta f} \\ -\underline{\tilde{\delta f}} & 0 \end{pmatrix}. \tag{4.2}$$

The magnitudes of $\hat{\delta f}$ are assumed to be small, meaning that we can ignore higher-order terms.

The Usadel equation, as stated in Eq. (3.133), can, in the absence of electromagnetic fields and spin-flip and spin-orbit scattering, be written as[1]

$$D\partial_x\big(\hat{g}\partial_x\hat{g}\big) = -\mathrm{i}[E\hat{\tau}_3 + \hat{M}, \hat{g}], \tag{4.3}$$

where we recall that $\hat{M} = \boldsymbol{h}\cdot\mathrm{diag}(\underline{\boldsymbol{\sigma}}, \underline{\boldsymbol{\sigma}}^*)$. In order to solve for the anomalous component, we take the upper right component of Eq. (4.3), yielding

$$D\partial_x^2\underline{\delta f} = -2\mathrm{i}E\underline{\delta f} - \mathrm{i}\left[(\boldsymbol{h}\cdot\underline{\boldsymbol{\sigma}})\underline{\delta f} - \underline{\delta f}(\boldsymbol{h}\cdot\underline{\boldsymbol{\sigma}}^*)\right]. \tag{4.4}$$

For a clear and suggestive notation, we will decompose the anomalous quasiclassical Green function using a singlet-triplet decomposition which is presented e.g. in an article by Jacobsen *et al.* [73],

$$\underline{\delta f} = (f_s + \boldsymbol{d}\cdot\underline{\boldsymbol{\sigma}})\mathrm{i}\underline{\sigma}_2 = \begin{pmatrix} \mathrm{i}d_y - d_x & d_z + f_s \\ d_z - f_s & d_x + \mathrm{i}d_y \end{pmatrix}. \tag{4.5}$$

Under a spin permutation of Eq. (4.5), it can be checked that $\boldsymbol{d}$ is invariant and f_s obtains a negative sign, suggesting that f_s is the spin-singlet component and $\boldsymbol{d}$ are the spin-triplet components.

Using Eq. (4.4), we can isolate the derivative of the singlet component f_s by adding the $(1,2)$ and $(2,1)$ components of Eq. (4.4). Similarly, one can isolate equations for the derivatives d_x, d_y and d_z by adding or subtracting other components. This results in

$$\frac{\mathrm{i}D}{2}\partial_x^2 f_s = Ef_s + \boldsymbol{h}\cdot\boldsymbol{d} \tag{4.6}$$

$$\frac{\mathrm{i}D}{2}\partial_x^2\boldsymbol{d} = E\boldsymbol{d} + \boldsymbol{h}f_s, \tag{4.7}$$

[1]The superconducting gap term of course vanishes in ferromagnets and in normal metals, and the anomalous Green function arises solely due to the proximity effect.

which are four in general coupled linear differential equations, which can be solved analytically.

The KL boundary condition for the right side of an interface is in the same manner found by inserting the expansion in Eq. (4.1) into Eq. (3.136). We denote by the subscript 1 (2) the left (right) material, so that the left-hand side of Eq. (3.136) becomes

$$\frac{1}{\Omega_2}\hat{g}_2\partial_x\hat{g}_2 = \frac{1}{\Omega_2}(\hat{\tau}_3 + \hat{\delta f}_2)\partial_x\hat{\delta f}_2 \approx \frac{1}{\Omega_2}\hat{\tau}_3\partial_x\hat{\delta f}_2, \tag{4.8}$$

where we have included only first-order terms in the small quantity $\hat{\delta f}$ and its derivative, and introduced the quantity $\Omega_j = (2L_j\zeta_j)^{-1}$. The right-hand side of the KL boundary condition becomes

$$[\hat{g}_1, \hat{g}_2] = [\hat{g}_1, \hat{\tau}_3 + \hat{\delta f}] \approx [\hat{g}_1, \hat{\tau}_3] = -2\,\mathrm{antidiag}\Big(\underline{f}_1, \tilde{\underline{f}}_1\Big)\,. \tag{4.9}$$

The upper right component of Eq. (4.8) is $\partial_x\delta\underline{f}_2/\Omega_2$, and for Eq. (4.9) it is $-2\underline{f}_1$, where $\underline{f}_1$ is the upper right component of $\hat{g}_1$. Equating the upper right components produces the linearized Kuprianov-Lukichev boundary conditions,

$$\partial_x\underline{f}_2 = -2\Omega_2\underline{f}_1. \tag{4.10}$$

The normal-derivative has reduced to a derivative in the x-direction because we have assumed a one-dimensional system.

4.1.2 Solving the weak proximity system

We start by shortly discussing the physical interpretation of the solutions to the four coupled differential equations in Eq. (4.6) and Eq. (4.7). For simplicity, we base this discussion on the first ferromagnetic regime of the system, where $\boldsymbol{h} = h\boldsymbol{e}_z$, but the results are easily generalized to an arbitrary magnetization. In this case, the equations for the singlet component f_s and the triplet component d_z are coupled through the exchange term, while the equations for the remaining two triplet components decouple. The decoupled triplet components will follow the same exponential decay as the singlet component does in a normal metal, decaying over distances of $\xi_E = \sqrt{D/E}$. Typically, the energy E is in the same order of magnitude as the temperature, which is much smaller than typical exchange fields. In other words, the perpendicular components d_x and d_y do not "feel" the exchange field, and decay as if the ferromagnet was a normal metal. These are the so-called long-ranged triplet components. The d_z-component, however, is coupled to the magnetic field and the singlet component and will decay with a much shorter decay length on the order of the ferromagnetic coherence length $\xi_F = \sqrt{D/h}$. The d_z-component is thus the so-called short-ranged triplet component in this case.

Generally, it can be shown that the component of $\boldsymbol{d}$ that is parallel with $\boldsymbol{h}$ is short-ranged, while the perpendicular components are long-ranged [73].

Physically, the above discussion is understood by considering the expansion in Eq. (4.5), and noting that the different components of the matrix in spin space correspond to different spin-1 states. d_z has components at the $(1,2)$ and $(2,1)$ matrix elements, meaning that it represents a spin-triplet with spin projection $S_z = 0$ in the z-direction. Similarly, d_x and d_y are seen to represent linear combinations of the $S_z = 1$ and $S_z = -1$ components. Symbolically, we write this as

$$f_s \sim |\uparrow\downarrow\rangle - |\downarrow\uparrow\rangle \quad d_x \sim |\downarrow\downarrow\rangle - |\uparrow\uparrow\rangle \quad d_y \sim |\downarrow\downarrow\rangle + |\uparrow\uparrow\rangle \quad d_z \sim |\uparrow\downarrow\rangle + |\downarrow\uparrow\rangle\,, \tag{4.11}$$

where we have used $|\uparrow\rangle$ and $|\downarrow\rangle$ to represent spin-up and spin-down eigenstates with respect to the z-axis, respectively. When placed in an exchange field along the z-direction, the short-ranged triplet d_z as well as the singlet is broken up by the exchange field through the effect of paramagnetic pair breaking, as discussed in Section 2.1.3. The long-ranged components are not affected by this effect, due to consisting of two spins with equal projection along the z-axis.

We now turn to solving Eq. (4.6) and Eq. (4.7) in F_1. The solutions for are

$$d_j(x) = A_j \mathrm{e}^{kx} + B_j \mathrm{e}^{-kx} \approx B\mathrm{e}^{-kx}, j = \{x, y\} \tag{4.12}$$

$$\begin{aligned} d_z(x) &= C_1\mathrm{e}^{k_- x} + C_2\mathrm{e}^{-k_- x} + C_3\mathrm{e}^{k_+ x} + C_4\mathrm{e}^{-k_+ x} \\ &\approx C_2\mathrm{e}^{-k_- x} + C_4\mathrm{e}^{-k_+ x} \end{aligned} \tag{4.13}$$

$$\begin{aligned} f_s(x) &= -C_1\mathrm{e}^{k_- x} + -C_2\mathrm{e}^{-k_- x} + C_3\mathrm{e}^{k_+ x} + C_4\mathrm{e}^{-k_+ x} \\ &\approx -C_2\mathrm{e}^{-k_- x} + C_4\mathrm{e}^{-k_+ x}, \end{aligned} \tag{4.14}$$

which can be verified by insertion into the equations of motion. Here, we have neglected the exponentially increasing functions, because the length of F_1 is assumed to be large. We have defined the four integration-constants $C_i, i \in \{1,2,3,4\}$, and the variables

$$k = \sqrt{-\frac{2\mathrm{i}E}{D}} \qquad\qquad k_\pm = \sqrt{-\frac{2\mathrm{i}(E \pm h)}{D}}. \tag{4.15}$$

The solutions in F_2, where $\boldsymbol{h} = h\boldsymbol{e}_x$ follows from interchanging $z \leftrightarrow x$.

A simple but tedious calculation, using the linearized KL boundary conditions, reveals that the d_x component of the anomalous Green function in the normal metal is given by[2]

$$d_x(x) = 4\Omega_1\Omega_2\Omega_3 \frac{1}{k^2} f_{BCS} \mathrm{e}^{-k(x-L_1)} \left(\frac{-\mathrm{e}^{-k_- L_1}}{k_-} + \frac{\mathrm{e}^{-k_+ L_1}}{k_+} \right), \tag{4.16}$$

[2]This quantity is independent on L_2 because it decays similarly in F_2 and in the normal metal.

where Ω_i is the transparency for interface i, L_1 is the length of the first ferromagnet, and

$$f_{BCS} = \mathcal{I}\Delta, \tag{4.17}$$

with

$$\mathcal{I} = \frac{\Theta(E^2-\Delta^2)\mathrm{sign}(E)}{\sqrt{E^2-\Delta^2}} - \frac{\mathrm{i}\Theta(\Delta^2-E^2)}{\sqrt{\Delta^2-E^2}}, \tag{4.18}$$

is the upper-right component of the anomalous Green function in a bulk conventional superconductor, which was calculated in Appendix A.3. A similar calculation can be done using transparent boundary conditions, where we assume that the value of the anomalous Green function is unchanged across the boundaries. The result of such a calculation is

$$d_x(x) = f_{BCS}\,\mathrm{e}^{-kx}\left(-\mathrm{e}^{-k_+L_1} + \mathrm{e}^{-k_+L_1}\right). \tag{4.19}$$

Since these expressions diverges as $E \to 0$, and we have assumed a weak proximity effect, the expressions are not valid for small energies, as this would produce a large proximity effect. The solutions in this section will nevertheless serve as inspiration when we discuss symmetries and suggest models for odd-frequency superconductivity in the following sections.

4.2 Criteria for odd-frequency solutions

Motivated by the solution in the last section, we will now look for criteria that we expect the retarded quasiclassical Green function to satisfy in the odd-frequency case. Our goal will be to find models for an odd-frequency superconductor that satisfy these properties, as well as reproduce results that are expected for such superconductors.

4.2.1 Tilde symmetries

We recall that the advanced and retarded quasiclassical Green functions are related through Eq. (C.4), a result that was derived in Appendix C.1. If we now consider the upper right 2×2 components of this equation, we get[3]

$$\underline{f}^A_{\sigma\sigma'}(E) = -\left[\underline{\tilde{f}}^R(E)\right]^\dagger_{\sigma\sigma'} = -\underline{f}^R_{\sigma'\sigma}(-E). \tag{4.20}$$

This relation can be regarded as a generalization of the Pauli principle, including also the possibility of having a pairing that is odd in energy [13]. Since we are

[3]In the general case, where we have not assumed a dirty material, this also includes an inversion in the momentum variable

considering materials in the dirty limit, which display s-wave superconductivity, triplets will be odd in frequency and singlets will be even in frequency. Because the anomalous Green function is symmetric (antisymmetric) when exchanging spin indices for triplets (singlets), we get

$$\underline{f}^A_{\sigma\sigma'}(E) = -\underline{f}^R_{\sigma\sigma'}(-E), \text{ for triplet odd-frequency} \tag{4.21}$$
$$\underline{f}^A_{\sigma\sigma'}(E) = +\underline{f}^R_{\sigma\sigma'}(-E), \text{ for singlet even-frequency.} \tag{4.22}$$

These symmetries, however, do nothing towards our goal of finding criteria for the retarded Green function. Instead, we want to derive symmetries for the retarded Green function directly.

Due to the particle-hole symmetry of quasiclassical theory, we expect that the tilde-conjugation, which essentially interchanges electrons and holes, should leave the magnitude of the quasiclassical Green function unchanged [78]. This corresponds to the magnitude of the quasiclassical Green functions being symmetric in energy. Thus, we expect at most a phase factor to appear under an application of the tilde operator,

$$\tilde{\underline{g}}^R = \mathrm{e}^{\mathrm{i}\gamma_g}\underline{g}^R \tag{4.23}$$
$$\tilde{\underline{f}}^R = \mathrm{e}^{\mathrm{i}\gamma_f}\underline{f}^R, \tag{4.24}$$

where γ_g and γ_f are real quantities. From the BCS solution in Eq. (A.23) with a real superconducting gap, we have

$$\tilde{\underline{g}}^R_{\mathrm{BCS}} = +\underline{g}^R_{\mathrm{BCS}} \tag{4.25}$$
$$\tilde{\underline{f}}^R_{\mathrm{BCS}} = -\underline{f}^R_{\mathrm{BCS}}, \tag{4.26}$$

and the same symmetries can easily be shown to also hold in an SN proximity structure. In an SF-structure, such as the one we solved for in the last chapter, we find that the singlet component $f_{s,F}$ and the triplet components $\boldsymbol{d}_F$ satisfy different symmetries,

$$\tilde{f}^R_{s,\mathrm{F}} = -f^R_{s,\mathrm{F}} \tag{4.27}$$
$$\tilde{\boldsymbol{d}}^R_{\mathrm{F}} = \boldsymbol{d}^R_{\mathrm{F}}, \tag{4.28}$$

while the normal Green function still satisfies $\tilde{\underline{g}} = \underline{g}$. This can be seen from Eq. (4.16) and Eq. (4.14), by noting that $\tilde{k}_+ = k_-$ and that $\tilde{k} = k$. That the normal Green function is invariant under tilde conjugation also makes sense from a physical standpoint, since we expect the density of states, which we recall is given as the real part of $\underline{g}$, to be symmetric in energy, again because of the particle-hole

symmetry of quasiclassical theory. Moreover, when we solve numerically for a more complicated proximity structure in Chapter 5, we find the same symmetries hold[4]. Motivated by the discussion above, and the symmetries of the actual solution for the odd-frequency anomalous Green function in a proximity structure, we make the following ansatz,

Criterion 1 *For a superconductor with a real gap,*

$$\tilde{\underline{g}}^R = \underline{g}^R \qquad \tilde{\underline{f}}^R = -\underline{f}^R \tag{4.29}$$

holds for singlet even-frequency paring, while

$$\tilde{\underline{g}}^R = \underline{g}^R \qquad \tilde{\underline{f}}^R = \underline{f}^R \tag{4.30}$$

holds for triplet odd-frequency pairing.

Later, this criterion will be vital when we make ansatzes for models of odd-frequency superconductors. If a generalization to a complex gap is needed, we will in analogy with the BCS solution simply add an extra phase factor to the anomalous Green function, or the order parameter, after using the above criterion.

4.2.2 Normalization

As discussed in Section 3.6.4, the quasiclassical Green function is assumed to be normalized, which we state as a second criterion,

Criterion 2 *The quasiclassical Green function is normalized, satisfying*

$$\underline{g}^2 - \underline{f}\tilde{\underline{f}} = \underline{1}. \tag{4.31}$$

When we later postulate models for the anomalous Green function, Eq. 4.31 will serve as the definition of the normal Green function $\underline{g}$, and we will then choose the sign in such a way as to give a positive density of states.

4.2.3 Sum rule of the spectral weight

A third criterion can be found by considering the spectral weight function defined in Eq. (3.147). Normally, the spectral weight satisfies the sum rule,

$$\int_{-\infty}^{\infty} dE A_\sigma(\boldsymbol{p}, E) = 1, \tag{4.32}$$

[4]This can be seen from Fig. 5.5a.

which can be shown e.g. from the Lehmann representation, as is done in [76]. Physically, this means that the probability of an electron with momentum $\boldsymbol{p}$ to be in any state is 1. In the quasiclassical approximation, however, we essentially assume that all states have momentum the Fermi momentum $\boldsymbol{p}_F$, meaning that the integral over any other momentum than the Fermi momentum vanishes, while for the Fermi momentum the integral becomes infinite. Thus, we will need to modify the sum rule for the spectral weight. We demand that the sum over the spectral weight should be the same for all systems, and compare the general case with the normal-metal case, where $\underline{g}^R = \underline{1}$, which was shown in Appendix A.2. We take the integral to go from $-\omega_0$ to ω_0, and take the limit as ω_0 goes to infinity,

$$\lim_{\omega_0\to\infty}\int_{-\omega_0}^{\omega_0} dE\,\Re\left\{\delta(\xi_{\boldsymbol{p}})g^R_{\sigma\sigma}(E,X,\boldsymbol{p}_F)\right\} = \lim_{\omega_0\to\infty}\int_{-\omega_0}^{\omega_0} dE\,\Re\left\{\delta(\xi_{\boldsymbol{p}})\right\}. \tag{4.33}$$

Finally, we integrate over momentum to remove the delta functions and average the quasiclassical Green function over the Fermi surface, using the approximation from Eq. (3.100). Moving all quantities to the left-hand side, and using that the particle-hole symmetry of quasiclassical theory implies a symmetric density of states, we can use the expression for the density of state in Eq. (3.149) to state the third criterion,

Criterion 3 *The normalized number of states is the same for all systems,*

$$\int_0^\infty dE\,\left\{\frac{N_\sigma(E)}{N_0} - 1\right\} = 0. \tag{4.34}$$

This criterion will be referred to as the criterion for conservation of the number of states in the following.

4.2.4 Vanishing pairing for large energies

As a final criterion, we expect the superconducting pairing to disappear for large energies, in analogy with the BCS pairing. Thus, we require

Criterion 4 *The superconducting pairing vanishes at energies far from the Fermi surface,*

$$\lim_{|E|\to\infty} \underline{f}(E) = 0. \tag{4.35}$$

Again, this can be seen to hold for our solutions of the proximity system in Eq. (4.16) and Eq. (4.19), as well as for the numerical solution of a realistic proximity system

in Chapter 5. Note that criterion fits well with the criterion in Eq. (4.34) since when the anomalous Green function vanishes for large energies, we get

$$\underline{g} = \underline{1}, \tag{4.36}$$

meaning that the normalized density of states becomes unity. This is required, but not sufficient for the criterion in Eq. (4.34) to hold; we also need e.g. that the integrand goes to zero fast enough for the integral in Eq. (4.34) to converge.

4.3 Models for odd-frequency Green functions

The exact pairing in an odd-frequency superconductor is difficult to derive from first principles, as the time dependence, which is antisymmetric, cannot be neglected in the way it is in e.g. BCS theory [13]. Instead, in a recent article, Johnsen and Linder [14] suggested a model of odd-frequency superconductivity where the quasiclassical Green functions were assumed to be on a BCS-like form, with the only difference being that the gap was assumed to be an odd function of energy. This causes the tilde-symmetry criterion in Eq. (4.30) to hold for such a model. This produced a density of state that at the Fermi energy was peaked for some parameter choices and gapped for others. The peaked models suggested in [14] did, however, display a density of states larger than one for all energies, thus not satisfying the criterion in Eq. (4.34). Moreover, the density of states for the gapped models was not conserved either. Although it was argued that this problem could be circumvented by flanking the density of states at large energies, it would still be useful to find a model that satisfies all criteria that are required for the actual quasiclassical Green function. To this end, we will in this chapter make ansatzes for simple models that satisfy the four criteria from the last section, while also being on a simple form resembling what was found in Section 4.1. We will then move on to study the physical implications of the models; whether the density of states is peaked or gapped, the resilience to spin-flip and spin-orbit scattering, and the sign of the Meissner response. These results will be compared with the conventional superconductor case, as well as the model in [13].

For the tilde symmetry from Eq. (4.30) to hold, a general anomalous Green function for a pure d_z triplet component can be written

$$\underline{f}(E) = [\mathcal{S}(E) + \mathrm{i}\mathcal{A}(E)]\,\underline{\sigma}_1, \tag{4.37}$$

where $\mathcal{S}$ and $\mathcal{A}$ are real functions that are symmetric and antisymmetric in energy, respectively. The normal Green function is found from the normalization condition,

and using the tilde symmetry of the odd-frequency solution, this becomes[5]

$$\underline{g} = \sqrt{\underline{1} + \underline{f}\underline{\tilde{f}}} = \underline{1}\sqrt{1+f^2} = \underline{1}\sqrt{1 - \mathcal{A}(E)^2 + \mathcal{S}(E)^2 + 2\mathrm{i}\mathcal{S}(E)\mathcal{A}(E)}. \tag{4.38}$$

This means that for g to follow the conservation of states criterion in Eq. (4.34), we must have that $\mathcal{S}$ and $\mathcal{A}$ are both nonzero[6]. This is the reason the peaked model in [14], which was real for all energies, does not satisfy this criterion.

A huge amount of different functions $\mathcal{S}$ and $\mathcal{A}$ can be chosen, and they must be chosen such that the spectral weight criterion holds. In analogy with the solution in Section 4.1, as well as the discussion to come in Chapter 5, we will let most of these solutions keep a factor of f_{BCS}, making many of the calculations more convenient, as well as being physically relevant. The models will thus in no way exhaust the different types of odd-frequency pairings, but rather serve as simple models that exhibit different physics.

4.3.1 Model 1: A BCS-like model with a symmetric function

Motivated by the analytic solution in the weak proximity case we found in Section 4.1 we use the BCS solution f_{BCS}, which of course has the appropriate symmetries for a singlet superconductor, and guess the solution

$$\underline{f}(E) = \mathrm{i}\mathcal{S}(E) f_{\mathrm{BCS}}(E)\underline{\sigma}_1, \tag{4.39}$$

where $\mathcal{S}(E)$ is a symmetric function in energy, and where we have also shifted the matrix structure in order to have only a d_z triplet component. We restrict $\mathcal{S}(E) \in \Re$, which means that this anomalous Green function satisfies the tilde symmetry relation in Eq. (4.30). If needed, one could let $\Delta \to |\Delta|\mathrm{e}^{\mathrm{i}\phi}$, to generalize to the complex case, but unless stated otherwise we will in the following assume Δ to be real[7]. This anomalous Green function vanishes for large energies, satisfying Eq. (4.35). We find the corresponding normal Green function by using the normalization condition in Eq. (4.31),

$$\begin{aligned}\underline{g} &= \sqrt{\underline{1} + \underline{f}^2} = \sqrt{1 - \mathcal{S}(E)^2\Delta^2\mathcal{I}^2}\underline{1} \\ &= \sqrt{1 - \mathcal{S}(E)^2\frac{\Delta^2}{E^2-\Delta^2}}\underline{1} = \sqrt{\frac{E^2 - (1+\mathcal{S}(E)^2)\,\Delta^2}{E^2-\Delta^2}}\underline{1},\end{aligned} \tag{4.40}$$

[5] From this equation, we note that even if we included an extra phase factor in f, this would cancel in this expression.

[6] If both are zero, we obtain the trivial normal metal solution.

[7] In this model as well as Model 3, Δ will sometimes be called the "gap" or "order parameter", but note that these models do not, in general, have gaps for $|E| < |\Delta|$, as the BCS solution has.

where we chose the positive root in order for the solution to reduce to a normal-metal solution in the case of $\Delta \to 0$[8]. It is easily seen that this function is peaked at zero energy and that it is larger than unity for $E < \Delta$. This quantity is purely real for energies $|E| < |\Delta|$ and $|E| > \sqrt{1+\mathcal{S}(E)}|\Delta|$, and purely imaginary in between. This means that if we want a model without a gap in the density of states, we must choose $\mathcal{S}$ such that it satisfies $\mathcal{S}(\Delta) = 0$. For this model to satisfy all criteria in Section 4.2, we only need to choose a function $\mathcal{S}(E)$ that causes the number of states to be conserved for all choices of Δ.

Model 1a Constant symmetric function

For concreteness, we will consider a specific choice of the symmetric function $\mathcal{S}(E)$, namely that of a real constant, $\mathcal{S}(E) = a \in \Re$. The real part of the normal Green function is, for a choice of $a = 1$, shown in Fig. 4.2, together with the BCS density of states. In order to use this model for other systems, where the meaning of the

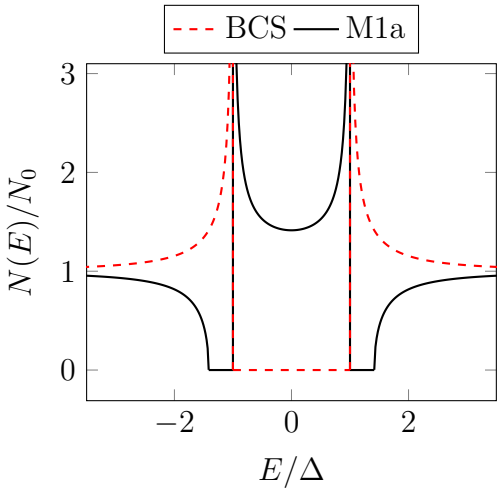

Figure 4.2: The density of states for a BCS superconductor and for Model 1a (M1a) with $a = 1$. See the main text for details.

factor Δ that appears in the f_{BCS}-factor is unclear, we can use it as a curve-fitting parameter, determining the width of the density of states in the system.

We now proceed to show that this model satisfies the criterion in Eq. (4.34). To this end, it will be convenient to substitute a new variable $b \equiv \sqrt{1+a^2}$. Inserting the expression in Eq. (4.40) into the left-hand side of the criterion in Eq. (4.34),

[8]Another justification for this choice is only the positive root produces a positive density of states.

and splitting the integrand into three parts, we find

$$\Delta \int_0^\infty dE' \left\{ \Re \left\{ g \right\} - 1 \right\} = \Delta \int_0^1 dE' \left\{ \sqrt{\frac{b^2 - E'^2}{1 - E'^2}} - 1 \right\} \tag{4.41a}$$

$$- \Delta \int_1^b dE' \left\{ 1 \right\} \tag{4.41b}$$

$$+ \Delta \int_b^\infty dE' \left\{ \frac{\sqrt{E'^2 - b}}{\sqrt{E'^2 - 1}} - 1 \right\}, \tag{4.41c}$$

where we have introduced the integration variable $E' \equiv E/\Delta$. The first term in Eq. (4.41a) is an elliptic integral, and the term can be shown to equal

$$\Delta \left(\mathcal{E} \left(\frac{1}{b} \right) b - 1 \right). \tag{4.42}$$

Here, we have introduced the complete elliptic integral of second kind as[9]

$$\mathcal{E}(k) \equiv \mathcal{E}(1, k), \tag{4.43}$$

where we have used the incomplete elliptic integral of the second kind,

$$\mathcal{E}(x, k) \equiv \int_0^x dt \sqrt{\frac{1 - k^2 t^2}{1 - t^2}}. \tag{4.44}$$

The term in Eq. (4.41b) is trivial and becomes $-\Delta(b - 1)$. For the term in Eq. (4.41c), a mathematical software can be used to show that it equals

$$\Delta \left(\mathcal{F}(b)\, b^2 - \mathcal{E} \left(\frac{1}{b} \right) b - \mathcal{E} \left(b, \frac{1}{b} \right) b + \mathcal{E}(b) - \mathcal{F}(b) + b \right), \tag{4.45}$$

where we have used the complete integral of first kind,

$$\mathcal{F}(k) \equiv \mathcal{F}(1, k), \tag{4.46}$$

given in terms of its incomplete counterpart,

$$\mathcal{F}(x, k) \equiv \int_0^x dt \frac{1}{\sqrt{(1 - k^2 t^2)(1 - t^2)}}. \tag{4.47}$$

Adding the results for the three terms, we find that the result becomes

$$\Delta \left(\mathcal{F}(b)\, b^2 - \mathcal{E} \left(\frac{1}{b} \right) b + \mathcal{E}(b) - \mathcal{F}(b) \right). \tag{4.48}$$

This expression is difficult to simplify symbolically, but by evaluating it for different values of b, it can be shown that it is identically zero for all values of b. Thus, this model does in fact satisfy all our criteria for odd-frequency quasiclassical Green functions.

[9] The reader is directed to [79] for a discussion of elliptic integrals.

Adding inelastic scattering

In order to remove the divergences at the gap edge, we add the effects of inelastic scattering through the Dynes approximation [80, 78], which was first used by Dynes *et al.* [81]. We thus let $E \to E + \mathrm{i}\epsilon\Delta$, where ϵ is the inelastic scattering parameter. This approximation yields good results for the effect on the density of states but does not capture the inelastic scattering effect for energy mode decays [78]. Since we are mainly interested in the spectral quantities such as the density of states for this model, we will employ this approximation. For small values of ϵ, this has the effect of "smoothing" out the divergences. We note that the density of states of Model 1a, as shown in Fig. 4.2, has an unconventional form. If we, however, treat the Dynes parameter ϵ as a general cure-fitting parameter, we can make the density of states look more like the one obtained from the realistic system where odd-frequency arises naturally, as we will find in Chapter 5. The density of states for different choices of ϵ is shown in Fig. 4.3. If we also treat the order parameter Δ as a general parameter, we find that the result is a density of states where the width can be adjusted by changing Δ, the height can be changed by changing a and ϵ. We emphasize that using Δ and ϵ in this manner is nothing more than a way of curve-fitting Model 1a to systems. From a numerical integration, it can also be seen that the number of states is still conserved, making the four criteria hold in this case as well.

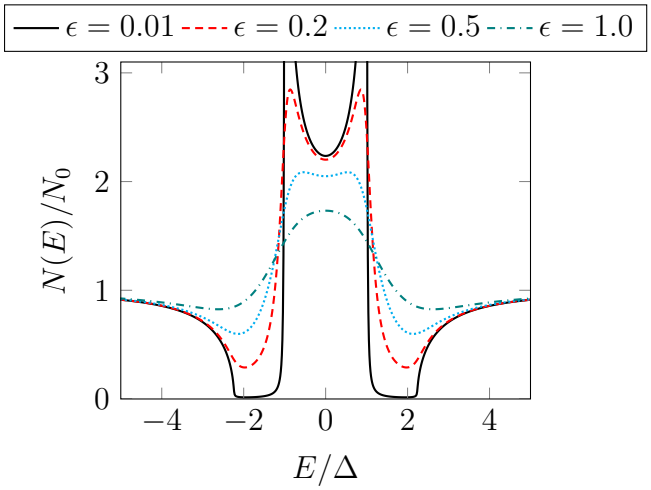

Figure 4.3: The density of states for Model 1a with $a = 2$ for different Dynes inelastic scattering parameters ϵ. See the main text for details.

4.3.2 Model 2: A step function model

We suggest an even simpler model which also satisfies the symmetry relations for a real order parameter superconductor, and which has a peaked density of states that roughly resembles what we will find in the realistic proximity system in Chapter 5. We propose the anomalous Green function

$$\underline{f} = f\underline{\sigma}_1, \tag{4.49}$$

with

$$f = \Theta(a^2 - E^2)c + \mathrm{isgn}(E)\Theta(E^2 - a^2)\Theta(b^2 - E^2)d, \tag{4.50}$$

where a, b, c, d are real parameters, and we restrict $|d| < 1$. It is easy to check that this function satisfies the criteria for the tilde symmetries and the vanishing anomalous Green functions in Eq. (4.30) and Eq. (4.35). The normal Green function becomes

$$\underline{g} = g\underline{1}, \tag{4.51}$$

with

$$g == c_2\Theta(a^2 - E^2) + d_2\Theta(E^2 - a^2)\Theta(b^2 - E^2) + \Theta(E^2 - b^2), \tag{4.52}$$

where we introduced the parameters $c_2 \equiv \sqrt{1 + c^2}$ and $d_2 \equiv \sqrt{1 - d^2}$ for later convenience. This function is real for all possible values of the parameters, since we restricted $|d| < 1$. The density of states is equal to the Green function and is plotted in Fig. 4.4. Using basic geometry it is then easy to see that we must require that the parameters satisfy

$$b = a\sqrt{1 + c^2} + (b - a)\sqrt{1 - d^2}, \tag{4.53}$$

in order for the number of states to be conserved. In other words, we must choose 3 free independent parameters to vary, and the last parameter is set by Eq. (4.53). Which parameters we want to be free may depend on the system we want to fit the distribution to. In the following, we take b to be the dependent parameter, satisfying

$$b = \frac{a\sqrt{1 + c^2} - a\sqrt{1 - d^2}}{1 - \sqrt{1 - d^2}}. \tag{4.54}$$

The density of states is shown in Fig. 4.4 for a particular choice of parameters.

4.3.3 Model 3: A BCS-like model with an antisymmetric function

As we will see later, Model 1 produces a Meissner effect that is consistent with that of induced odd-frequency superconductivity in a heterostructure, but does not

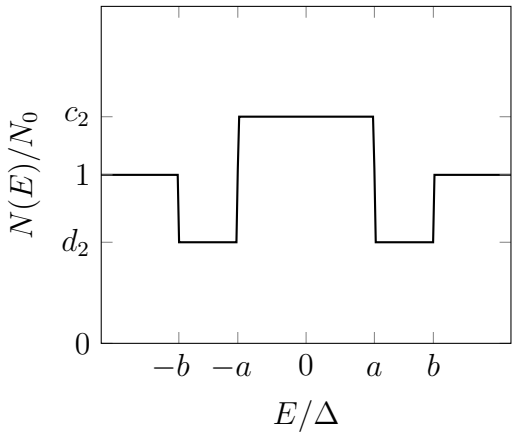

Figure 4.4: The density of states for Model 2. See the main text for details.

give a stable solution for a bulk superconductor, a topic which will be explained in more detail in Section 4.5.1. For this reason, we suggest a third model,

$$\underline{f}(E) = \mathcal{A}(E) f_{\mathrm{BCS}} \underline{\sigma}_1, \tag{4.55}$$

where $\mathcal{A}$ is a real antisymmetric function, thus satisfies the tilde conjugation relation that is appropriate for the odd-frequency case. As a side note, we notice that using

$$\mathcal{A}(E) = \frac{\Delta(E)\mathcal{I}_2(E)}{f_{\mathrm{BCS}}}, \tag{4.56}$$

with

$$\mathcal{I}_2 = \frac{\mathrm{sign}(E)\,\Theta(E^2 - |\Delta(E)|^2)}{\sqrt{E^2 - |\Delta(E)|^2}} - \frac{\mathrm{i}\Theta(|\Delta(E)|^2 - E^2)}{\sqrt{|\Delta(E)|^2 - E^2}}, \tag{4.57}$$

with an antisymmetric function $\Delta(E)$, we get the model that was used in [14]. This model gives simple expressions that resemble the BCS solution, but does not in general satisfy the conservation of the number of states for the choices of $\Delta(E)$ that was used in the paper. We define the normal Green function through the normalization condition,

$$\underline{g} = \sqrt{\underline{1} + \underline{f}\underline{\tilde{f}}} = \sqrt{1 + \Delta^2 \mathcal{A}(E)^2 \mathcal{I}^2}\underline{1} = \sqrt{\frac{E^2 - \Delta^2(1 - \mathcal{A}(E)^2)}{E^2 - |\Delta|^2}}\underline{1}. \tag{4.58}$$

From Eq. (4.58), we see that the density of states for this model is nonzero for energies $|E| < |\Delta|\sqrt{1 - \mathcal{A}(E)^2}$, zero for $|\Delta|\sqrt{1 - \mathcal{A}(E)^2} < |E| < \Delta$, and then nonzero again for $|E| > |\Delta|$. We also see that the density of states is never peaked at the Fermi energy since the numerator is always smaller than the denominator at low energies.

Model 3a: Sign function

For concreteness, we will in the following consider the antisymmetric function

$$\mathcal{A}(E) = \alpha \,\mathrm{sign}(E) \tag{4.59}$$

where α is a positive real number. This produces

$$\underline{g} = \sqrt{\frac{E^2 - \Delta^2(1-\alpha^2)}{E^2 - |\Delta|^2}}\underline{1}, \tag{4.60}$$

which for $\alpha \geq 1$ produces the same gap in the density of states as in a BCS superconductor. Initially, this result may seem to be at odds with that the general result that systems with odd-frequency pairing should have a density of states larger or equal to one at $E = 0$, as was derived in Appendix C.2. This apparent paradox is understood by noting that for the Green functions to be continuous, we should demand that the sign function in Eq. (4.59) goes to zero for small energies. This causes the density of states to be nonzero in a narrow peak around $E = 0$. However, since we can choose this peak to be arbitrarily narrow, and since the height of the peak is finite, the contribution to the density of states vanishes, and we can ignore this peak in the following. The same holds also for other choices of $\mathcal{A}(E)$ that produce a gap at the Fermi energy[10]. From Eq. (4.60), we recognize the $\alpha = 1$ case as the exact BCS solution for the normal Green function. The sum rule of the spectral function is thus inherited for this model with $\alpha = 1$ as well. It is then obvious that since $\alpha > 1$ gives a density of states higher than this at all energies, the number of states cannot be conserved, and thus we must demand $\alpha \leq 1$ for the solution to satisfy the criteria in Section 4.2.

For $\alpha < 1$ we find the density of states,

$$\underline{g} = \sqrt{\frac{E'^2 - \beta^2}{E'^2 - 1}}\underline{1}, \tag{4.61}$$

where we have introduced $\beta = \sqrt{1-\alpha^2}$, and again used the notation $E' = E/\Delta$. This is real for $|E'| < \beta$, imaginary for $\beta < |E'| < 1$, and real again for $|E| > 1$. The density of states for two values of β is shown in Fig. (4.5). We note that this is the same integral as for Model 1, and one can show, that the number of states is conserved for this model as well. Thus, this model also satisfies all criteria for odd-frequency superconductors. It does, however, have a density of states at $E = 0$ smaller than unity for all choices of β. By adding a large Dynes inelastic scattering parameter, as we did for Model 1a, the density of states is changed, but still smaller than unity for $E = 0$. A plot showing the density of states for $\beta = 0.8$ and different Dynes parameters is shown in Fig. 4.6.

[10]This includes the model used in [14].

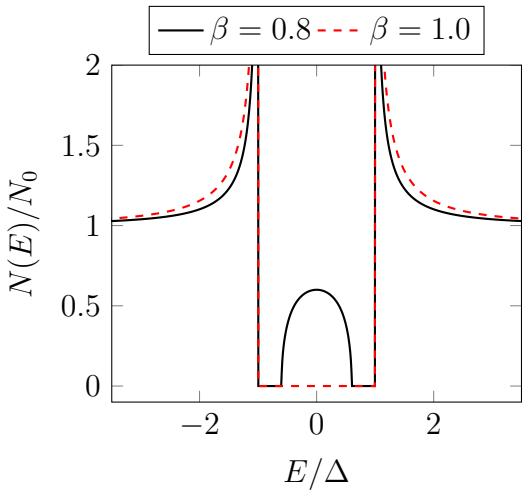

Figure 4.5: The density of states for Model 3a for different values of β. See the main text for details.

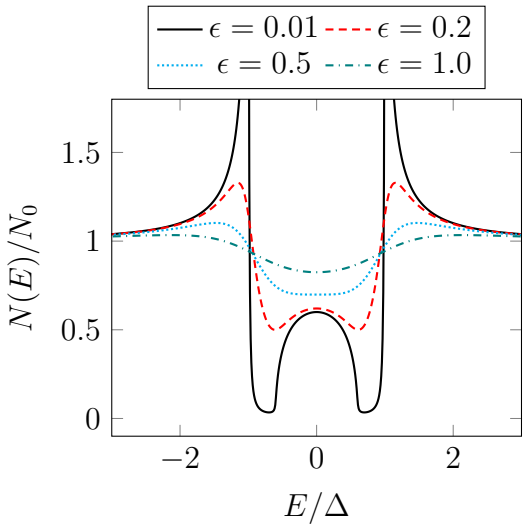

Figure 4.6: The density of states for Model 3a with $\beta = 0.8$ for different Dynes inelastic scattering parameters ϵ. See the main text for details.

4.4 Spin mode renormalization

We proceed by considering a bulk odd-frequency superconductor that has the form of the models in the last section. We apply a spin-voltage to such a system and calculate how the spin mode is affected by spin-flip and spin-orbit impurity

scattering in the system. Even if the odd-frequency pairing arises due to the proximity effect in an SF-heterostructure, and thus is a function of position, we can apply the spin-voltage perpendicular to the material, as illustrated in Fig. 4.7, and thus justify using the models from the last section, which are position-independent. Here, we will use the models for odd-frequency superconductors to study the

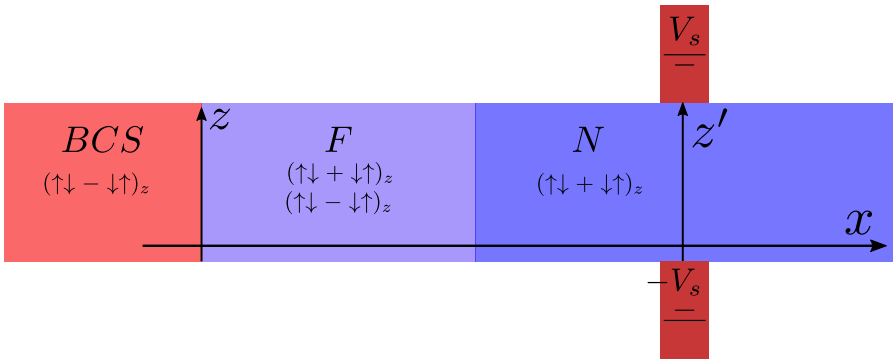

Figure 4.7: The proximity system in consideration. A conventional superconductor (BCS) in contact with a ferromagnet (F) that has a non-homogeneous magnetization that causes the singlets and the triplets with $S_z = \pm 1$ to decay, meaning that there is only an $S_z = 0$ triplet component in the normal metal (N). A spin voltage V_s is applied across the normal metal with induced odd-frequency superconductivity in a narrow area, where the triplet amplitude is constant, thus meaning that we can treat the material as a bulk material in the calculation of the non-equilibrium modes.

spin mode in the system. We will thus not include the effects the spin-flip and spin-orbit scattering has on the equilibrium Green function, but instead study how the non-equilibrium solutions are changed by the scattering. We include a general superconducting term in the self-energy, which would need to be present in a bulk odd-frequency superconducting system.

The Keldysh component of the Usadel equation in the odd-frequency superconductor with spin-flip and spin-orbit scattering reads

$$D\partial_x(\check{g}\partial_x\check{g})^K = -\mathrm{i}\left[\hat{E}\tau_3 + \check{\sigma}_{\mathrm{so}} + \check{\sigma}_{\mathrm{sf}} + \hat{D}^T(E), \hat{g}\right]^K, \tag{4.62}$$

where we have introduced the superconducting self-energy term

$$\hat{D}^T(E) = \mathrm{antidiag}(D(E), D(E), -D(E), -D(E)), \tag{4.63}$$

where the energy dependence of $D(E)$ is unknown for our systems[11]. It is possible to derive the form of the order parameter for each model by working backward from

[11]We have used the notation $D(E)$ for the unknown gap matrix to separate it from the quantity Δ, which is used in our models.

the Usadel equation, but we will here only need the matrix structure, as this will cause the effect on the spin mode decay to vanish. This is consistent with the fact that superconductors display long-range order [14]. This is further justified when we in Chapter 5 use a heterostructure to study odd-frequency superconductivity, and find that the spin modes behave in the same way as in a normal metal when neglecting spin-orbit and spin-flip scattering. For our three models, we can write, in order to get a suggestive form resembling the BCS solution in Eq. (4.18),

$$\underline{f}^R \equiv \mathcal{I}_f \Delta \underline{\sigma}_1 \tag{4.64}$$

$$\underline{g}^R \equiv \mathcal{I}_g E \underline{\sigma}_3, \tag{4.65}$$

meaning that the full retarded Green function can be written

$$\hat{g}^R = \mathcal{I}_g E \hat{\tau}_3 + \mathcal{I}_f \Delta \hat{J}_3, \tag{4.66}$$

where $\hat{J}_3 \equiv \text{antidiag}(1, 1, -1, -1)$.

In a detailed calculation, we show in Appendix F that the Usadel equation can be isolated for the spin mode in such a system. The equation reads

$$\partial_x^2 h^z = \frac{h^z}{D\tau_{\text{sf}}} + \frac{h^z}{D\tau_{\text{so}}} \left(1 + \frac{4\Delta^2 \Re\{\mathcal{I}_f\}^2}{1 + E^2|\mathcal{I}_g|^2 - |\mathcal{I}_f|^2\Delta^2} \right). \tag{4.67}$$

By a similar derivation, but with a singlet gap matrix, it can be shown that the equation of motion only results in a sign swap in the numerators in Eq. (F.26), meaning that we will get

$$\partial_x^2 h^z = \frac{h^z}{D\tau_{\text{sf}}} \left(1 + \frac{4\Delta^2 \Re\{\mathcal{I}_f\}^2}{1 + E^2|\mathcal{I}_g|^2 - |\mathcal{I}_f|^2\Delta^2} \right) + \frac{h^z}{D\tau_{\text{so}}}. \tag{4.68}$$

The results above is consistent with the results found for the specific model in [14]. We can find the normal-metal case by letting $\Delta \to 0$ in Eq. (4.67) or Eq. (4.68), which yields

$$\partial_x^2 h^z \equiv \frac{h^z}{D\tau_{\text{sf}}} + \frac{h^z}{D\tau_{\text{so}}}. \tag{4.69}$$

Comparing this to Eq. (4.67) and Eq. (4.68), we see that we can introduce an energy-dependent effective scattering parameter,

$$\frac{1}{\tau_i^{\text{eff}}} = \frac{1}{\tau_i} \left(1 + \frac{4\Delta^2 \Re\{\mathcal{I}_f\}^2}{1 + E^2|\mathcal{I}_g|^2 - |\mathcal{I}_f|^2\Delta^2} \right), \tag{4.70}$$

where $i = \text{sf}$ for an even-frequency superconductor, and $i = \text{so}$ for an odd-frequency superconductor. Thus, we have shown that for odd-frequency models that can be written in the form in Eq. (4.64), there will be no renormalization of the spin-flip

scattering, while there will be a renormalization of the spin-flip scattering as long as $\Re\{\mathcal{I}_f\} \neq 0$. For an even-frequency singlet superconductor, the roles of spin-flip and spin-orbit scattering is reversed. As a general remark, we thus conclude that for models where Eq. (4.70) holds, we have spin-orbit (spin-flip) renormalization in odd-frequency (even-frequency) systems when the normal Green function has a real part. This is in agreement with results in the literature [50, 82, 14, 18].

It can be seen from the normalization condition in Eq. (4.38), that for a Green function that is either purely real or purely imaginary at each energy, a real normal Green function is associated with an increase in the density of states. For such models, an increase in the density of states at an energy E is associated with a renormalization of the spin-flip scattering for singlet superconductors, and renormalization of the spin-orbit scattering for odd-frequency superconductors. As an example, it was found in [14] that there is spin-orbit renormalization for all energies because a model with a purely real normal Green function was used. In this approximate model, the density of states was also found to be larger than unity for all energies. Another example is the BCS superconductor, which has a spin-flip renormalization and a density of states higher than unity for all energies above the gap. We make the general remark that in order for the number of states to be conserved, the anomalous Green function must, at least in some energy domain, have a nonzero real part[12], causing renormalization of the spin modes for some energies. In the following, we will consider our models from Section 4.3, and evaluate the specific renormalization of the spin-orbit scattering lengths in each case.

4.4.1 Spin mode renormalization in a singlet superconductor

We start by considering the BCS superconductor case, where

$$\mathcal{I}_f = \mathcal{I}_g = \mathcal{I}, \tag{4.71}$$

from which we find that the effective spin-flip scattering length in Eq. (4.70) becomes[13]

$$\frac{1}{\tau_{\text{sf}}^{\text{eff}}} = \frac{1}{\tau_{\text{sf}}}\left[\frac{E^2+\Delta^2}{E^2-\Delta^2}\right] \tag{4.72}$$

[12]The only other possibility is that the anomalous Green function is identically zero, which is the trivial case of a normal metal.

[13]For energies below the gap, we find that both the numerator and denominator of Eq. (F.26) vanishes, meaning that we strictly should go back to Eq. (F.25), and there assume that $E > \Delta$. That is, for energies $E < \Delta$, we do not get any information about the spin mode in the superconductor from Eq. (F.25), as both sides vanish. This works out in the end, because the density of states is zero for the same energies that our equation vanishes for.

This should only be applied for energies above the band gap. We know, however, that for energies below the band gap there are no single-particle states available, and since the spin-singlet does not carry spin, we know that the spin mode only has contributions above the gap. Ultimately, it is the spin accumulation, which also is dependent on the local density of states, which is the observable quantity, and this will get zero contribution from energies below the gap because the density of states here is zero.

From Eq. (4.72), it is seen that the effects of spin-flip scattering become larger compared to a normal metal, making it difficult to sustain a spin mode in such a superconductor with many magnetic impurities. We note that the renormalization effect diverges for $E \to \Delta$, as the spin-flip scattering time τ_{sf} goes to zero.

4.4.2 Spin mode renormalization in Model 1a

In our first model of odd-frequency superconductivity, with the choice $\mathcal{S}(E) = a$, we have

$$\mathcal{I}_f\Delta = \frac{\mathrm{i}a\Delta\text{sign}(E)\,\Theta(E^2-\Delta^2)}{\sqrt{E^2-\Delta^2}} + \frac{a\Delta\Theta(\Delta^2-E^2)}{\sqrt{\Delta^2-E^2}} \tag{4.73}$$

$$\begin{aligned}\mathcal{I}_g E = &\sqrt{\frac{E^2-(1+a^2)\Delta^2}{E^2-\Delta^2}}\left[\Theta(E^2-\Delta^2(1+a^2)) + \Theta(\Delta^2-E^2)\right] \\ &+ \mathrm{i}\,\text{sign}(E)\sqrt{\frac{(1+a^2)\Delta^2-E^2}{E^2-\Delta^2}}\Theta(E^2-\Delta^2)\Theta(\Delta^2(1+a^2)-E^2).\end{aligned} \tag{4.74}$$

Inserting this into our general result in Eq. (4.70), we find that the spin-orbit scattering time becomes

$$\frac{1}{\tau_{\text{so}}^{\text{eff}}} = \frac{1}{\tau_{\text{so}}}\left[1 + \frac{2\Delta^2 a^2\Theta(\Delta^2-E^2)}{\Delta^2-E^2}\right]. \tag{4.75}$$

This expression is valid for energies outside the gap, which in this model is for $1 < |E/\Delta| < \sqrt{1+a^2}$. We conclude that this specific model renormalizes the spin-orbit scattering for energies below the gap, and not for energies above the gap. It is easily seen that the spin-orbit scattering effect is enhanced, meaning that spin modes will decay quicker in systems where spin-orbit scattering is present than in the normal metal or BCS superconductor case. This effect diverges as $E \to \Delta$.

4.4.3 Spin mode renormalization in Model 2

Using the general form of the full Nambu-spin space Green function from Eq. (3.107), we find that the retarded and advanced Green functions for the second model can

be written as

$$\hat{g}^R(E) = \left[\sqrt{1+c^2}\hat{\tau}_3 + c\hat{J}_4\right]\Theta(a^2-E^2) + \Theta(E^2-b^2)\hat{\tau}_3 + \left[\sqrt{1-d^2}\hat{\tau}_3 + \mathrm{i}\,\mathrm{sign}(E)d\hat{J}_4\right]\Theta(E^2-a^2)\Theta(b^2-E^2) \quad (4.76)$$

and $\hat{g}^A = -\hat{g}^R$. Using this, we find

$$\mathcal{I}_g E = \sqrt{1+c^2}\Theta(a^2-E^2) + \sqrt{1-d^2}\Theta(E^2-a^2)\Theta(b^2-E^2) + \Theta(E^2-b^2) \quad (4.77)$$
$$\mathcal{I}_f \Delta = c\Theta(a^2-E^2) + \mathrm{i}d\Theta(E^2-a^2)\Theta(b^2-E^2), \quad (4.78)$$

which can be inserted into the expression for the effective spin-orbit scattering time in Eq. (4.70), producing

$$\frac{1}{\tau_{\mathrm{so}}^{\mathrm{eff}}} = \frac{1}{\tau_{\mathrm{so}}}\left[1 + 2c^2\Theta(a^2-E^2)\right], \quad (4.79)$$

while of course the spin-flip scattering is the same as in the normal metal. Again, we observe a renormalized spin-orbit scattering where the anomalous Green function is real, but this quantity does not diverge at the band edge.

4.4.4 Spin mode renormalization in Model 3a

For the third model, with $\mathcal{A}(E) = \alpha\mathrm{sign}(E)$, we have

$$\mathcal{I}_f \Delta = \frac{\alpha\Delta\Theta(E^2-\Delta^2)}{\sqrt{E^2-\Delta^2}} - \frac{\mathrm{i}\alpha\Delta\mathrm{sign}(E)\,\Theta(\Delta^2-E^2)}{\sqrt{\Delta^2-E^2}} \quad (4.80)$$

$$\mathcal{I}_g E = \sqrt{\frac{E^2-\Delta^2\beta^2}{E^2-\Delta^2}}\left[\Theta(E^2-\Delta^2) + \Theta(\Delta^2\beta^2-E^2)\right] \quad (4.81)$$

$$+ \mathrm{i}\,\mathrm{sign}(E)\sqrt{\frac{1-\frac{\Delta^2}{E^2}\beta^2}{E^2-\Delta^2}}\Theta(E^2-\Delta^2\beta^2)\Theta(\Delta^2-E^2), \quad (4.82)$$

where we again used $\beta = 1-\alpha^2$ to simplify notation. Using this, we find that the spin-orbit scattering time in Eq. (4.70) becomes

$$\frac{1}{\tau_{\mathrm{so}}^{\mathrm{eff}}} = \frac{1}{\tau_{\mathrm{so}}}\left[1 + \frac{2\Delta^2\alpha^2}{E^2-\Delta^2}\Theta(E^2-\Delta^2)\right], \quad (4.83)$$

which diverges as $E \to \Delta$. This is, in contrast to the result for Model 1a, a renormalization for energies outside the gap.

4.5 Meissner response

The Meissner effect is the fundamental property of conventional superconductivity, as we discussed briefly in Section 2.1.2. In this section, we will consider how the Meissner effect arises in a superconductor from the Maxwell equations, before we move on to calculating the Meissner response in our models, comparing them to the response in a conventional superconductor.

4.5.1 Conventional and unconventional Meissner response

We consider the Maxwell equation in the potential formulation, which is derived e.g. in a textbook by Griffiths [28][14],

$$(\boldsymbol{\nabla}^2\boldsymbol{A} - \partial_t^2\boldsymbol{A}) - \boldsymbol{\nabla}(\boldsymbol{\nabla}\cdot\boldsymbol{A} + \partial_t\phi) = -\boldsymbol{j}, \tag{4.84}$$

where $\boldsymbol{j}$ is the electric current. In the following, we will study the Meissner effect in a superconductor in equilibrium, meaning that time-derivatives vanish. Additionally, we know from Section 3.2 that in the London gauge, the magnetic vector potential is divergenceless[15],

$$\boldsymbol{\nabla}\cdot\boldsymbol{A} = 0, \tag{4.85}$$

so that Eq. (4.84) reduces to

$$\boldsymbol{\nabla}^2\boldsymbol{A} = -\boldsymbol{j}. \tag{4.86}$$

We recall from Section 3.2.1 that the London equation, as stated in Eq. (3.20), gives a relation between the magnetic vector potential and the current density, valid for a conventional superconductor. Using this, the Eq. (4.84) reads

$$\boldsymbol{\nabla}^2\boldsymbol{A} = \frac{\boldsymbol{A}}{\lambda_L^2}, \tag{4.87}$$

where we defined the London penetration depth [33],

$$\lambda_L = \sqrt{\frac{m}{e^2 n}}, \tag{4.88}$$

where n can be interpreted as the spin-averaged number of superconducting electrons [33]. This equation has exponential solutions, meaning that magnetic fields are expelled from the bulk of materials, corresponding to a conventional superconducting (perfect) diamagnetic Meissner effect. To see this, we consider a

[14] In our units, we have set the permittivity and permeability to unity.

[15] In for potentials that do not change in time, this requirement is met not only by the Coulomb and London gauge but also the Lorenz gauge.

one-dimensional superconducting system of length L in the x-direction, subject to a constant applied magnetic field strength $\boldsymbol{H} = H_z \boldsymbol{e}_z$, which means that we can choose $\boldsymbol{A} = A_y(x)\boldsymbol{e}_y$. The magnetic field in the superconductor is then given in terms of the magnetization $\boldsymbol{M}$ as [28][16]

$$\boldsymbol{B} = \boldsymbol{H} + \boldsymbol{M} = (1 + \chi)\boldsymbol{H}, \tag{4.89}$$

where we in the second equation have assumed a linear material so that the magnetization is proportional with the magnetic field strength $\boldsymbol{H}$. The proportionality constant χ is the magnetic susceptibility. Letting the edges of the material be at $x = 0$ and $x = L$, we get the following boundary conditions,

$$\frac{dA_y}{dx}(x = 0) = H_z \qquad\qquad \frac{dA_y}{dx}(x = L) = H_z, \tag{4.90}$$

Solving Eq. (4.87) with these boundary conditions, we find

$$A_y(x) = -H_z\lambda_L \frac{\mathrm{e}^{\lambda_L^{-1}L} - 1}{\mathrm{e}^{\lambda_L^{-1}L} - \mathrm{e}^{-\lambda_L^{-1}L}} \mathrm{e}^{-\lambda_L^{-1}x} + H_z\lambda_L \frac{\mathrm{e}^{-\lambda_L^{-1}L} - 1}{\mathrm{e}^{\lambda_L^{-1}L} - \mathrm{e}^{-\lambda_L^{-1}L}} \mathrm{e}^{\lambda_L^{-1}x}. \tag{4.91}$$

The magnetic field, which is exclusively in the z-direction, is then found by taking the derivative of the magnetic vector potential,

$$B_z(x) = H_z \frac{\mathrm{e}^{\lambda_L^{-1}L} - 1}{\mathrm{e}^{\lambda_L^{-1}L} - \mathrm{e}^{-\lambda_L^{-1}L}} \mathrm{e}^{-\lambda_L^{-1}x} + H_z \frac{\mathrm{e}^{-\lambda_L^{-1}L} - 1}{\mathrm{e}^{\lambda_L^{-1}L} - \mathrm{e}^{-\lambda_L^{-1}L}} \mathrm{e}^{\lambda_L^{-1}x} \tag{4.92}$$

For later, we consider also an unconventional response where the current is given as

$$\boldsymbol{j} = \frac{\boldsymbol{A}}{\lambda_L^2}, \tag{4.93}$$

where we for simplicity assume that the proportional factor is the same as in the conventional case. This can be interpreted as a negative density n [83, 84, 85]. This leads to the equation of motion for the vector potential,

$$\boldsymbol{\nabla}^2 \boldsymbol{A} = -\frac{\boldsymbol{A}}{\lambda_L^2}, \tag{4.94}$$

which for the same material as considered above has the oscillating solutions

$$A_y(x) = H_z\lambda_L \sin(\lambda_L^{-1}x) + H_z\lambda_L \frac{\cos(\lambda_L^{-1}L) - 1}{\sin(\lambda_L^{-1}L)} \cos(\lambda_L^{-1}x). \tag{4.95}$$

[16] In our units, with $\mu_0 = 1$, the magnetic field $\boldsymbol{B}$, the magnetic field strength $\boldsymbol{H}$, and the magnetization $\boldsymbol{M}$ is all given in the same units.

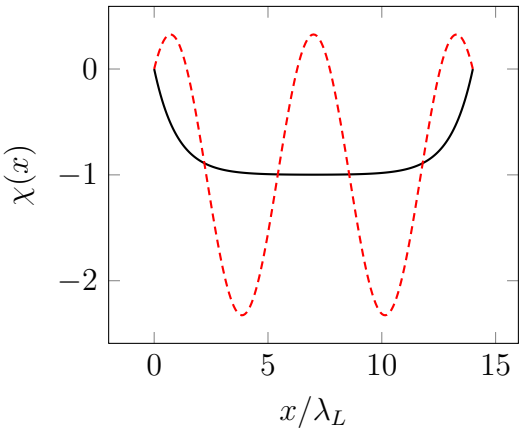

Figure 4.8: The magnetic susceptibility χ of a material with length $L = 14\lambda_L$ with a conventional (solid) and unconventional (dashed) Meissner response. The values of $\chi < -1$ are unphysical. See the main text for details.

The magnetic field again has only a component in the z-direction, and found by differentiating A_y,

$$B_z(x) = H_z \cos(\lambda_L^{-1} x) - H_z \frac{\cos(\lambda_L^{-1} L) - 1}{\sin(\lambda_L^{-1} L)} \sin(\lambda_L^{-1} x). \tag{4.96}$$

The magnetic susceptibility at a given point is given through Eq. (4.89),

$$\chi(x) = \frac{B_z(x)}{H_z} - 1, \tag{4.97}$$

and describes the degree that the material has become magnetized by the external magnetic field. The magnetic susceptibilities for the conventional and unconventional Meissner responses are plotted together in Fig. 4.8. It is seen from the figure that the unconventional Meissner response leads to a magnetic field that oscillates, taking both negative and positive values. Recalling that a paramagnetic (diamagnetic) material has $\chi > 0$ ($\chi < 0$), we note that materials with an unconventional Meissner response can in general display both diamagnetic and paramagnetic behavior, while the system with the conventional Meissner response displays a diamagnetic effect, which fully suppresses magnetic fields in the bulk. For this reason, we will sometimes refer to systems with an unconventional Meissner response as being locally paramagnetic. It is important to note that values of $|\chi| > 1$ indicate an instability in the system, as explained further in an article by Yokoyama *et al.* [84]. For values where $\chi < -1$, we find that the energy density, which in our units can be shown to be $\boldsymbol{B}^2/(1+\chi)$ [28], becomes negative, indicating that the energy can be lowered by increasing the magnetic field. This is an indication of

either a breakdown of the linear response approximation we are using or of a phase transition [84].

In general, the unconventional current response leads to instability in a homogeneous bulk system, but can be found in e.g. superconductor-ferromagnet heterostructures [83, 19, 86], as we will find in Section 5.3.2. Such proximity systems are, however, stabilized by the superconductor in the system, which displays the conventional diamagnetic Meissner effect. For a further discussion of the sign of the Meissner response in odd-frequency systems, the reader is directed to the article by Linder and Balatsky [13].

4.5.2 Quasiclassical Meissner response

In this section, we calculate the electrical current from Eq. (3.152)[17] in the quasiclassical approximation for a bulk material, in order to study the Meissner response of the material. We assume the system to be in equilibrium, where we recall from Eq. (3.146) that the distribution matrix is given as $\tanh(E/2T)\hat{1}$.

In a bulk material the derivative in Eq. (3.152) vanishes, and only the term proportional to $\boldsymbol{A}$ survives,

$$\boldsymbol{j} = -\frac{\mathrm{i}\boldsymbol{A}N_0e^2D}{16}\int_{-\infty}^{\infty} dE\,\mathrm{Tr}\Big\{\hat{\tau}_3\left(\check{g}\big[\hat{\tau}_3,\check{g}\big]\right)^K\Big\}. \tag{4.98}$$

The trace can be simplified as,

$$\begin{aligned}
&\mathrm{Tr}\Big\{\hat{\tau}_3\left(\check{g}\big[\hat{\tau}_3,\check{g}\big]\right)^K\Big\}\\
=&\mathrm{Tr}\big\{\hat{\tau}_3\left(\hat{g}^R\big[\hat{\tau}_3,\hat{g}^K\big]+\hat{g}^K\big[\hat{\tau}_3,\hat{g}^A\big]\right)\big\}\\
=&\tanh\left(\frac{E}{2T}\right)\mathrm{Tr}\big\{\hat{\tau}_3\left(\hat{g}^R\big[\hat{\tau}_3,\hat{g}^R-\hat{g}^A\big]+\left(\hat{g}^R-\hat{g}^A\right)\big[\hat{\tau}_3,\hat{g}^A\big]\right)\big\}\\
=&\tanh\left(\frac{E}{2T}\right)\mathrm{Tr}\Big\{\left(\hat{\tau}_3\hat{g}^R\right)^2-\left(\hat{\tau}_3\hat{g}^A\right)^2\Big\},
\end{aligned} \tag{4.99}$$

where we have assumed the system to be in equilibrium and used the normalization conditions from Eq. (3.104) in the last line. Using the general form of the quasiclassical Green function as shown in Eq. (3.107), together with the identity for the advanced Green function in Eq. (3.109), we find (dropping the "R" superscript on

[17] We here use the matrix $\hat{\tau}_3$ instead of $\hat{\rho}_4$, as they are equivalent.

the 2×2 matrices for simpler notation)

$$\hat{\tau}_3 \hat{g}^R = \begin{pmatrix} \underline{g} & \underline{f} \\ \underline{\tilde{f}} & \underline{\tilde{g}} \end{pmatrix} \tag{4.100}$$

$$\hat{\tau}_3 \hat{g}^A = -\begin{pmatrix} \underline{g}^\dagger & \underline{\tilde{f}}^\dagger \\ \underline{f}^\dagger & \underline{\tilde{g}}^\dagger \end{pmatrix}, \tag{4.101}$$

so that the elements in Eq. (4.99) become

$$\left(\hat{\tau}_3 \hat{g}^R\right)^2 = \begin{pmatrix} \underline{g}^2 + \underline{f}\underline{\tilde{f}} & \underline{g}\underline{f} + \underline{f}\underline{\tilde{g}} \\ \underline{\tilde{f}}\underline{g} + \underline{\tilde{g}}\underline{\tilde{f}} & \underline{\tilde{g}}^2 + \underline{\tilde{f}}\underline{f} \end{pmatrix} \tag{4.102}$$

$$\left(\hat{\tau}_3 \hat{g}^A\right)^2 = \begin{pmatrix} (\underline{g}^\dagger)^2 + \underline{\tilde{f}}^\dagger \underline{f}^\dagger & \underline{g}^\dagger \underline{\tilde{f}}^\dagger + \underline{\tilde{f}}^\dagger \underline{\tilde{g}}^\dagger \\ \underline{f}^\dagger \underline{g}^\dagger + \underline{\tilde{g}}^\dagger \underline{f}^\dagger & (\underline{\tilde{g}}^\dagger)^2 + \underline{f}^\dagger \underline{\tilde{f}}^\dagger \end{pmatrix}. \tag{4.103}$$

We now perform the trace in Eq. (4.99), and using that $\mathrm{Tr}\{\underline{A}\} = \mathrm{Tr}\{\underline{A}^{Tr}\}$, we obtain

$$\begin{aligned} \mathrm{Tr}\left\{\left(\hat{\tau}_3 \hat{g}^R\right)^2 - \left(\hat{\tau}_3 \hat{g}^A\right)^2\right\} &= \mathrm{Tr}\left\{\underline{g}^2 + \underline{f}\underline{\tilde{f}} + \underline{\tilde{g}}^2 + \underline{\tilde{f}}\underline{f} - (\underline{g}^*)^2 - \underline{\tilde{f}}^* \underline{f}^* - (\underline{\tilde{g}}^*)^2 - \underline{f}^* \underline{\tilde{f}}^*\right\} \\ &= 2\mathrm{i}\mathrm{Tr}\left\{\Im\left\{\underline{g}^2 + \underline{f}\underline{\tilde{f}} + \underline{\tilde{g}}^2 + \underline{\tilde{f}}\underline{f}\right\}\right\} \\ &= 4\mathrm{i}\mathrm{Tr}\left\{\Im\left\{\underline{1} + \underline{f}\underline{\tilde{f}} + \underline{\tilde{f}}\underline{f}\right\}\right\} \\ &= 4\mathrm{i}\mathrm{Tr}\left\{\Im\left\{\underline{f}\underline{\tilde{f}} + \underline{\tilde{f}}\underline{f}\right\}\right\}, \end{aligned} \tag{4.104}$$

where we in the third line used the normalization conditions, $\underline{g}^2 = \underline{1} + \underline{f}\underline{\tilde{f}}$ and $(\underline{g}^*)^2 = \underline{1} + \underline{f}^* \underline{\tilde{f}}^*$. In order to simplify the integral further, we note that the equilibrium distribution function $\tanh(E/2T)$ is an antisymmetric function in energy. For an integral with symmetric integration limits, such as in Eq. (4.99), we thus have for an arbitrary function $W(E)$,

$$\begin{aligned} \int_{-\omega}^{\omega} dE \tanh\left(\frac{E}{2T}\right) \tilde{W}(E) &= \int_{\omega}^{-\omega} (-dE) \tanh\left(\frac{-E}{2T}\right) \tilde{W}(-E) \\ &= -\int_{-\omega}^{\omega} dE \tanh\left(\frac{E}{2T}\right) W(E)^*. \end{aligned} \tag{4.105}$$

Using this identity in last term in Eq. (4.104), we write the final expression for the

electric current as

$$\begin{aligned}\boldsymbol{j} &= \boldsymbol{A}\frac{N_0e^2D}{4}\int_{-\infty}^{\infty}dE\,\tanh\left(\frac{E}{2T}\right)\mathrm{Tr}\Big\{\Im\big\{\underline{f}\underline{\tilde{f}}-\underline{f}^*\underline{\tilde{f}}^*\big\}\Big\}\\ &= \boldsymbol{A}\frac{N_0e^2D}{4}\int_{-\infty}^{\infty}dE\,\tanh\left(\frac{E}{2T}\right)\mathrm{Tr}\Big\{\Im\big\{2\mathrm{i}\Im\{\underline{f}\underline{\tilde{f}}\}\big\}\Big\}\\ &= \boldsymbol{A}\frac{N_0e^2D}{2}\int_{-\infty}^{\infty}dE\,\tanh\left(\frac{E}{2T}\right)\mathrm{Tr}\Big\{\Im\big\{\underline{f}\underline{\tilde{f}}\big\}\Big\}\\ &= \boldsymbol{A}\frac{N_0e^2D}{2}I(x),\end{aligned} \tag{4.106}$$

where we for later convenience have defined the integral

$$I(x) = \int_{-\infty}^{\infty}dE\,\tanh\left(\frac{E}{2T}\right)\mathrm{Tr}\Big\{\Im\big\{\underline{f}\underline{\tilde{f}}\big\}\Big\}, \tag{4.107}$$

which will determine whether the Meissner response is conventional or unconventional.

4.5.3 Meissner response in a BCS superconductor

We consider a bulk BCS s-wave superconductor, where we have $\underline{f} = \mathcal{I}\mathrm{i}\Delta\underline{\sigma}_2$, with $\mathcal{I}$ given by Eq. (4.18). Here, we must remember that we have a factor $E \to E + \mathrm{i}\delta$ in the retarded Green function, and $E \to E - \mathrm{i}\delta$ in the advanced Green function, as explained in detail in Appendix A.3. Since $\underline{f}$ was introduced as a part of the retarded Green function, we use the positive energy shift here. We thus get

$$\begin{aligned}\mathrm{Tr}\Big\{\Im\big\{\underline{f}\underline{\tilde{f}}\big\}\Big\} &= 2|\Delta|^2\Im\left\{\frac{1}{(E+\mathrm{i}\delta)^2-|\Delta|^2}\right\}\\ &= 2|\Delta|^2\Im\left\{\frac{E^2-|\Delta|^2-2\mathrm{i}\delta E}{(E^2-|\Delta|^2)^2+4\delta^2E^2}\right\}\\ &= \frac{-4|\Delta|^2E\delta}{4E^2\delta^2+(E^2-|\Delta|^2)^2}\\ &= \frac{-2|\Delta|^2\mathrm{sign}(E)\,\delta'}{\delta'^2+(E^2-|\Delta|^2)^2},\end{aligned} \tag{4.108}$$

where we in the second line ignored the term $\mathcal{O}(\delta^2)$, and $\delta' = 2|E|\delta$ is another positive infinitesimal[18]. This expression has the form of a Lorentzian, which has the property

$$\lim_{\delta\to 0}\frac{\delta}{\delta^2+x^2} = \pi\delta(x), \tag{4.109}$$

[18]It is necessary for the infinitesimal to be positive, otherwise we would have in effect used the negative energy shift corresponding to the advanced Green function.

where $\delta(x)$ is the Dirac delta function. Taking the limit of Eq. (4.108) as the infinitesimal quantity δ' approaches zero, we get

$$\begin{aligned}\lim_{\delta'\to 0}\frac{-2|\Delta|^2\mathrm{sign}(E)\,\delta'}{\delta'^2+(E^2-|\Delta|^2)^2} &= -2\pi|\Delta|^2\mathrm{sign}(E)\,\delta(E^2-|\Delta|^2)\\ &= \frac{-2\pi|\Delta|^2\mathrm{sign}(E)}{|\Delta|}\left[\delta(E-|\Delta|)+\delta(E+|\Delta|)\right],\end{aligned} \tag{4.110}$$

where we in the last line have used the delta function identity

$$\delta(p(x)) = \sum_i \frac{1}{|\partial_x p(x_i)|}\,(x-x_i)\,, \tag{4.111}$$

where x_i are the roots of the polynomial $p(x)$. The current in equilibrium becomes

$$\begin{aligned}\boldsymbol{j} &= -\boldsymbol{A}\pi|\Delta|N_0e^2D\int_{-\infty}^{\infty}dE\,\tanh\left(\frac{E}{2T}\right)\mathrm{sign}(E)\left[\delta(E-|\Delta|)+\delta(E+|\Delta|)\right]\\ &= -\boldsymbol{A}2\pi|\Delta|N_0e^2D\int_{0}^{\infty}dE\,\tanh\left(\frac{E}{2T}\right)\delta(E-|\Delta|)\\ &= -\boldsymbol{A}2\pi|\Delta|N_0e^2D\tanh\left(\frac{|\Delta|}{2T}\right)\\ &= -K_{\mathrm{BCS}}\boldsymbol{A},\end{aligned} \tag{4.112}$$

where we in the second line used that $[\delta(E-|\Delta|)+\delta(E+|\Delta|)]$ is a symmetric function in E[19], and where we in the last line defined the positive quantity K_{BCS}, for which the specific form will not be of relevance to us. The relation $\boldsymbol{j} = -K_{\mathrm{BCS}}\boldsymbol{A}$ means that the supercurrent is a shielding current, as we expect to find in a conventional superconductor that displays the diamagnetic Meissner effect.

4.5.4 Meissner response in Model 1

We now move on to considering the first model of odd-frequency superconductivity, with[20]

$$\underline{f}^R = \mathcal{S}(E)\mathrm{i}\mathcal{I}\Delta\underline{\sigma}_1, \tag{4.113}$$

which means that we get[21]

$$\mathrm{Tr}\Big\{\Im\{\underline{f}\underline{\tilde{f}}\}\Big\} = -2\mathcal{S}(E)^2|\Delta|^2\Im\left\{\frac{1}{(E+\mathrm{i}\delta)^2-|\Delta|^2}\right\}, \tag{4.114}$$

[19]This follows from the Dirac delta function property that $\delta(-x)=\delta(x)$.

[20]We allow the order parameter to be complex in this section.

[21]We assume that we can choose $\mathcal{S}(E)$ in such a way that we do not have to include the energy shift $E\to E+\mathrm{i}\delta$.

which is just $-\mathcal{S}(E)^2$ times the result in Eq. (4.108) the expression in the BCS case. Thus, we can immediately conclude that the current becomes

$$\begin{aligned}\boldsymbol{j} &= \boldsymbol{A}\frac{N_0 e^2 D}{\pi}\int_{-\infty}^{\infty} dE\,\mathcal{S}(E)^2 \tanh\left(\frac{E}{2T}\right)\text{sign}(E)\left[\delta(E-|\Delta|)+\delta(E+|\Delta|)\right] \\ &= K_1\boldsymbol{A},\end{aligned} \tag{4.115}$$

where we have introduced the positive constant K_1 in the last line. This means that we get an unconventional Meissner response for this model. Following the discussion in Section 4.5.1, we see that this suggests that this model could be useful as a model for the odd-frequency behavior in e.g. a proximity system since these can produce a locally paramagnetic Meissner response. This model does, however, not describe a Meissner response that gives a stable system for a bulk superconductor. We note that this also holds for the model presented in [14] since their model is on the form considered here. In an article by Higashitani [87], a possible mechanism for the paramagnetic Meissner response in odd-frequency superconductors was suggested. It was found that the paramagnetic response was associated with a peaked density of states at the Fermi energy, which is exactly the behavior one generally finds for Model 1. This current has the opposite sign compared to the BCS case, as found in Eq. (4.112), in addition to a different constant. For concreteness, we consider Model 1a, with $\mathcal{S}(E) = a \in \Re$. We can then pull a outside the integral in Eq. (4.115), yielding

$$\boldsymbol{j} = K_{BCS}a^2\boldsymbol{A}. \tag{4.116}$$

4.5.5 Meissner response in Model 2

Inserting the expressions for the Green functions of Model 2 into Eq. (4.106) we find that

$$\Im\{f\tilde{f}\} = 0, \tag{4.117}$$

meaning that this model does not give any Meissner response. This suggests that even though a simple model like this can model the density of states and the spin-orbit scattering of a material, it is unable to produce a Meissner effect. More generally, it can be seen that for a model where the imaginary and real parts never overlap, such as the three models we have used in this chapter, and we consider either pure odd-frequency or pure even-frequency amplitudes, an energy shift is required to get a nonzero Meissner response. In models that do not include the energy variable, such as Model 2, Eq. (4.106) will thus vanish. This is because, when the imaginary and the real part does not overlap, and if we do not include an energy shift, we have

$$\Im\{f\tilde{f}\} = \pm\Im\{f^2\} = \pm\Im\{\Re\{f\}^2 - \Im\{f\}^2\} = 0, \tag{4.118}$$

where we have used that $\underline{f}^2 = \underline{1}f^2$ when we have either a system with only one singlet or triplet component, and the upper (lower) sign holds for odd(even)-frequency superconductors with a real gap, according to our criterion in Eq. (4.29) and Eq. (4.30). In systems where the imaginary and real parts overlap, such as the system we consider in Chapter 5, this argumentation does not hold.

4.5.6 Meissner response in Model 3

For the third model, we have that for a general function $\mathcal{A}(E)$,

$$\underline{f} = \mathcal{A}(E)\mathcal{I}\underline{\sigma}_1, \tag{4.119}$$

where we assumed $\mathcal{A}(E)$ to be a real and antisymmetric function in E. Using this model, we get

$$\mathrm{Tr}\Big\{\Im\{f\tilde{f}\}\Big\} = 2\Im\{f^2\} = \mathcal{A}(E)^2\Im\{\mathcal{I}^2\} = 2\mathcal{A}(E)^2\Im\left\{\frac{1}{(E+\mathrm{i}\delta)^2 - |\Delta|^2}\right\}, \tag{4.120}$$

which again is similar to the BCS case with an extra factor of $\mathcal{A}(E)^2$. We thus get that the current becomes

$$\begin{aligned}\boldsymbol{j} &= \boldsymbol{A}\pi N_0 e^2 D \int_{-\infty}^{\infty} dE\, \mathcal{A}(E)^2 \tanh\left(\frac{E}{2T}\right) \mathrm{sign}(E)\left[\delta(E-|\Delta|) + \delta(E+|\Delta|)\right] \\ &= -K_3\boldsymbol{A},\end{aligned} \tag{4.121}$$

where K_3 is a new positive constant. Here, we used that the integrand is symmetric and positive for all energies to conclude that K_3 must be positive as well. This is a diamagnetic Meissner effect, which is a similar response as we get in a BCS superconductor. This also fits well with the article by Higashitani [87], where it was suggested that a peaked density of states was associated with a paramagnetic Meissner effect. The diamagnetic Meissner response means that there is no stability issue when applying this model to a bulk odd-frequency system. In a recent paper, however, Fominov *et al.* [83] studied the coexistence between the diamagnetic and paramagnetic odd-frequency superconducting phases and found that such systems gave rise to unphysical properties. Because the paramagnetic odd-frequency state arises in e.g. proximity systems, as we will see in Section 5.3, it was argued that this state was not realizable in a physical system. For a review of the stability of odd-frequency solutions, the reader is referred to the article by Linder and Balatsky [13].

As a side note, we notice that using the choice $\mathcal{A}(E) = \alpha\mathrm{sign}(E)$ with $\alpha = 1$, we find that the constant K_3 takes the same value as in the BCS case. This model thus

has the same Meissner response and density of states as a BCS superconductor, while at the same time satisfying all of our criteria for an odd-frequency superconductor in Section 4.2. It is an extremely simple model, while also describing a diamagnetic Meissner effect.

Chapter 5

Numerical Solutions of Proximity Systems

The Usadel equation is a nonlinear differential equation, which can only be solved analytically in a few special cases [45]. In this chapter, we introduce parametrizations that can be used to solve the Usadel equation numerically for much more general systems. We start by introducing the Riccati parametrization, which is useful when solving for the retarded Green function. A Python program was written that solves the retarded part of the Usadel equation in a proximity system. We show how the proximity effect gives rise to odd-frequency superconductivity in heterostructures, and design a proximity system that naturally displays only triplet odd-frequency superconductivity. This system is used to compare with our models in Section 4.3, as well as serving as a check of our criteria in Section 4.2.

In a recent article, Johnsen and Linder [14] predicted that the spin-injection in an odd-frequency superconductor can be larger than that in an even-frequency superconductor or even a normal metal, using a model that did not satisfy the sum rule of the spectral weight[1]. In this chapter, we investigate whether we can design a realistic system where this is the case, without violating the sum rule of the spectral weight, which we stated as a criterion in Eq. (4.34). To that end, we will introduce a convenient parametrization of the distribution matrix, which was used to write the Keldysh component of the Usadel equation a convenient and compact form. This parametrization was used to make another Python program, which solves for the distribution matrix in a non-equilibrium system. We also study how the spin-flip and spin-orbit scattering lengths are renormalized in such a system, and discuss how they differ from the model used in [14]as well as our models in Section 4.3. Finally, we also calculate the Meissner response in the system and compare it with our models from Chapter 3

[1]The spectral function and its sum rule was discussed in detail in Section 4.2.

5.1 The Riccati parametrization

Solving the retarded part of the Usadel equation in Eq. (3.133) is in general a difficult task, and analytically one can only hope to find solutions for some very simple systems. In some cases, as was done in Section 4.1, the Green functions can be assumed to deviate little from well-known solutions such as the BCS solution or the normal-metal solution, allowing for linearization and analytical solution. For general systems, one can only hope to achieve numerical solutions. In this chapter, we will introduce the Riccati parametrization, allowing us to write the retarded component of the Usadel equation in a form suitable for numerical calculations. This can be used to solve for the retarded Green function, which describes the equilibrium properties of the system. These can then later be used in the calculation of the distribution matrix, which describes the non-equilibrium properties of the system. We can split the calculation up this way because the distribution function does not enter the calculation of the retarded Green functions in the systems we are considering. If one e.g. wanted to include self-consistent calculations for the order parameter in a superconductor, we would have to solve for the retarded Green functions and the distribution function simultaneously as the self-consistent gap equation leads to mixing between the retarded and the Keldysh components.

The retarded component of the Usadel equation is a 4×4 matrix equation, with in total amounts to 16 components to solve for. However, these components are not all independent. We also have to take into account the normalization conditions in Eq. (3.105). The normalization condition in total has 8 independent equations, meaning that we have 8 remaining free variables to solve for. This is apparent through Eq. (3.107), where we only have the two 2×2 matrices $\underline{g}$ and $\underline{f}$ as independent variables. To exploit the reduced number of variables, we introduce the Riccati parametrization[2], which reduces the Usadel equation to a 2×2 matrix equation with elements that automatically satisfy the normalization conditions. In this section, we will closely follow the work of Jacobsen *et al.* [73], who presents a derivation of the Riccati parametrized Usadel equations and KL boundary conditions, as well as generalizing them to also include spin-orbit coupling. We will not repeat the derivation here, but simply state the most important results and discuss how they simplify in special cases.

The Riccati parametrization is defined by introducing a 2×2 matrix γ. We also introduce the normalization matrix N, which is a normalization matrix given in terms of the independent variables γ and its tilde conjugate $\tilde{\gamma}$ as $N = (\underline{1} - \gamma\tilde{\gamma})^{-1}$. For these matrices, we will drop the bar notation, as there is no ambiguity about the dimensionality. Additionally, since we only use this parametrization to solve

[2]The parametrization gets its name from the fact that it transforms the Eilenberger equation into the differential Riccati equation [45].

for the retarded components of the quasiclassical Green function, we will drop the superscripts indicating the retarded component. We parametrize the retarded quasiclassical Green function as [73]

$$\hat{g} = \begin{pmatrix} N & 0 \\ 0 & -\tilde{N} \end{pmatrix} \begin{pmatrix} \underline{1} + \gamma\tilde{\gamma} & 2\gamma \\ 2\tilde{\gamma} & \underline{1} + \tilde{\gamma}\gamma \end{pmatrix}. \tag{5.1}$$

Comparing with the general expression for the Green function in Eq. (3.107), we find

$$\underline{g} = N(1 + \gamma\tilde{\gamma}) = 2N - \underline{1} \tag{5.2}$$

$$\underline{f} = 2N\gamma, \tag{5.3}$$

where we have used the definition of N to rewrite the first expression. It can easily be checked that these expressions satisfy the normalization conditions automatically. Moreover, the Riccati parametrization has the advantage that the parameters, which are the components of $\gamma, \tilde{\gamma}$, have magnitudes that are bounded in the domain $[0, 1]$. This can be seen heuristically by using the definition of N, and looking at e.g. the anomalous Green function in Eq. (5.3). For very small values of γ and its tilde conjugate, the normalization matrix N becomes close to one, meaning that we find $\underline{f} \approx \underline{0}$. For γ on the order of unity, we find that N becomes huge, meaning that $\underline{f}$ becomes huge as well. Thus, a finite variation of the parameters corresponds to an infinite variation in the quasiclassical Green functions. A similar discussion also holds for the normal Green function in Eq. (5.2). Having such a bounded domain makes the Riccati parametrization a numerically stable parametrization [88].

Usadel equation and KL boundary conditions in the Riccati parametrization

We want to be able to solve the Usadel equation for a ferromagnetic system, in contact with a superconductor via the proximity effect. From the components of the Usadel equation for the retarded component, it can be shown that the corresponding parametrized Usadel equation can be written

$$D\partial_x^2\gamma = -2\mathrm{i}E\gamma - \mathrm{i}\boldsymbol{h} \cdot (\boldsymbol{\sigma}\gamma - \gamma\boldsymbol{\sigma}^*) - 2(\partial_x\gamma)\tilde{N}\tilde{\gamma}(\partial_x\gamma), \tag{5.4}$$

in a ferromagnet in the absence of a magnetic vector potential. The effects of spin-orbit spin-flip scattering have been neglected, and we have also neglected the effects of the magnetic vector potential. The corresponding KL boundary conditions can, for a boundary with coordinate 1 to the left and 2 to the right, be

written as[3]

$$\partial_x \gamma_1 = \Omega_1 \left(1 - \gamma_1 \tilde{\gamma}_2\right) N_2 \left(\gamma_2 - \gamma_1\right) \tag{5.5}$$
$$\partial_x \gamma_2 = \Omega_2 \left(1 - \gamma_2 \tilde{\gamma}_1\right) N_1 \left(\gamma_2 - \gamma_1\right). \tag{5.6}$$

These equations and boundary conditions will allow us to solve the equilibrium part of the Usadel equation in a ferromagnet in contact with another material.

BCS and normal metal solution in the Riccati parametrization

We now proceed to show how the Riccati matrices γ and N look in a bulk BCS superconductor. This will be useful because we will consider systems that are in contact with such superconductors, meaning that the Riccati matrices will enter through the boundary conditions in the last section. Using Eq. (5.2) and the BCS solution from Appendix A.3, we can isolate N,

$$N_{BCS} = \frac{1}{2}(1 + E\mathcal{I})\underline{1}, \tag{5.7}$$

where we recall that

$$\mathcal{I} = \frac{\Theta(E^2 - \Delta^2)\mathrm{sign}(E)}{\sqrt{E^2 - \Delta^2}} - \frac{\mathrm{i}\Theta(\Delta^2 - E^2)}{\sqrt{\Delta^2 - E^2}}. \tag{5.8}$$

Since N_{BCS} is a diagonal matrix it can easily be inverted, meaning that we can isolate γ from Eq. (5.3),

$$\gamma_{BCS} = \frac{1}{2} N_{\mathrm{BCS}}^{-1} \underline{f} = \frac{\Delta \mathcal{I}}{1 + E\mathcal{I}} (\mathrm{i}\underline{\sigma}_2) \tag{5.9}$$

The normal metal solution is easily obtained by letting $\Delta \to 0$, producing $N = \underline{1}$ and $\gamma = \underline{0}$. This indicates that for small proximity effects γ is small, meaning that $N = \underline{1}$ and $\underline{f} = 2\gamma$ to first order in γ. Here, we will instead solve the equations numerically, so that no such approximation is needed.

5.2 Numerical solutions of proximity systems

We introduce different proximity systems with increasing complexity, with the final goal of having a proximity system with pure odd-frequency superconductivity. The goal of this section is not only to introduce the reader to the proximity effect in metals and ferromagnets and to design a system of pure odd-frequency

[3]The two equations are related by performing $1 \leftrightarrow 2$, as well as an extra negative sign arising from the derivative changing direction from $1 \to 2$ to $2 \to 1$.

superconductivity but also to use the results to verify the Python program, which solves the Usadel equation for the retarded quasiclassical Green functions. This will be done by qualitatively checking whether the solutions for the simple systems reproduce characteristic effects from known theory. In this section, we will assume that the superconductor has a temperature $T = 0$, meaning that the order parameter is $\Delta = \Delta_0$. Energies will be given in units of Δ_0, and lengths in units of the superconducting coherence length ξ. The systems we will consider are in contact with a conventional superconductor at $x = 0$ and with the vacuum at $x = L$ We assume that the superconductor is not affected by the inverse proximity effect, meaning that we can use the BCS bulk solution in the boundary conditions.

5.2.1 Superconductor-normal metal (SN) heterostructure

In Section 2.2, we discussed how superconducting properties leak from a superconductor (S) to a normal metal (N), when the materials are put in contact with each other. Inside the normal metal, the Cooper pairing is not energetically favorable due to the mismatch between the energy of electrons and holes in the Andreev reflection at the interface, leading to decaying solutions on distances of order $\xi_E = \sqrt{D/E}$. In Fig. 5.1, the anomalous Green function and the density of states in the normal metal part of an SN heterostructure are shown. The existence of a minigap is clear from Fig. 5.1b, matching well with the theory of SN heterostructures [89].

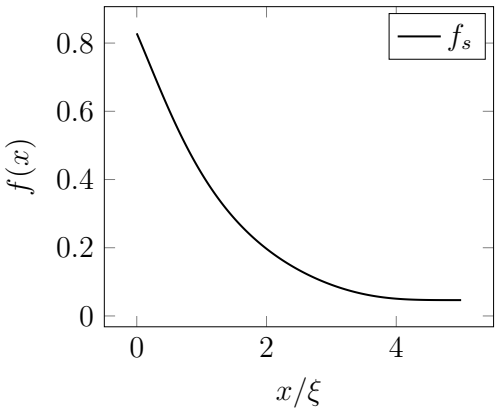

(a) The magnitude of the singlet anomalous Green function for $E = 0.5\Delta_0$.

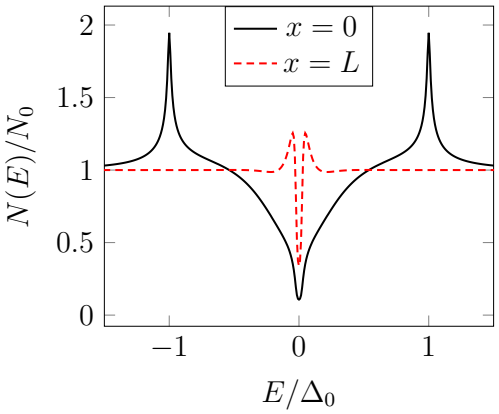

(b) The density of states at different positions.

Figure 5.1: The proximity effect for a normal metal in proximity with a superconductor. The length of the normal metal is $L = 5\xi$, and the SN interface is characterized by $\zeta = 0.1$. See the main text for details.

5.2.2 Superconductor-ferromagnet (SF) heterostructure

If one instead considers the proximity effect in an FS structure, the Cooper pairs will be torn apart even faster, because the paramagnetic effect of pair breaking will destroy Cooper pairs consisting of electrons with different spins. We also expect to find the FFLO effect, as discussed in Section 2.1.3. Fig. 5.2a shows the absolute value of the amplitudes of the singlet component f_s and the triplet component d_z in such a proximity structure, where the strength of the exchange field is $h = 3\Delta_0$. From this figure, we observe the FFLO effect. By comparing Fig 5.2 with Fig. (5.1), we see that the decay length is much smaller in the ferromagnet than in the normal metal, indicating that the effect of paramagnetic pair breaking is present. This is especially clear from Fig. 5.2b, where the minigap that was present in the SN heterostructure has been closed at $x = L$.

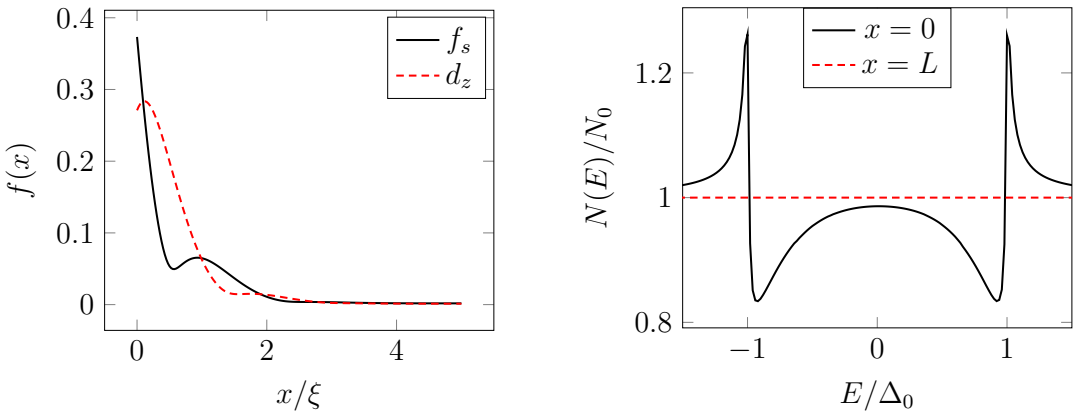

(a) The magnitude of the singlet and the d_z triplet anomalous Green function for $E = 0.5\Delta_0$.

(b) The density of states at different positions.

Figure 5.2: The proximity effect in the ferromagnet with magnetization in the z-direction in proximity with a superconductor. The ferromagnet has length $L = 5\xi$, and the SF interface is characterized by $\zeta = 0.1$. See the main text for details.

5.2.3 SF heterostructure with a non-homogeneous magnetization

We are considering dirty materials, meaning that the SF heterostructure in the last section induces triplets which are odd in frequency. To study the properties of odd-frequency systems, however, it would be instructive if we could make a system with a pure odd-frequency component. This will never happen in a system like

the one considered above because the d_z component and the f_s component decay equally fast for systems with magnetization in the z-direction. We know, however, from our discussion in Section 4.1, that the d_x and d_y triplet components do not "feel" an exchange field parallel with the z-axis, and decay as in a normal metal. In order to induce a pure odd-frequency amplitude, we let the magnetic field with $|\boldsymbol{h}| = 3\Delta_0$ rotate from being parallel with the z-direction at $x = 0$, to pointing in the x-direction at $x = \xi$. This will induce both d_z and d_x triplets, and during the last portion of the material, the d_z triplets will be long-ranged, and should thus survive while the other components decay.

The resulting Green function amplitudes and density of states for such a system are shown in Fig. 5.3. From Fig. 5.3a, we see that at end of the system, the singlet component f_s and the triplet component d_x have decayed, with only the desired triplet component d_z surviving. From Fig. 5.3b, we see that the triplet components produce a peak in the density of states at the Fermi energy.

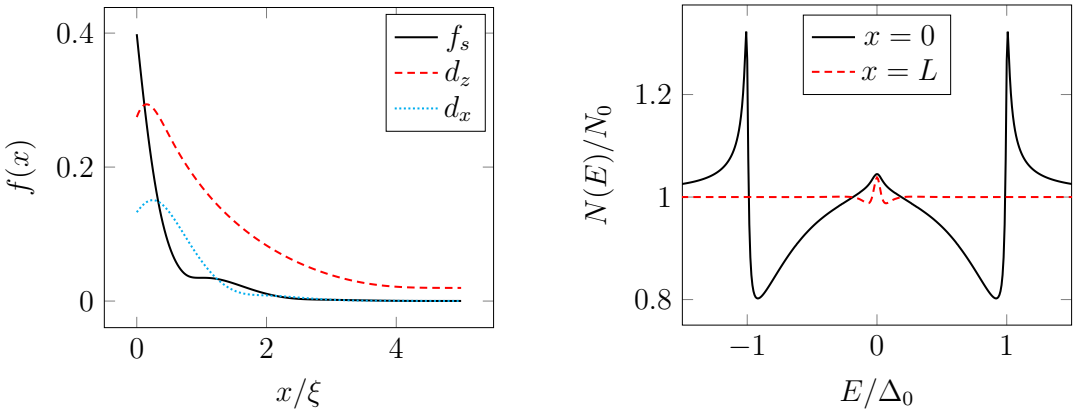

(a) The magnitude of the singlet and the triplet anomalous Green function for $E = 0.5\Delta_0$.

(b) The density of states at different positions.

Figure 5.3: The proximity effect inside a ferromagnet with rotating magnetization in proximity with a BCS superconductor. The calculation was performed for a ferromagnet of length $L = 5\xi$, and a boundary with $\zeta = 0.1$. The exchange field, which has a magnitude of $h = 3\Delta_0$, rotates uniformly from being in the z-direction at $x = 0$, to pointing in the x-direction at $x = \xi$, and remains in this position for the rest of the ferromagnet. See the main text for details.

In the system considered above, a pure odd-frequency pairing has been induced in a ferromagnet. We now want to modify this system so that we remove the ferromagnetism. To do this, we place a normal metal in proximity to this system. This will lead to a normal metal with purely odd-frequency amplitudes, which can be

used to study the signatures of odd-frequency superconductivity. The setup is shown in Fig. 5.4a. As an approximation to this system, we consider a system consisting of a single ferromagnet but where the magnetization is suppressed exponentially, making the last part of the system a normal metal. This approximation is shown in Fig. 5.4b. We will in the following refer to this system as the *odd-frequency proximity system*.

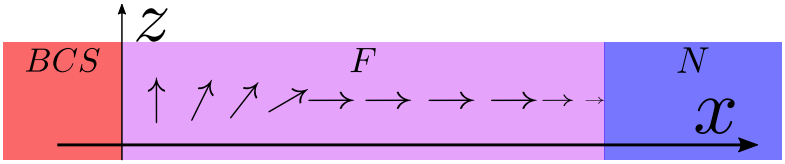

(a) The system that displays pure odd-frequency superconductivity consists of a conventional bulk superconductor (BCS), a ferromagnet with a rotating magnetization (F), a ferromagnet with a constant magnetization, a ferromagnet with a rapidly decaying magnetization (indicated by the arrows), and a normal metal (N). The lengths in the figure are not to scale.

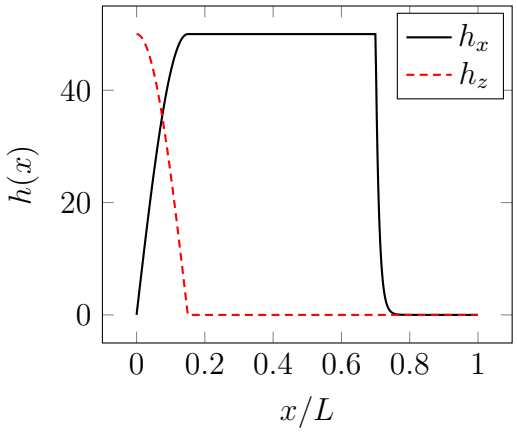

(b) The magnetic field in ferromagnet and normal metal.

Figure 5.4: We approximate the two ferromagnetic parts and the normal metal part of the heterostructure with single material with a non-homogeneous magnetization.

5.3 Analysis of the odd-frequency proximity system in equilibrium

We continue working with the odd-frequency proximity system that was introduced in the last section and discuss properties such as density of states and symmetries of the quasiclassical Green functions. To get a significant effect, we want the

anomalous Green function component d_z to be as large as possible at the end of the system. This can be done by making the system short, and by making the interface resistance ζ small. At the same time, we must make sure that the singlet component and the triplet component d_x decay fast enough to vanish. This can be done by choosing a large exchange field. We, therefore, require that $d_z/f_s > 10$ for all energies at the end of the system to ensure that the odd-frequency pairing dominates completely in this region of space. Trial and error shows that using values $h = 50\Delta_0$, $\zeta = 0.1$ and $L = 0.75\xi$ produce good results. We use a Dynes parameter of $\epsilon = 0.01\Delta_0$ in order to remove divergences. In the following, we consider how the Green functions look at the end of this material, that is at the vacuum edge, where we to a good approximation have only odd-frequency triplet states.

5.3.1 Symmetries and density of states

The quasiclassical Green function d_z and the density of states at $x = L$ in the odd-frequency proximity system are found using the Python program and plotted in Fig. 5.5. In contrast to a BCS superconductor, and thus also to our three models, we find that the real and imaginary parts of both the anomalous and normal Green functions overlap. This is shown in Fig. 5.5a. It can be seen from

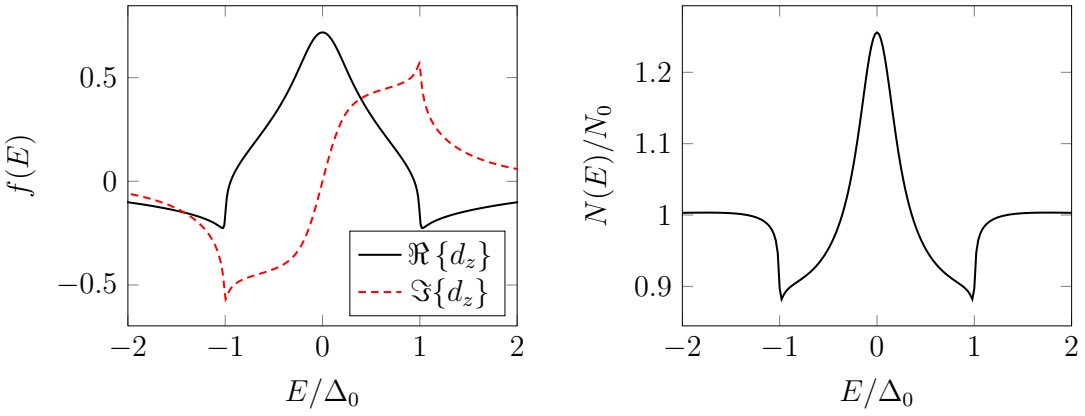

(a) The real and imaginary part of the anomalous Green function.

(b) The density of states.

Figure 5.5: The proximity effect at $x = L$ in the odd-frequency proximity system. Parameters used are $h = 50\Delta_0$, $\zeta = 0.1$, $L = 0.75\xi$, and $\epsilon = 0.01\Delta_0$. See the main text for details.

the figure that the solution has inherited properties of the BCS superconductor through the proximity effect, as the function changes rapidly at the gap edge. We

observe that the real part is symmetric, while the imaginary part is antisymmetric, which of course is consistent with and further justifies the tilde symmetry criterion in Eq. (4.30). Additionally, the anomalous Green function disappears for large energies, consistent with the criterion in Eq. (4.35). This is also consistent with our discussion in Appendix C.2. The density of states at the vacuum edge in our system with induced odd-frequency superconductivity is shown in Fig. 5.5b. The density of states is peaked for energies close to the Fermi energy. By numerical integration, it can be checked that the number of states is conserved, as required in the criterion Eq. (4.34). Finally, the criterion of normalization is automatically satisfied by the Riccati parametrization, meaning that this solution satisfies all the criteria we argued for in Section 4.2.

Finally, we compare the density of states to our analytical models, as shown in Fig. 5.6. It is that the density of states loosely resembles the density of states for Model 1a with a large Dynes parameter. A curve fit between this model and the numerical results is shown in Fig. 5.6a. This is only a good fit for small energies, and around the band gap there is a large discrepancy between the two. Even

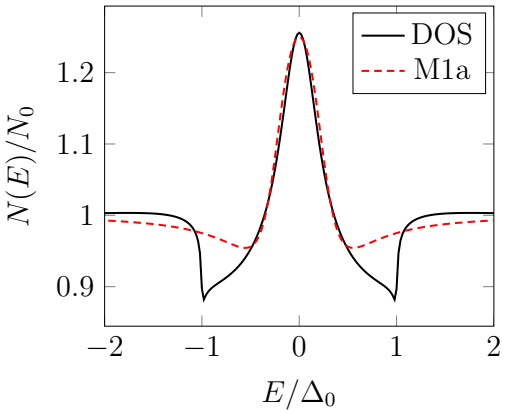

(a) A curve fit using Model 1a (M1a). Parameters used are $\Delta = 0.18\Delta_0$, $\delta = 0.27\Delta_0$, and $a = 1.3$.

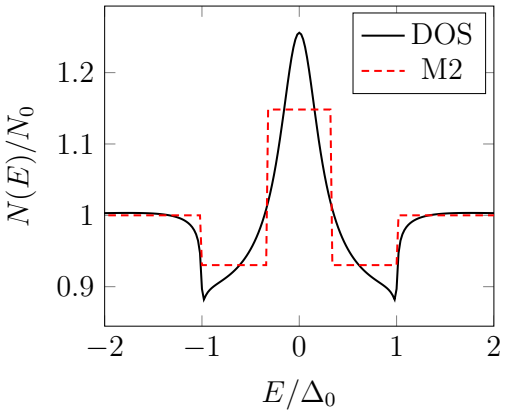

(b) A curve fit using Model 2 (M2). Parameters used are $a = 0.32$, $b = 1.0$,$c = 0.56$, and $d = 0.37$.

Figure 5.6: Different models fitted to the density of states from the proximity structure. See the main text for details.

though the fit is not very good, and depends on the inclusion of the large Dynes parameter, this is an indication that the solutions in the odd-frequency proximity system has some resemblance to Model 1. By choosing a more advanced symmetric function $\mathcal{S}(E)$, a better fit could be obtained. From the discussion in Section 4.3.1, we know that this function should be chosen such that it satisfies $\mathcal{S}(\Delta) = 0$, in order to produce a density of states with no gaps. A curve fit with Model 2 is

shown in Fig. 5.6b, and it can be seen that this roughly approximates the shape of the density of states.

5.3.2 The Meissner response

We follow the same method of calculating the Meissner response as in Section 4.5, using linear response. This is done by numerically calculating the integral $I(x)$ in Eq. (4.107) for the proximity system. The result is shown in Fig. 5.7. We find that

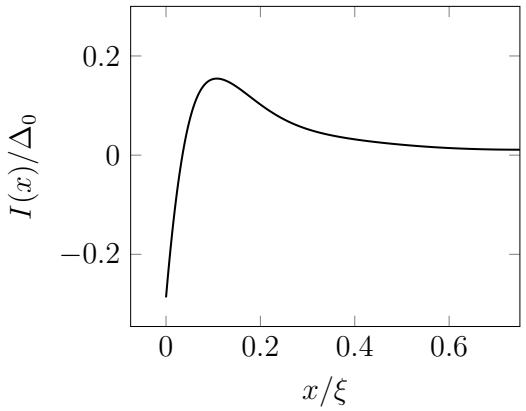

Figure 5.7: The integral $I(x)$ determining the sign of the Meissner response inside the proximity system. See the main text for details.

the integral is negative close to the superconductor, but changes its sign inside the odd-frequency proximity system. This is due to the system transitioning from being dominated by the even-frequency singlet component close to the superconductor to being dominated by the odd-frequency triplet component. This matches our discussion in Section 4.5.1 well. Inside the system, where odd-frequency pairing dominates, the Meissner response has oscillating solutions, which are stabilized by the BCS superconductor and the diamagnetic part of the proximity system. This means that Model 1 describes the physics of odd-frequency superconductivity induced by such a proximity system well. Additionally, Model 1 has a peaked density of states, just like this proximity system. Model 2 has a peaked density of states as well but does not give any Meissner response. Model 3 has a diamagnetic Meissner response and a gap in the density of states, thus bearing little resemblance to the odd-frequency paring induced in the odd-frequency proximity system. It could, as discussed in Section 4.5.1, describe a bulk odd-frequency superconductor because the diamagnetic Meissner effect gives stable solutions for the magnetic field.

5.4 Parametrization of the non-equilibrium equations

In this section, we will introduce a convenient parametrization of the Keldysh component of the Usadel equation. This section will follow the work of Ouassou *et al.* [78]. For a general quasiclassical self-energy term $\check{\sigma}$, the Keldysh component of the Usadel equation reads

$$D\boldsymbol{\nabla}\left(\check{g}\boldsymbol{\nabla}\check{g}\right)^K = -\mathrm{i}\left[\check{\sigma},\check{g}\right]^K, \tag{5.10}$$

where we have neglected the magnetic vector potential. First, it is convenient to introduce an 8-vector h, through the equation

$$\hat{h} = \sum_{j=0}^{7} h_j\hat{\rho}_j, \tag{5.11}$$

where the matrices are given as

$$\begin{aligned}
&\hat{\rho}_0 \equiv \hat{\tau}_0\hat{\sigma}_0 && \hat{\rho}_1 \equiv \hat{\tau}_0\hat{\sigma}_1 && \hat{\rho}_2 \equiv \hat{\tau}_0\hat{\sigma}_2 && \hat{\rho}_3 \equiv \hat{\tau}_0\hat{\sigma}_3\\
&\hat{\rho}_4 \equiv \hat{\tau}_3\hat{\sigma}_0 && \hat{\rho}_5 \equiv \hat{\tau}_3\hat{\sigma}_1 && \hat{\rho}_6 \equiv \hat{\tau}_3\hat{\sigma}_2 && \hat{\rho}_7 \equiv \hat{\tau}_3\hat{\sigma}_3.
\end{aligned}$$

Assuming the self-energy to be of first order in the quasiclassical Green functions, we can write it as

$$\check{\sigma} = \hat{v} + \hat{w}\check{g}\hat{w}, \tag{5.12}$$

where we have introduced the zeroth and first-order self-energy terms as $\hat{v}$ and $\hat{w}$, respectively. By comparing with the Usadel equation in Eq. (3.133), we see that the kinetic term, the superconducting term, and the ferromagnetic terms are examples of zeroth-order terms, while the spin-flip and spin-orbit scattering terms are examples of first-order terms. It can be shown that by introducing the quantities

$$\boldsymbol{Q}_{nm} = \frac{D}{4}\mathrm{Tr}\left\{\hat{\rho}_m\hat{\rho}_n\hat{g}^R\boldsymbol{\nabla}\hat{g}^R - \hat{\rho}_n\hat{\rho}_m\hat{g}^A\boldsymbol{\nabla}\hat{g}^A\right\} \tag{5.13}$$

$$M_{nm} = \frac{D}{4}\mathrm{Tr}\left\{\hat{\rho}_n\hat{\rho}_m - \hat{\rho}_n\hat{g}^R\hat{\rho}_m\hat{g}^A\right\} \tag{5.14}$$

$$V_{nm} = \frac{\mathrm{i}}{4}\mathrm{Tr}\left\{\left[\hat{\rho}_n,\hat{v}\right](\hat{g}^R\hat{\rho}_m - \hat{\rho}_m\hat{g}^A)\right\} \tag{5.15}$$

$$W_{nm} = \frac{\mathrm{i}}{4}\mathrm{Tr}\left\{\left[\hat{\rho}_n,\hat{w}\right](\hat{g}^R\hat{w}\hat{g}^R\hat{\rho}_m - \hat{\rho}_m\hat{g}^A\hat{w}\hat{g}^A + \hat{g}^R\left[\hat{\rho}_m,\hat{w}\right]\hat{g}^A)\right\}, \tag{5.16}$$

the kinetic equations can be written compactly as

$$M_{nm}\boldsymbol{\nabla}^2 h_m = -(\boldsymbol{\nabla}M_{nm} + \boldsymbol{Q}_{nm})\cdot\boldsymbol{\nabla}h_m - (\boldsymbol{\nabla}Q_{nm} + V_{nm} + W_{nm})h_m. \tag{5.17}$$

This equation is convenient to use in a numerical solver. We can also make this equation dimensionless by dividing it by Δ_0, and giving lengths in units of the superconducting coherence length $\xi = \sqrt{D/\Delta_0}$, and energies in units of Δ_0.

5.5 Spin modes and spin accumulation

Using the parametrization in the last section, a program was written in Python that solves the kinetic equation for the distribution matrix in the full system introduced in Section 5.2.3. This allows us to study non-equilibrium phenomena such as the response to applying voltages or spin voltages. Johnsen and Linder [14] predicted recently that the spin accumulation can be larger in an odd-frequency system than in a superconductor or even in the normal state. Predictions were also made about the renormalization of the spin-flip and spin-orbit scattering lengths. In this section, we aim to investigate these predictions numerically for a realistic proximity system. We will apply a spin-voltage across the proximity system from Section 5.3, and study the spin accumulation and the decay of spin modes close to the vacuum edge, where we have pure odd-frequency amplitude.

In the calculations to come, we have made several assumptions. For once, we have ignored the effects of spin-orbit and spin-flip scattering on the equilibrium Green functions calculated in Section 5.3. Secondly, we have assumed that the right-hand side of the system is in contact with a vacuum, while still applying a spin voltage. This could be fixed by instead calculating the equilibrium Green functions for a system with a normal-metal edge instead of the vacuum edge. This gives the same functional form for the quasiclassical Green functions, with a peaked density of states that is slightly lower. We will neglect the temperature dependence of the order parameter, as we are interested in comparing different models at a constant temperature. This corresponds to assuming that the temperature is $T = 0$ in the odd-frequency system while allowing the temperature in the reservoirs to vary. When calculating the spin accumulation numerically, we introduce an integration cutoff at $E = \pm 3\Delta_0$. It can be shown numerically that neglecting the contributions from energies higher than this cutoff is a very good approximation in the situations we will consider. Finally, we use continuous boundary conditions for the non-equilibrium calculations, since using e.g. the KL-boundary conditions would only lower the spin mode in all materials, and not affect the qualitative nature of the spin mode [14].

We start by considering a spin-voltage of magnitude $V_\uparrow = -V_\downarrow = V_s$, meaning that the normal voltage vanishes, and we get the boundary conditions for the

energy mode,

$$h_0(x=0) = \frac{1}{2}\left[\tanh\left(\frac{E+eV_s}{2T}\right) + \tanh\left(\frac{E-eV_s}{2T}\right)\right] \tag{5.18}$$

$$h_0(x=L) = \frac{1}{2}\left[\tanh\left(\frac{E-eV_s}{2T}\right) + \tanh\left(\frac{E+eV_s}{2T}\right)\right], \tag{5.19}$$

and for the spin mode,

$$h_7(x=0) = \frac{1}{2}\left[\tanh\left(\frac{E+eV_s}{2T}\right) - \tanh\left(\frac{E-eV_s}{2T}\right)\right] \tag{5.20}$$

$$h_7(x=L) = \frac{1}{2}\left[\tanh\left(\frac{E-eV_s}{2T}\right) - \tanh\left(\frac{E+eV_s}{2T}\right)\right], \tag{5.21}$$

while the other modes vanish. In Fig. 5.8, the boundary condition $h_7(x=L)$ is plotted against energy for different spin voltages and temperatures. A high spin voltage and temperature correspond to a wide distribution, while a small spin voltage and low temperature make the distribution narrow. This indicates that for lower temperatures and spin voltages, the density of states at the Fermi energy becomes increasingly more important for spin accumulation. Thus, we expect the spin accumulation to be high in an odd-frequency system such as the one we are considering and very low in the gapped conventional superconductor. The figure also justifies our integration cutoff, as we see that the spin-mode vanishes for energies $\pm 3\Delta_0$ for temperatures and spin voltages in the range we will be using.

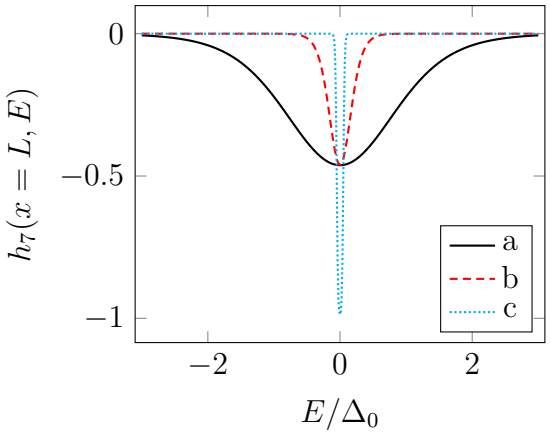

Figure 5.8: The boundary distribution $h_7(x=L)$ is plotted against energy for $T=0.5T_c$ (solid), $eV_s=0.5\Delta_0$ (dashed), $T=0.1T_c$, $eV_s=0.1\Delta_0$, and $T=0.01T_c$, $eV_s=0.05\Delta_0$ (dotted). See the main text for details.

5.5.1 Without scattering

We set $T = 0.5T_c$ and $eV_s = 0.5\Delta_0$, and calculate the spin mode in the absence of spin-flip and spin-orbit scattering. The spin mode is used to calculate the spin accumulation, using Eq. (3.151). The result is shown in Fig. 5.9a. It is apparent from the figure that the spin accumulation in the normal metal and the odd-frequency system are almost identical, while the BCS superconductor has a much smaller spin accumulation. This is consistent with our result in Eq. (4.70) in Chapter 4. It is thus the density of states that determines the spin accumulation in this case; the BCS superconductor has no states inside the gap, meaning that the spin accumulation becomes small. The odd-frequency system has a peaked density of states at zero energy, but also a lowered density of states for small but nonzero energies. Thus, by using $T = 0.5T_c$ and $eV_s = 0.5\Delta_0$, corresponding to a broad spin mode at the boundaries, the spin accumulation becomes similar in the normal metal and the odd-frequency superconductor.

We then choose $T = 0.01T_c$ and $eV_s = 0.05\Delta_0$, corresponding to a much narrower spin mode. The spin accumulation for these parameters is shown in Fig. 5.9b. We observe that the spin accumulation in the BCS superconductor vanishes, which is expected for a narrow spin mode at the boundaries, while the odd-frequency superconductor obtains a higher spin mode. Thus, we have shown numerically that for narrow spin modes, one can obtain higher spin accumulation in an odd-frequency superconductor than in a normal metal. For higher temperatures and spin voltages, the spin accumulation will be approximately equal to that of a normal metal.

From both of the subfigures in Fig. 5.9, we see that while the spin accumulation in the odd-frequency superconductor starts at a higher value close to the applied voltage, it drops off quickly. This can be understood by considering the spin accumulation for the whole system, which is shown in Fig. 5.10. The spin accumulation in the full system is of course also affected by the non-homogenous magnetic field in the ferromagnetic part of the system. This is what causes the spin accumulation to drop of faster in this system. It seems reasonable to expect that in a bulk material of the type that we find in the odd-frequency part of our system, the spin accumulation will drop off as in a normal metal, and the spin accumulation will be even higher than in this heterostructure.

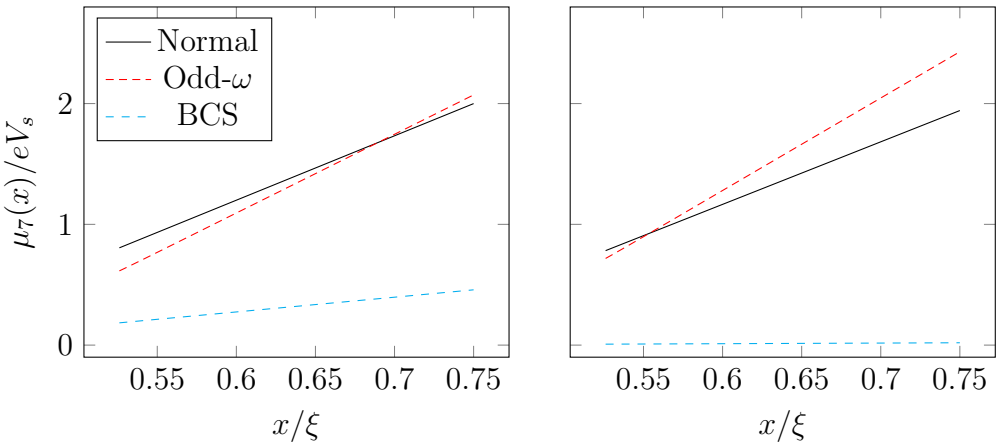

(a) $T = 0.5T_c$, $eV_s = 0.5\Delta_0$ (b) $T = 0.01T_c$, $eV_s = 0.05\Delta_0$.

Figure 5.9: The spin accumulation for different spin voltages V_s and reservoir temperatures T in the odd-frequency part of the system, compared with a BCS superconductor and a normal metal. See the main text for details.

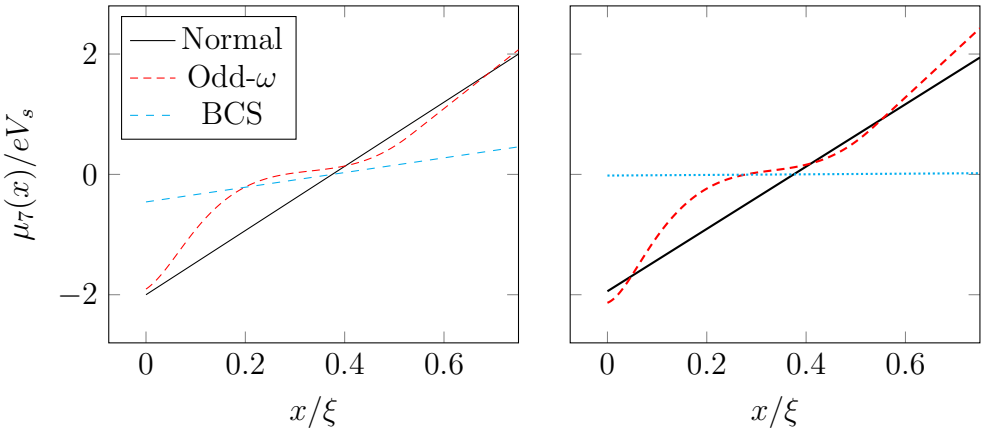

(a) $T = 0.5T_c$ and $eV_s = 0.5\Delta_0$. See the main text for details.

(b) $T = 0.01T_c$ and $eV_s = 0.05\Delta_0$.

Figure 5.10: The spin accumulation for different reservoir temperatures T and spin voltages V_s in the full proximity system compared with a BCS superconductor and a normal metal of the same length.

5.5.2 Spin-flip scattering

We define the spin-flip scattering length $l_{\text{sf}} = \sqrt{D\tau_{\text{sf}}}$, and calculate the spin modes and spin accumulation in a system with $l_{\text{sf}} = 0.0375\xi$. The result for two different energies is shown in Fig. 5.11 for a reservoir temperature of $T = 0.5T_c$ and a spin voltage of $eV_s = 0.5\Delta_0$. We observe that the spin-flip scattering length of the BCS superconductor is renormalized, and for energies $E \approx \Delta_0$, this renormalization becomes huge. The spin mode in the normal metal and in the proximity odd-frequency system is not renormalized. These results are consistent with the general discussion we had in Section 4.4, where we found that odd-frequency pairing is unaffected by spin-flip impurity scattering.

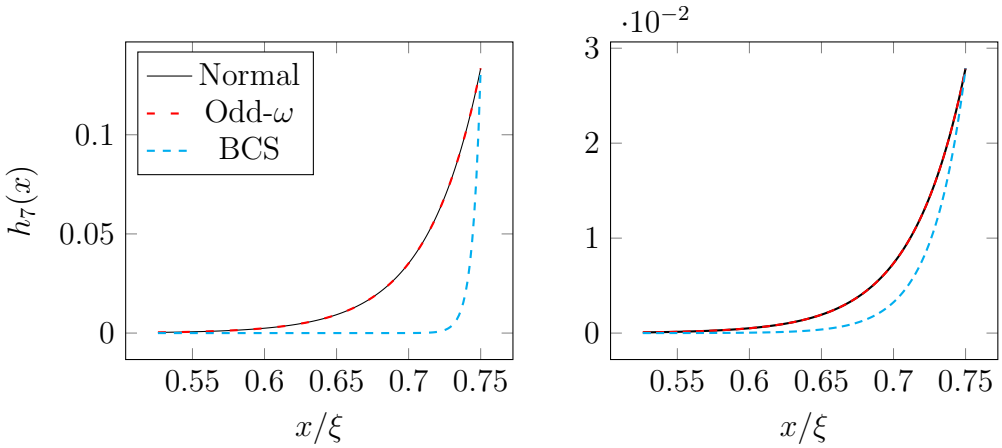

Figure 5.11: Spin modes in the presence of spin-flip scattering with scattering length $l_{\text{sf}} = 0.0375\xi$. In the left pane, $E = 1.02\Delta_0$, and in the right pane, $E = 1.50\Delta_0$. The temperature of the reservoir is $T = 0.5T_c$, and the spin-voltage is $eV_s = 0.5\Delta_0$. The ordinate label and the legend are shared for the two axes. See the main text for details.

Using Eq. (3.151), we find the spin accumulation in the system, as shown in Fig. 5.12. In the right pane, we have normalized each spin accumulation to be able to only see the differences in decay rates. This effectively hides the differences in the density of states of the different systems. The decay rates of the spin accumulation is inherited from the decay rates of the spin modes, and, as expected, we find that the spin accumulation decays faster in the BCS superconductor compared with the normal metal and odd-frequency superconductor, which decays with the same rate.

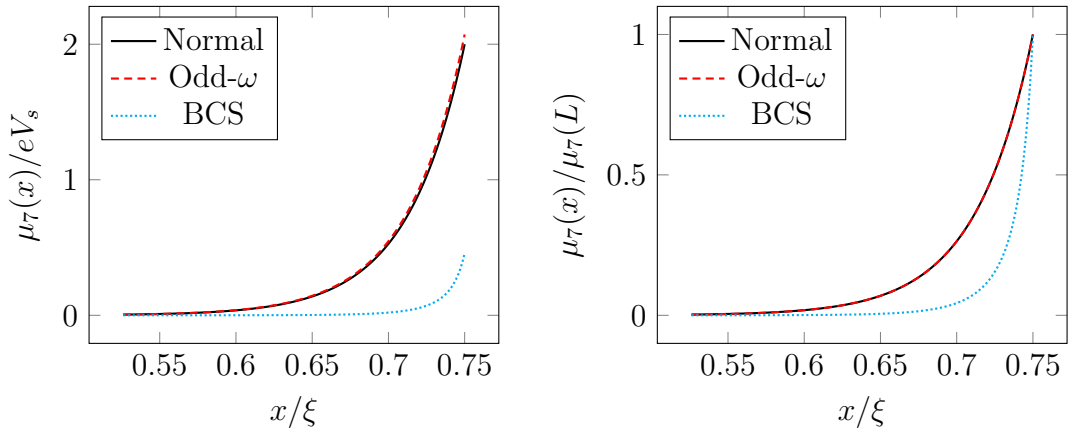

Figure 5.12: The spin accumulation in the presence of spin-flip scattering with scattering length $l_{\text{sf}} = 0.0375\xi$. The temperature of the reservoir is $T = 0.5T_c$, and the spin-voltage is $eV_s = 0.5\Delta_0$. The spin accumulations in the right panel have been normalized by dividing by the value of the spin accumulation at $x = L$. See the main text for details.

5.5.3 Spin-orbit scattering

We define the spin-orbit scattering length $l_{\text{so}} = \sqrt{D\tau_{\text{so}}}$, and calculate the spin modes and spin accumulation in a system with $l_{\text{so}} = 0.0375\xi$. The spin mode decays exponentially, as shown in Fig. 5.13, where the spin mode is plotted for two different energies. The normal metal and BCS superconductor experience no renormalization of the spin-orbit length, while the odd-frequency superconductor decays faster. Qualitatively, this is consistent with both the discussion in Section 4.4 and in [14]. The renormalization does, however, not diverge at the band gap or anywhere else, which is in contrast with [14]. This result can be understood from the general result in Eq. 4.70, and by observing from Fig. 5.5a that the anomalous Green function of this system has a real part that is large at zero energy and does not diverge for any energies. This means that while the spin accumulation will be smaller for the odd-frequency model, it does not decay much faster than the BCS superconductor and the normal metal. The spin accumulation is shown in Fig. 5.14. These results bear some resemblance with the results from Model 2, which has a spin-orbit renormalization for small energies where the density of states is peaked, but differ drastically from those of Model 1a and Model 3a. By choosing the specific functions in Model 1 and Model 3 in such a way that there is no divergence at the gap edge[4], one could obtain models that better capture the spin-orbit impurity scattering in the proximity structure we have considered here.

[4]This can be done e.g. for Model 1 by choosing the function $\mathcal{S}(E)$ such that $\mathcal{S}(\Delta) = 0$.

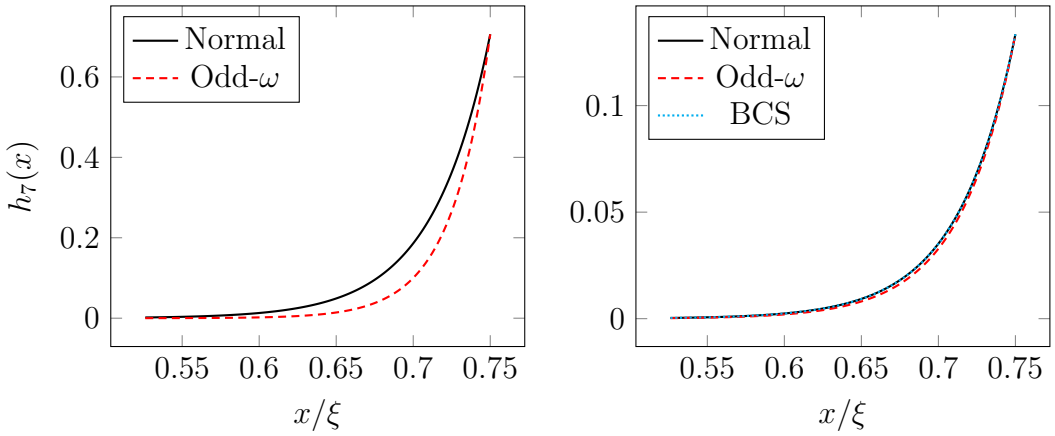

Figure 5.13: Spin modes in the presence of spin-orbit scattering with scattering length $l_{\text{so}} = 0.0375\xi$. In the left pane, $E = 0.02\Delta_0$, and in the right pane, $E = 1.02\Delta_0$. The temperature of the reservoir is $T = 0.5T_c$, and the spin-voltage is $eV_s = 0.5\Delta_0$. The ordinate label is shared for the two axes. See the main text for details.

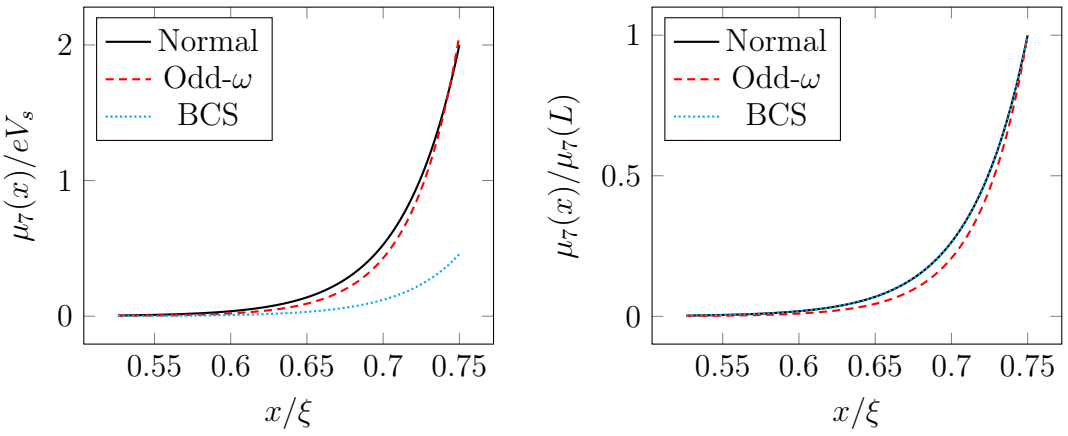

Figure 5.14: The spin accumulation in the presence of spin-orbit scattering with scattering length $l_{\text{so}} = 0.0375\xi$. The temperature of the reservoir is $T = 0.5T_c$, and the spin-voltage is $eV_s = 0.5\Delta_0$. The spin accumulations in the right panel have been normalized by dividing by the value of the spin accumulation at $x = L$. See the main text for details.

Chapter 6

Conclusion and Outlook

In this thesis, quasiclassical theory in the dirty limit was derived and used to study superconducting odd-frequency systems. Such systems have attracted much interest recently, due to the possibility of having long-ranged spin-polarized supercurrents, which could be used in applications in energy-efficient computing [6]. Moreover, the pairing in such systems is non-local and antisymmetric in time [13], making odd-frequency superconductivity interesting also from a fundamental physics point of view.

We proposed four criteria for the quasiclassical Green functions in odd-frequency superconductors, based on general arguments as well as analytical and numerical solutions of proximity systems. Using these criteria in addition to solutions of superconductor-ferromagnet systems, we proposed ansatzes for three models describing odd-frequency superconducting systems with physically reasonable behavior. Model 1 consists of the BCS solution multiplied with a symmetric function $\mathcal{S}(E)$, and we introduced Model 1a as the special case where $\mathcal{S}(E)$ is a constant. Model 2 was constructed to be as simple as possible, as a step function model with a peaked density of states. Finally, Model 3 consists of the BCS solution multiplied with an antisymmetric function $\mathcal{A}(E)$, and we introduced Model 3a as the special case where $\mathcal{A}(E) = \alpha \text{sign}(E)$, with $\alpha \leq 1$.

We calculated the density of states, the renormalization of the spin-flip and spin-orbit scattering lengths, and the Meissner response for these models. Model 1 and Model 2 generally have a peaked density of states around the Fermi energy, while the density of states of Model 3 is lowered, and in some cases, such as for Model 3a, gapped close to the Fermi energy. A general result was derived, stating that the spin-orbit scattering length is renormalized in odd-frequency systems, while the spin-flip scattering length is renormalized in even-frequency systems. In both cases, this renormalization depended on the real part of the anomalous Green function being nonzero. This was used to argue that in general, there must at least be some energy domains where such a renormalization takes place for

all possible models. It was found that Model 1, in contrast with conventional superconductors, can display an unconventional and locally paramagnetic Meissner response. This, along with the peaked density of states, makes Model 1 suitable for describing odd-frequency superconductivity induced by the proximity effect in heterostructures. Model 3 has a diamagnetic Meissner response similar to that of a conventional superconductor, making bulk solutions avoid the stability issues found in systems with a paramagnetic Meissner response. This makes Model 3 a candidate for a bulk odd-frequency superconductor. Model 2 displays no Meissner effect, indicating that it is too primitive to capture the electromagnetic properties of a superconductor.

In the final chapter, we solved numerically for the quasiclassical Green functions in a realistic system displaying odd-frequency superconductivity. We found a peaked density of states, and it was found that this system generally has a higher spin accumulation than a conventional superconductor. This is consistent with Model 1 and Model 2, supporting the claim that these models can describe proximity systems. For low temperatures and spin voltages, the spin accumulation was shown to be higher than in the normal state. This confirms the predictions made in [14], using a realistic system that satisfies the sum rule of the spectral weight. The spin-orbit scattering length was renormalized, while the spin-flip scattering length was unchanged in the odd-frequency part of this system, consistent with our results from the analytic part. The Meissner effect in the proximity structure was found to be unconventional in the part where odd-frequency pairing dominates, again consistent with Model 1.

The results in this thesis suggest several further tasks. To get a model that captures the physics of realistic proximity systems better, effort should be put into finding an approximate functional form of the real and imaginary parts of the quasiclassical Green function of the odd-frequency proximity system. This could be done by considering Model 1 for functions satisfying $\mathcal{S}(\Delta) = 0$, which makes the density of states non-gapped for all energies. One could then find the symmetric function $\mathcal{S}$ that best fits the numerical results, while also making sure that the model satisfies the sum rule of the spectral weight.

Another possible direction could be to drop the constraints of our three models and directly curve-fit a new function to the numerical results. This approach results in anomalous Green functions which have overlapping real and imaginary parts, which would make analytical calculations more difficult, but would better describe the physics in a proximity structure. This approach would, however, probably result in an unconventional Meissner response, making the model inapplicable to bulk systems.

The possibility of combining models should also be investigated. By e.g. adding Models 3 and 2, it should be possible to find a model that has a peaked density of

states as well as a diamagnetic Meissner effect. Moreover, by adding solutions in this way, it should also be possible to find models that have nonzero real and imaginary parts for all energies, thus experiencing spin-orbit scattering renormalization for all energies, which seems physically reasonable. Finally, the prospect of using Model 3, alone or in combination with e.g. Model 2, as a model for a bulk odd-frequency system should be explored further. Model 3a can be chosen in such a way that it has the same density of stats and Meissner response as a conventional superconductor, and the further implications of the model should be studied to understand whether such a system is physically realizable, and what the physical implications of such a system would be.

Appendix A

Simple Green Function Solutions

We solve for the Green functions in some simple systems in equilibrium. This appendix serves as an application of the theory of Green functions developed in Chapter 3, deriving results that are used extensively in the main text, as well as highlighting important details such as the infinitesimal convergence factors added to the energy variable of the Green functions. Parts of this appendix are based on the master's thesis by Morten [25].

A.1 Kinetic one-particle Hamiltonian

We consider a system where free particles of mass m move in a box of volume $\mathcal{V}$. The one-particle free-particle Hamiltonian is in the position representation given as

$$\mathcal{H}(\boldsymbol{r}) = -\frac{\boldsymbol{\nabla}^2}{2m} - \mu, \tag{A.1}$$

where μ is the chemical potential of the system, which we assume is a constant. In the following, we solve for the Green function by using two different methods: first by solving the Heisenberg equation of motion for the field operators from Eq. (2.17) directly, and then by Fourier transforming the equations of motion themselves, before solving the equation. The first calculation is useful because it will illuminate the important aspect of infinitesimal convergence factors when defining the Fourier transformed Green function, and the second method is useful because it generalizes the easiest to more complicated systems.

Solving the Heisenberg equation of motion directly

The second quantized version of the Hamiltonian in Eq. (A.1) reads

$$\begin{aligned} H(t) &= \int d\boldsymbol{r}' \psi^\dagger(\boldsymbol{r}', t) \left(-\frac{\boldsymbol{\nabla}^2}{2m} - \mu \right) \psi(\boldsymbol{r}', t) \\ &= \frac{1}{\mathcal{V}^2} \int d\boldsymbol{r}' \sum_{\boldsymbol{p}''\boldsymbol{p}'} \mathrm{e}^{\mathrm{i}\boldsymbol{p}''\cdot\boldsymbol{r}'} c^\dagger_{\boldsymbol{p}''}(t) \left(-\frac{\boldsymbol{\nabla}^2}{2m} - \mu \right) \mathrm{e}^{-\mathrm{i}\boldsymbol{p}'\cdot\boldsymbol{r}'} c_{\boldsymbol{p}'}(t) \\ &= \frac{1}{\mathcal{V}^2} \int d\boldsymbol{r}' \sum_{\boldsymbol{p}''\boldsymbol{p}'} \mathrm{e}^{\mathrm{i}\boldsymbol{p}''\cdot\boldsymbol{r}'} c^\dagger_{\boldsymbol{p}''}(t) \xi_{\boldsymbol{p}''} \mathrm{e}^{-\mathrm{i}\boldsymbol{p}'\cdot\boldsymbol{r}'} c_{\boldsymbol{p}'}(t) \\ &= \sum_{\boldsymbol{p}'} \xi_{\boldsymbol{p}'} c^\dagger_{\boldsymbol{p}'}(t) c_{\boldsymbol{p}'}(t), \end{aligned} \tag{A.2}$$

where we have changed into momentum basis, defined the function $\xi_{\boldsymbol{p}} = \boldsymbol{p}^2/2m - \mu$, and used the definition of the delta function in the last line. Using the anticommutation relation of the creation and annihilation operators it is then easy to show that

$$\left[H(t), c_{\boldsymbol{p}}(t)\right] = -\xi_{\boldsymbol{p}} c_{\boldsymbol{p}}(t) \tag{A.3}$$

$$\left[H(t), c_{\boldsymbol{p}}(t)\right] = \xi_{\boldsymbol{p}} c^\dagger_{\boldsymbol{p}}(t), \tag{A.4}$$

from which we can solve the Heisenberg equation of motion from Eq. (2.17) to get

$$c_{\boldsymbol{p}}(t) = \mathrm{e}^{-\mathrm{i}\xi_{\boldsymbol{p}} t} c_{\boldsymbol{p}}(0) \tag{A.5}$$

$$c^\dagger_{\boldsymbol{p}}(t) = \mathrm{e}^{\mathrm{i}\xi_{\boldsymbol{p}} t} c^\dagger_{\boldsymbol{p}}(0). \tag{A.6}$$

Inserting this into the definition of the retarded Green function, we obtain

$$G(\boldsymbol{p}, t_1 - t_2) = -\mathrm{i}\Theta(t_1 - t_2) \mathrm{e}^{-\mathrm{i}\xi_{\boldsymbol{p}}(t_1 - t_2)}. \tag{A.7}$$

In order to get the Green function as a function of energy, we perform a Fourier transformation in the relative time variable,

$$\begin{aligned} G(\boldsymbol{p}, E) &= -\mathrm{i} \int_{-\infty}^{\infty} dt\, \mathrm{e}^{\mathrm{i}Et} \Theta(t) \mathrm{e}^{-\mathrm{i}\xi_{\boldsymbol{p}} t} \\ &= -\mathrm{i} \int_{0}^{\infty} dt\, \mathrm{e}^{\mathrm{i}t(E - \xi_{\boldsymbol{p}})}. \end{aligned} \tag{A.8}$$

Care is needed when evaluating this expression, since this integral does not strictly converge. The integral is problematic both because the integrand does not converge as $t \to \infty$, and because the integral goes to infinity for $E - \xi_{\boldsymbol{p}} = 0$. In order to fix

both of these problems, the usual procedure is to perform the analytic continuation in $E \to E + \mathrm{i}\delta$, and then take the limit $\delta \to 0$ in the end [27]. In order for the integrand to converge, we see that we must choose $\delta > 0$, thus making an analytic continuation in the upper half plane. Using this, the integral becomes trivial,

$$G(\boldsymbol{p}, E) = \frac{1}{E - \xi_{\boldsymbol{p}} + \mathrm{i}\delta}. \tag{A.9}$$

We observe that the Fourier-transformed Green function has poles at $E = \xi_{\boldsymbol{p}} - \mathrm{i}\delta$, in the lower half-plane, while it is analytic in the upper half-plane. It can in the same manner be shown that for the advanced Green function, the analytic continuation must be performed in the lower half-plane, $E \to E - \mathrm{i}\delta$. Moreover, this pole is located at the single-particle energies, with an infinitesimal shift. These results have been derived for a free single-particle Hamiltonian, but is valid in general [27].

Fourier transforming the Green function equation of motion

We now perform the same calculation by first Fourier transforming the equation of motion. First, we insert the Hamiltonian from Eq. (A.1) into the equation of motion for the Green function, as was stated in a Nambu-spin space generalized version in Eq. (3.36),

$$\left[\mathrm{i}\partial_{t_1} - \mathcal{H}(\boldsymbol{r}_1)\right] G^R(\boldsymbol{r}_1, t_1; \boldsymbol{r}_2, t_2) = \delta(\boldsymbol{r}_1 - \boldsymbol{r}_2)\delta(t_1 - t_2). \tag{A.10}$$

This is easiest solved by Fourier transforming the entire equation into the energy-momentum-domain, solving for the transformed Green function, and then performing the inverse Green function if we want to go back into position-space. Assuming we are in a stationary system, G^R is only a function of the relative time $t = t_1 - t_2$. We can then use that $\partial_{t_1} G(t) = \partial_t G(t)$, and performing a Fourier transform of Eq. (A.10), we obtain

$$\left[E + \mathrm{i}\delta - \mathcal{H}(\boldsymbol{r}_1)\right] G^R(\boldsymbol{r}_1, \boldsymbol{r}_2, E) = \delta(\boldsymbol{r}_1 - \boldsymbol{r}_2), \tag{A.11}$$

where we have again added the infinitesimal imaginary part to E, and used integration by parts. Since we are considering a bulk material, we also assume that the Green function is a function of relative coordinate only. Fourier transforming in the relative coordinate, again using integration by parts, we find

$$G^R(\boldsymbol{p}, E) = \frac{1}{E - \xi_p + +\mathrm{i}\delta}, \tag{A.12}$$

with $\xi_{\boldsymbol{p}} = \boldsymbol{p}^2/2m - \mu$. This is, of course, the same results we found using the first method.

The quasiclassical approximation

In the quasiclassical approximation, we assume that $E << \mu$, which means that the retarded Green function in Eq. (A.9) is strongly peaked at the Fermi level μ. In order to obtain the quasiclassical expression, we integrate over energies and get

$$\begin{aligned} g^R(E, \boldsymbol{p}_F, X) &= \frac{\mathrm{i}}{\pi} \int_{-\omega_c}^{\omega_c} d\xi_{\boldsymbol{p}} \, \frac{1}{E + \mathrm{i}\delta - \xi_{\boldsymbol{p}}} \\ &= \frac{\mathrm{i}}{\pi} \int_{-\omega_c}^{\omega_c} d\xi_{\boldsymbol{p}} \, \frac{E + \mathrm{i}\delta + \xi_{\boldsymbol{p}}}{(E + \mathrm{i}\delta)^2 - \xi_{\boldsymbol{p}}^2} \\ &= \frac{\mathrm{i}(E + \mathrm{i}\delta)}{\pi} \int_{-\omega_c}^{\omega_c} d\xi_{\boldsymbol{p}} \, \frac{1}{(E + \mathrm{i}\delta)^2 - \xi_{\boldsymbol{p}}^2} \\ &= \frac{\mathrm{i}(E + \mathrm{i}\delta)}{2\pi(E + \mathrm{i}\delta)} d\xi_{\boldsymbol{p}} \int_{-\omega_c}^{\omega_c} d\xi_{\boldsymbol{p}} \left[\frac{-1}{\xi_{\boldsymbol{p}} - (E + \mathrm{i}\delta)} + \frac{1}{\xi_{\boldsymbol{p}} + (E + \mathrm{i}\delta)} \right] \\ &= \frac{\mathrm{i}}{2\pi}(-2\pi\mathrm{i}) = 1 \end{aligned} \tag{A.13}$$

where we in the second line we ignored the antisymmetric term in $\xi_{\boldsymbol{p}}$, in the third line we have expanded in partial fractions, and in the last line we have performed the residue integration[1], which is the same whether we do it in the upper or lower half-plane.

A.2 Nambu-spin generalization

We now generalize the result for the Green functions for a normal metal in Nambu-spin space. The Hamiltonian in Nambu-spin space reads

$$\hat{H} = -\frac{\boldsymbol{\nabla}^2}{2m}\hat{1} - \mu\hat{1}, \tag{A.14}$$

and the Green function equation of motion is

$$\left[\mathrm{i}\partial_{t_1}\hat{\tau}_3 - \hat{H}(\boldsymbol{r}_1)\right] \hat{G}^R(\boldsymbol{r}_1, t_1; \boldsymbol{r}_2, t_2) = \delta(\boldsymbol{r}_1 - \boldsymbol{r}_2)\delta(t_1 - t_2). \tag{A.15}$$

Performing the Fourier transform, we get, similarly to the last section,

$$\begin{aligned} G^R(\boldsymbol{p}, E) &= \left[(E + \mathrm{i}\delta)\hat{\tau}_3 - \xi_p\hat{1}\right]^{-1} \\ &= \frac{E + \mathrm{i}\delta}{(E + \mathrm{i}\delta)^2 - \xi_{\boldsymbol{p}}^2}\hat{\tau}_3 + \frac{\xi_{\boldsymbol{p}}}{(E + \mathrm{i}\delta)^2 - \xi_{\boldsymbol{p}}^2}\hat{1} \end{aligned} \tag{A.16}$$

[1]For this, we have replaced the limits $\omega_c \to \infty$. The reader is directed to the master's thesis of [26] for a discussion about the limits of the quasiclassical Green function.

where we have performed the matrix inverse in the last equation.

When performing the integral in the quasiclassical approximation, the second term in Eq. (A.16) vanishes due to being antisymmetric in $\xi_{\boldsymbol{p}}$, so the expression becomes

$$\hat{g}^R(E, \boldsymbol{p}_F, X) = \frac{\mathrm{i}}{\pi} \int_{-\omega_c}^{\omega_c} \frac{E + \mathrm{i}\delta}{(E + \mathrm{i}\delta)^2 - \xi_{\boldsymbol{p}}^2} \hat{\tau}_3 = \hat{\tau}_3, \tag{A.17}$$

where we have used the results from the last section in order to do the integral.

A.3 BCS equilibrium solution

We now proceed solve for the Green functions for a bulk BCS superconductor. In a bulk superconductor, the Hamiltonian is

$$\hat{H} = -\frac{\boldsymbol{\nabla}^2}{2m}\hat{1} - \mu\hat{1} + \hat{\Delta}, \tag{A.18}$$

which yields

$$\begin{aligned} \hat{G}^R(E, \boldsymbol{p}) &= \left[(E + \mathrm{i}\delta)\hat{\tau}_3 - \xi_p\hat{1} - \hat{\Delta}\right]^{-1} \\ &= \frac{1}{(E + \mathrm{i}\delta)^2 - |\Delta|^2 - \xi_{\boldsymbol{p}}^2} \left[(E + \mathrm{i}\delta)\hat{\tau}_3 + \xi_{\boldsymbol{p}}\hat{1} - \hat{\Delta}\right], \end{aligned} \tag{A.19}$$

where the evaluation of the matrix inverse can be checked explicitly. Again, the term with $\xi_{\boldsymbol{p}}$ in the numerator vanishes when we perform the quasiclassical integral. Since, in the BCS bulk case, $\hat{\Delta}$ is independent of energy, we only need to calculate the integral

$$\int_{-\omega_c}^{\omega_c} d\xi_{\boldsymbol{p}} \frac{1}{(E + \mathrm{i}\delta)^2 - |\Delta|^2 - \xi_{\boldsymbol{p}}^2}. \tag{A.20}$$

This integral is the same as in Eq. (A.13), under the substitution $(E + \mathrm{i}\delta)^2 \to (E + \mathrm{i}\delta)^2 - |\Delta|^2$. We thus have to calculate this separately for $E^2 - |\Delta|^2 > 0$ and $E^2 - |\Delta|^2 < 0$. In the following, it will be convenient to define the quantity $E_+ \equiv E + \mathrm{i}\delta$, thus simplifying notation slightly.

In the domain where $E^2 - |\Delta|^2 > 0$,

$$\begin{aligned}
&\int_{-\omega_c}^{\omega_c} d\xi_{\boldsymbol{p}} \frac{1}{(E+\mathrm{i}\delta)^2 - |\Delta|^2 - \xi_{\boldsymbol{p}}^2} \\
=&\int_{-\omega_c}^{\omega_c} d\xi_{\boldsymbol{p}} \left[\frac{1}{\sqrt{(E+\mathrm{i}\delta)^2 - |\Delta|^2} - \xi_{\boldsymbol{p}}} \frac{1}{\sqrt{(E+\mathrm{i}\delta)^2 - |\Delta|^2} + \xi_{\boldsymbol{p}}} \right] \\
=&\frac{1}{2\sqrt{E_+^2 - |\Delta|^2}} \int_{-\omega_c}^{\omega_c} d\xi_{\boldsymbol{p}} \left[\frac{1}{\sqrt{E_+^2 - |\Delta|^2} - \xi_{\boldsymbol{p}}} + \frac{1}{\sqrt{E_+^2 - |\Delta|^2} + \xi_{\boldsymbol{p}}} \right] \\
=&\frac{1}{2\sqrt{E_+^2 - |\Delta|^2}} \int_{-\omega_c}^{\omega_c} d\xi_{\boldsymbol{p}} \left[\frac{1}{\sqrt{E^2 - |\Delta|^2} + \mathrm{i}E\delta - \xi_{\boldsymbol{p}}} + \frac{1}{\sqrt{E^2 - |\Delta|^2} + \mathrm{i}E\delta + \xi_{\boldsymbol{p}}} \right] \\
=&\frac{\pi}{\mathrm{i}} \frac{\mathrm{sign}(E)}{\sqrt{(E+\mathrm{i}\delta)^2 - |\Delta|^2}},
\end{aligned} \tag{A.21}$$

We have expanded the square root to the first order in δ in the denominator in the fourth equation. In the last equation, we have performed the contour integrations, which produced a factor of $\mathrm{sign}(E)$ because the two factors in the line above have a difference in the sign of the residue at their poles.

For the domain where $E^2 - |\Delta|^2 < 0$, we calculate

$$\begin{aligned}
&\int_{-\omega_c}^{\omega_c} d\xi_{\boldsymbol{p}} \frac{1}{E_+^2 - |\Delta|^2 - \xi_{\boldsymbol{p}}^2} \\
=&\int_{-\omega_c}^{\omega_c} d\xi_{\boldsymbol{p}} \left[\frac{1}{\mathrm{i}^2 \left(|\Delta|^2 - E_+^2\right) - \xi_{\boldsymbol{p}}^2} \right] \\
=&\int_{-\omega_c}^{\omega_c} d\xi_{\boldsymbol{p}} \left[\frac{1}{\mathrm{i}\sqrt{|\Delta|^2 - E_+^2} - \xi_{\boldsymbol{p}}} \frac{1}{\mathrm{i}\sqrt{|\Delta|^2 - E_+^2} + \xi_{\boldsymbol{p}}} \right] \\
=&\frac{1}{2\mathrm{i}\sqrt{|\Delta|^2 - E_+^2}} \int_{-\omega_c}^{\omega_c} d\xi_{\boldsymbol{p}} \left[\frac{1}{\mathrm{i}\sqrt{|\Delta|^2 - E_+^2} - \xi_{\boldsymbol{p}}} + \frac{1}{\mathrm{i}\sqrt{|\Delta|^2 - E_+^2} + \xi_{\boldsymbol{p}}} \right] \\
=&\frac{1}{2\mathrm{i}\sqrt{|\Delta|^2 - E_+^2}} \int_{-\omega_c}^{\omega_c} d\xi_{\boldsymbol{p}} \left[\frac{1}{\mathrm{i}\sqrt{|\Delta|^2 - E^2} + \mathrm{i}E\delta - \xi_{\boldsymbol{p}}} + \frac{1}{\mathrm{i}\sqrt{|\Delta|^2 - E^2} + \mathrm{i}E\delta + \xi_{\boldsymbol{p}}} \right] \\
=&\frac{\pi}{\mathrm{i}} \frac{-\mathrm{i}}{\sqrt{|\Delta|^2 - E_+^2} + \xi_{\boldsymbol{p}}}
\end{aligned} \tag{A.22}$$

The factor proportional to δ does not influence the contour integrals, since the poles are placed on the imaginary axis. Thus, we find that the retarded Green

function is given as

$$\hat{g}(E, \boldsymbol{R}, \boldsymbol{p}_F) = \mathcal{I}\left(E_+\hat{\tau}_3 + \hat{\Delta}\right), \tag{A.23}$$

with

$$\mathcal{I} = \frac{\Theta(E^2 - \Delta^2)\mathrm{sign}(E)}{\sqrt{E_+^2 - \Delta^2}} - \mathrm{i}\frac{\Theta(\Delta^2 - E^2)}{\sqrt{\Delta^2 - E_+^2}}. \tag{A.24}$$

In the main part of the thesis, we will normally not write out the infinitesimal factor explicitly, and instead reinstate it when it influences the results.

Appendix B

Schrödinger Field Theory

In this section, we introduce the concepts of second quantization and field operators in the context of the Schrödinger field; the field that satisfies the same equation as the wave functions from standard quantum mechanics. This section is based on the book by Economou [75].

We start by considering the Schrödinger equation for a classical field $\psi(\boldsymbol{r}, t)$,

$$\mathrm{i}\partial_t \psi(\boldsymbol{r}, t) = \mathcal{H}\psi(\boldsymbol{r}, t) = \left(-\frac{1}{2m}\boldsymbol{\nabla}^2 + V(\boldsymbol{r})\right)\psi(\boldsymbol{r}, t), \tag{B.1}$$

where $\mathcal{H} = p^2/2m + V$ is the Hamiltonian of the system we consider, and V is an arbitrary potential. The Lagrangian density that produces this equation of motion when we apply the principle of stationary action is

$$\mathcal{L} = \mathrm{i}\psi^\dagger \partial_t \psi - \frac{1}{2m}\boldsymbol{\nabla}\psi^\dagger \boldsymbol{\nabla}\psi - V\psi^\dagger\psi. \tag{B.2}$$

ψ is a scalar function, satisfying $\psi^\dagger = \psi^*$, but we use the dagger notation for convenience when we later quantize the field. The canonical momentum of the field is given in the standard way,

$$\Pi = \frac{\partial \mathcal{L}}{\partial\left(\partial_t \psi\right)} = \mathrm{i}\psi^\dagger. \tag{B.3}$$

From quantum mechanics we know that the general solution of Eq. (B.1) is given by

$$\psi(\boldsymbol{r}, t) = \sum_n c_n \mathrm{e}^{-\mathrm{i}E_n t}\psi_n(\boldsymbol{r}), \tag{B.4}$$

where ψ_n are the stationary energy eigenfunctions, satisfying

$$\mathcal{H}\psi_n = E_n \psi_n. \tag{B.5}$$

We can take the eigenfunctions as orthonormal, and it is assumed that these constitute a complete set. In (B.4), we assumed that the spectrum is discrete, but the arguments in this section will be similar for continuous spectra.

From classical field theory, we know that the field and the canonical momenta satisfies the Poisson bracket relations,

$$\{\psi(\boldsymbol{r}), \Pi(\boldsymbol{r}')\}_P = \delta(\boldsymbol{r} - \boldsymbol{r}') \quad \{\psi(\boldsymbol{r}), \psi(\boldsymbol{r}')\}_P \quad = 0 \quad \{\Pi(\boldsymbol{r}), \Pi(\boldsymbol{r}')\}_P = 0, \quad \text{(B.6)}$$

where the subscript indicates that these are Poisson brackets. The canonical quantization procedure consists of promoting the fields to operators, and Poisson brackets to commutation or anticommutation relations, depending on whether the particles described are fermions or bosons. Since we want to describe electrons, we choose the fermionic anticommutation relations,

$$\{\}_P \to \mathrm{i}\{\}. \quad \text{(B.7)}$$

Inserting the result from (B.3) the anticommutation relations reduce to

$$\{\psi(\boldsymbol{r}), \psi^\dagger(\boldsymbol{r}')\} = \delta(\boldsymbol{r} - \boldsymbol{r}') \qquad \{\psi(\boldsymbol{r}), \psi(\boldsymbol{r}')\} = 0 \qquad \{\psi^\dagger(\boldsymbol{r}), \psi^\dagger(\boldsymbol{r}')\} = 0, \quad \text{(B.8)}$$

which of course is the usual anticommutation relations for a fermionic field. Similarly, if we insert Eq. (B.4) into these relations, we get for the first equation that

$$\sum_{n,n'} \mathrm{e}^{-\mathrm{i}(E_n - E_{n'})t} \{c_n, c_{n'}^\dagger\} \psi_n(\boldsymbol{r}) \psi_{n'}^*(\boldsymbol{r}'). = \delta(\boldsymbol{r} - \boldsymbol{r}') \quad \text{(B.9)}$$

In order to isolate the anticommutator, we first multiply with $\psi_{n''}^*(\boldsymbol{r})$ and integrate over $\boldsymbol{r}$. Using the orthonormality of the energy eigenfunctions, we obtain

$$\sum_{n'} \mathrm{e}^{-\mathrm{i}(E_{n''} - E_{n'})t} \{c_{n''}, c_{n'}^\dagger\} \psi_{n'}^*(\boldsymbol{r}'). = \psi_{n''}^*(\boldsymbol{r}'), \quad \text{(B.10)}$$

and after multiplying with $\psi_n(\boldsymbol{r}')$ and integrating over $\boldsymbol{r}'$ we get

$$\{c_{n''}, c_n^\dagger\} = \delta_{nn''} \mathrm{e}^{+\mathrm{i}(E_{n''} - E_n)t} = \delta_{nn''}. \quad \text{(B.11)}$$

Similar calculations for the other anticommutation relations the total set of anti-commutation relations

$$\{c_n, c_{n'}^\dagger\} = \delta_{nn'} \qquad \{c_n, c_{n'}\} = 0 \qquad \{c_n^\dagger, c_{n'}^\dagger\} = 0, \quad \text{(B.12)}$$

where we have repeated the first result for completion. Thus, the anticommutation relations also hold for the energy eigenfunction basis.

Appendix C

Symmetries of the Quasiclassical Green Functions

In this appendix, we will derive symmetry relations of the quasiclassical Green function. We start with some general symmetries and then move on to symmetries specific to a real order parameter. Part of this chapter is based on the master's thesis of Morten [25].

C.1 General symmetries

In this section, we derive general symmetries of the quasiclassical Green functions. The 4×4 matrix $\hat{G}^{R/A}$ was defined in Eq. (3.26a) to involve the complex conjugates at the lower row components, and we now calculate the corresponding components of the quasiclassical Green functions. For the lower right components,

$$\begin{aligned}
&\frac{\mathrm{i}}{\pi}\int d\xi_p \int dx \mathrm{e}^{-\mathrm{i}x\cdot p}\underline{G}^{R/A}(X+\frac{1}{2}x, X-\frac{1}{2}x)^* \\
=&-\left[\frac{\mathrm{i}}{\pi}\int d\xi_p \int dx \mathrm{e}^{-\mathrm{i}x\cdot(-p)}\underline{G}^{R/A}(X+\frac{1}{2}x, X-\frac{1}{2}x)\right]^* \\
=&-\underline{g}^{R/A}(-E,-\boldsymbol{p}_E)^* = -\underline{\tilde{g}}^{R/A},
\end{aligned} \tag{C.1}$$

and the same is found for the anomalous Green function, allowing us to write the 4×4 quasiclassical retarded Green function as

$$\hat{g}^{R/A} = \begin{pmatrix} \underline{g}^{R/A} & \underline{f}^{R/A} \\ -\underline{\tilde{f}}^{R/A} & -\underline{\tilde{g}}^{R/A} \end{pmatrix} \tag{C.2}$$

We now move on to proving the general result relating the retarded and advanced quasiclassical Green function to each other. From the definitions of the Green

functions in Eq. (3.27) and Eq. (3.29) in Section 3.3.1,

$$\begin{aligned}\hat{\tau}_3\left[\hat{G}^A(2,1)\right]^\dagger\hat{\tau}_3 &= \hat{\tau}_3\left[\mathrm{i}\hat{\tau}_3\Theta(t_1-t_2)\left\langle\left\{\psi(2),\psi^\dagger(1)\right\}\right\rangle\right]^\dagger\hat{\tau}_3\\ &= \hat{\tau}_3\left[-\mathrm{i}\Theta(t_1-t_2)\left\langle\left\{\psi(1),\psi^\dagger(2)\right\}\right\rangle\hat{\tau}_3\right]\hat{\tau}_3\\ &= -\mathrm{i}\hat{\tau}_3\Theta(t_1-t_2)\left\langle\left\{\psi(1),\psi^\dagger(2)\right\}\right\rangle\\ &= \hat{G}^R(1,2)\end{aligned} \tag{C.3}$$

Using this in the definition of the advanced quasiclassical Green function, we get

$$\begin{aligned}\hat{g}^A(E,\boldsymbol{p},X) &= \frac{\mathrm{i}}{\pi}\int d\xi_p\int dx\mathrm{e}^{-\mathrm{i}x\cdot p}\hat{G}^A(X+\frac{1}{2}x,X-\frac{1}{2}x)\\ &= \frac{\mathrm{i}}{\pi}\int d\xi_p\int dx\mathrm{e}^{-\mathrm{i}x\cdot p}\hat{\tau}_3\left[\hat{G}^R(X-\frac{1}{2}x,X+\frac{1}{2}x)\right]^\dagger\hat{\tau}_3\\ &= \left[\frac{-\mathrm{i}}{\pi}\int d\xi_p\int dx\mathrm{e}^{+\mathrm{i}x\cdot p}\hat{\tau}_3\hat{G}^R(X-\frac{1}{2}x,X+\frac{1}{2}x)\hat{\tau}_3\right]^\dagger\\ &= -\hat{\tau}_3\left[\frac{\mathrm{i}}{\pi}\int d\xi_p\int dx\mathrm{e}^{-\mathrm{i}x\cdot p}\hat{G}^R(X+\frac{1}{2}x,X-\frac{1}{2}x)\right]^\dagger\hat{\tau}_3\\ &= -\hat{\tau}_3\left(\hat{g}^R\right)^\dagger\hat{\tau}_3\end{aligned} \tag{C.4}$$

This result is extremely useful since it removes the necessity of solving the Usadel equation for the advanced part when we already have found the solution for the retarded part[1].

C.2 Density of states at zero energy

Here, we will derive a relation describing how the symmetries of the quasiclassical Green function determine the effect of the density of states at the Fermi energy. Specifically, we will show that for triplet odd-frequency pairing, the density of states must be larger or equal to one, while for singlet even-frequency, it must be lowered. Consider a system with both triplet and singlet pairing, described by

$$\underline{f} = \begin{pmatrix} 0 & d_z+f_s \\ d_z-f_s & 0\end{pmatrix}, \tag{C.5}$$

and consider the case of the energy relative to the Fermi energy to be $E=0$, meaning that $\tilde{f}(0)=f^*(0)$. We get, temporarily suppressing the $E=0$ argument,

[1]We could of course also solve the Usadel equation for the advanced part and obtain the retarded part from Eq. (3.109).

and introducing the quantity $c \equiv fs^* d_z - f_s d_z^*$,

$$\underline{g}^2 = \underline{1} + \underline{f}\underline{\tilde{f}} = \begin{pmatrix} 1 + |d_z|^2 - |f_s|^2 + 2\mathrm{i}\Im\{c\} & 0 \\ 0 & 1 + |d_z|^2 - |f_s|^2 - 2\mathrm{i}\Im\{c\} \end{pmatrix}. \quad \text{(C.6)}$$

Taking the square root of this equation yields an expression for the quasiclassical Green function. In order to get the spin averaged density of states, we average over the spin-up and spin-down pairing density, and take the real part of the quasiclassical Green function,

$$\begin{aligned} N(E=0) &= \frac{N_0}{2} \Re \left\{ g_{\uparrow\uparrow} + g_{\downarrow\downarrow} \right\} \\ &= \frac{N_0}{2} \Re \left\{ \sqrt{1 + |d_z|^2 - |f_s|^2 + 2\mathrm{i}\Im\{c\}} + \sqrt{1 + |d_z|^2 - |f_s|^2 - 2\mathrm{i}\Im\{c\}} \right\}. \end{aligned} \quad \text{(C.7)}$$

In the case of a weak proximity effect, we expand the square root to first order, and get[2]

$$N(E=0) = N_0 \left(1 + \frac{|d_z|^2 - |f_s|^2}{2} \right). \quad \text{(C.8)}$$

This shows that in the weak regime, singlets will always lower the zero-energy density of states, while triplets will increase it.

In the case of a strong proximity effect, we cannot expand the square root, and the expression will not reduce in the same way as in the weak proximity regime. If we however consider systems with only singlets or only triplets, we find that

$$N(E=0) = \begin{cases} N_0 \sqrt{1 - |f_s|^2}, & \text{pure even-frequency singlet paring,} \\ N_0 \sqrt{1 + |d_z|^2}, & \text{pure odd-frequency triplet paring with } S_z = 0. \end{cases} \quad \text{(C.9)}$$

We see that triplets increase the density of states at zero energy, while singlets decrease it.

This can be understood better from the symmetries of the quasiclassical Green functions. We consider a real gap, such that we can use the symmetry criteria from Eq. (4.29) and Eq. (4.30). From the normalization condition in (3.105), it can be seen that if one considers a singlet superconductor with $\underline{f} = \mathrm{antidiag}(f_s, -f_s)$, one obtains

$$\underline{g} = \sqrt{\underline{1} + \underline{f}\underline{\tilde{f}}} = \underline{1}\sqrt{1 + f_s^2} = \underline{1}\sqrt{1 + \Re\{f_s\}^2 - \Im\{f_s\}^2 + 2\mathrm{i}\Re\{f_s\}\Im\{f_s\}}. \quad \text{(C.10)}$$

[2]This can be seen either due to taking the real part or due to the imaginary numbers canceling each other.

Repeating the same with an $S_z = 0$ triplet with $\underline{f} = \text{antidiag}(d_z, d_z)$, we find that the same relation holds,

$$\underline{g} = \underline{1}\sqrt{1 + \Re\{d_z\}^2 - \Im\{d_z\}^2 + 2\mathrm{i}\Re\{d_z\}\Im\{d_z\}}. \tag{C.11}$$

The symmetry criterion for the even-frequency singlet in Eq. (4.29) says that the real part of f_s is antisymmetric in E, while the imaginary part is symmetric. This, of course, implies a vanishing real part at $E = 0$, which from Eq. (C.10) implies the result for the even-frequency singlets from Eq. (C.9). Similarly, the symmetry criterion for the odd-frequency triplet in Eq. (4.30) says that the imaginary part of f_s is antisymmetric in E, while the real part is symmetric. This, together with Eq. (C.11) implies the result for odd-frequency triplets from Eq. (C.9).

Appendix D

Electrodynamics

In this section, we will derive the Hamiltonian for a classical particle in an electromagnetic field, and show how the magnetic vector potential $\boldsymbol{A}$ enters[1]. We will also discuss the distinction between the canonical and the kinetic momentum. Much of the theory of electromagnetism used in this section is based on Griffiths [28].

Classical electrodynamics is defined by the Maxwell equations,

$$\boldsymbol{\nabla} \cdot \boldsymbol{E} = \rho \qquad \boldsymbol{\nabla} \cdot \boldsymbol{B} = 0 \qquad \boldsymbol{\nabla} \times \boldsymbol{E} = -\partial_t \boldsymbol{B} \qquad \boldsymbol{\nabla} \times \boldsymbol{B} = \boldsymbol{J} + \partial_t \boldsymbol{E}, \tag{D.1}$$

where we have set the permittivity and permeability to unity. These equations describe the dynamics of the electric field $\boldsymbol{E}$ and the magnetic field $\boldsymbol{B}$ in terms of the charge density ρ and the electrical current $\boldsymbol{J}$. Together with the Lorentz force law,

$$\boldsymbol{F} = q(\boldsymbol{E} + \boldsymbol{v} \times \boldsymbol{B}), \tag{D.2}$$

describing the force $\boldsymbol{F}$ on a particle with velocity $\boldsymbol{v}$, these equations completely describe all classical electromagnetic phenomenon.

We start of our derivation of the Hamiltonian by guessing a Lagrangian L, which when inserted into the Lagrangian equations,

$$\partial_i L - \frac{d}{dt} \partial_{v_i} L = 0, \tag{D.3}$$

where $i = \{x, y, z\}$, should produce the Lorentz force law. By trial and error, we guess the Lagrangian

$$L = \frac{1}{2} m v^2 - q\phi + q\boldsymbol{A} \cdot \boldsymbol{v}, \tag{D.4}$$

[1]This is useful since we obtain quantum mechanics by using the classical Hamiltonian, along with the promotion of observable quantities to operators.

where $v = |\boldsymbol{v}|$, ϕ is the electrostatic potential and $\boldsymbol{A}$ the magnetic vector potential. The fields are given in terms of the potentials as

$$\boldsymbol{B} = \boldsymbol{\nabla} \times \boldsymbol{A} \tag{D.5}$$

$$\boldsymbol{E} = -\boldsymbol{\nabla}\phi - \partial_t \boldsymbol{A}, \tag{D.6}$$

Noting that,

$$\partial_x L = q(\boldsymbol{v} \cdot \partial_x \boldsymbol{A} - \partial_x) \tag{D.7}$$

$$\frac{d}{dt}\partial_{v_x} L = m\frac{d}{dt}v_x + q(\boldsymbol{v} \cdot \nabla A_x + \partial_t A_x), \tag{D.8}$$

where we have used the definition of a total derivative in the second equation. Inserting into (D.3), we get for the x-component,

$$\begin{aligned} m\frac{dv_x}{dt} &= q\boldsymbol{v} \cdot \partial_x \boldsymbol{A} - q(\boldsymbol{v} \cdot \boldsymbol{\nabla})A_x - q(\partial_x \phi + \partial_t A_x) \\ &= q\left(v_y \left[\partial_x A_y - \partial_y A_x\right] + v_z \left[\partial_x A_z - \partial_z A_x\right]\right) + eE_x \\ &= q\left(v_y \left[\boldsymbol{\nabla} \times A\right]_z - v_z \left[\boldsymbol{\nabla} \times A\right]_y\right) + qE_x \\ &= q\left(v_y \boldsymbol{B}_z - v_z \boldsymbol{B}_y\right) + qE_x \\ &= q\left(\left[\boldsymbol{v} \times \boldsymbol{B}\right]_x + E_x\right), \end{aligned} \tag{D.9}$$

which is exactly the x-component of the Lorentz force law in Eq. (D.2). The calculation for the other components is completely similar. This proves that the Lagrangian in Eq. (D.4) is the correct one for a particle moving in an electromagnetic field.

The canonical momentum is

$$\boldsymbol{p} = \nabla_{\boldsymbol{v}} L = m\boldsymbol{v} + q\boldsymbol{A}, \tag{D.10}$$

and the Hamiltonian is given by the Legendre transformation

$$H = \boldsymbol{p} \cdot \boldsymbol{v} - L = \frac{1}{2}mv^2 + q\phi = \frac{1}{2m}\left(\boldsymbol{p} - q\boldsymbol{A}\right)^2 + q\phi, \tag{D.11}$$

meaning that we have transformed from the Lagrangian, which is a function of $\boldsymbol{r}, \dot{\boldsymbol{r}}$, to the Hamiltonian, which is a function of $\boldsymbol{r}, \boldsymbol{p}$. Note that it is the so-called kinetic momentum,

$$\boldsymbol{P} \equiv \boldsymbol{p} - q\boldsymbol{A} = \frac{1}{2}m\boldsymbol{v}, \tag{D.12}$$

which is the quantity that appears in the Hamiltonian. This makes sense from a physical standpoint, since the magnetic field should not contribute to the energy of the particle.

Finally, we discuss conservation laws for these momenta. It is sometimes mentioned that the canonical momenta are conserved for a particle moving in an electromagnetic field. Here, we will argue that in general neither the canonical momentum nor the kinetic momenta are conserved for such a particle. Using Eq. (D.9), we see that

$$\frac{d\boldsymbol{P}}{dt} = q\left([\boldsymbol{v} \times (\boldsymbol{\nabla} \times \boldsymbol{A})] - \boldsymbol{\nabla}\phi - \partial_t \boldsymbol{A}\right), \tag{D.13}$$

meaning that the kinetic momentum for a particle in an electromagnetic field is not conserved. This is of course to be expected, since the particle is influenced by electric and magnetic forces, in the Newtonian formalism. The equation of motion for the canonical momenta becomes

$$\frac{d\boldsymbol{p}}{dt} = q\left([\boldsymbol{v} \times (\boldsymbol{\nabla} \times \boldsymbol{A})] - \boldsymbol{\nabla}\phi + (\boldsymbol{v} \cdot \boldsymbol{\nabla}) \cdot \boldsymbol{A}\right), \tag{D.14}$$

which in general is nonzero as well. As a final remark, we see that if the potentials are position-independent, we get that the canonical momentum is conserved, which is a consequence of Noether's theorem [68].

Appendix E

The Dyson Equation

In this section, we will show the equivalence of the Dyson equation and a generalized equation of motion for the Green function,

$$\left[\mathrm{i}\hat{\tau}_3\partial_{t_1} - \hat{H}_0(1)\right]\check{G}(1,2) - \left[\check{\Sigma}\bullet\check{G}\right](1,2) = \delta(1-2)\check{1}, \tag{E.1}$$

where $\check{\Sigma}(1,2)$ is a general 2-body self-energy term, and we use the shorthand notation $(1,2) \equiv (x_1, x_2)$. The bullet product is given by

$$\left[\check{\Sigma}\bullet\check{G}\right](1,2) = \int dx_3 \check{\Sigma}(1,3)\check{G}(3,2). \tag{E.2}$$

Eq. (E.1) corresponds to the right-handed equation of motion of the Green function with a scalar potential if $\check{\Sigma}(1,2) = \delta(1-2)V(1)\check{1}$, so that the equation of motion reads

$$\left[\mathrm{i}\hat{\tau}_3\partial_{t_1} - \hat{H}_0(\boldsymbol{r_1}) - V(1)\hat{1}\right]\check{G}(1,2) = \delta(1-2)\check{1}. \tag{E.3}$$

Let $\check{G}_0$ be the Green function that solves Eq. (E.1) without the self-energy term,

$$\left[\mathrm{i}\hat{\tau}_3\partial_{t_1} - \hat{H}_0(1)\right]\check{G}_0(1,2) = \delta(1-2)\check{1}. \tag{E.4}$$

For suggestive notation, we define the differential operator $\hat{L}(1) \equiv \mathrm{i}\hat{\tau}_3\partial_{t_1} - \hat{H}_0(1)$, and the source term $\check{s}(1,2) \equiv \delta(1-2)\check{1} + [\check{\Sigma}\bullet\check{G}](1,2)$. We can then write Eq. (E.1) as

$$L(1)\check{G}(1,2) = \check{s}(1,2), \tag{E.5}$$

which is a function $\check{G}$ acted upon by a differential operator, and $\check{G}_0$ is the Green function of the differential operator $\hat{L}(1)$. As usual, the solution of the differential equation with the source term, which in this case is Eq. (E.1), is given as the

integral over the source terms, and the Green function of the differential operator,

$$\check{G}(1,2) = \int dx_3 \check{G}_0(1,3)\check{s}(3,2) \tag{E.6}$$

$$= \int dx_3 \check{G}_0(1,3)\left(\delta(3-2)\check{1} + \int dx_4 \check{\Sigma}(3,4)\check{G}(4,2)\right) \tag{E.7}$$

$$= \check{G}_0(1,2) + \left[G_0 \bullet \check{\Sigma} \bullet \check{G}\right](1,2), \tag{E.8}$$

which is the Dyson equation, which can be iterated by inserting the expression for $\check{G}$ into the right-hand side. In the case of a scalar potential $\check{\Sigma}(1,2) = V(1)\delta(1-2)\check{1}$, this reduces to

$$\check{G}(1,2) = \check{G}_0(1,2) + \int dx_3 \check{G}_0(1,3)V(3)\check{G}(3,2). \tag{E.9}$$

Thus, we have shown that the Dyson equation in Eq. (E.6) is equivalent to Eq. (E.1). In the case of a scalar potential, this means that Eq. (E.4) is equivalent to Eq. (E.9).

Appendix F

Spin Mode Renormalization in a Triplet Superconductor

In this appendix, we consider the Usadel equation,

$$D\partial_x(\check{g}\partial_x\check{g})^K = -\mathrm{i}\left[\hat{E}\tau_3 + \check{\sigma}_{\mathrm{so}} + \check{\sigma}_{\mathrm{sf}} + \hat{D}^T(E), \hat{g}\right]^K, \tag{F.1}$$

and find the equation of motion for the non-equilibrium spin mode. The distribution function is diagonal, and we define the components of the distribution matrix as $\hat{h} = \mathrm{diag}(h_1, h_2, h_3, h_4)$.

We start by considering the left-hand side of Eq. (F.1). The term inside the first derivative can be written

$$(\check{g}\partial_x\check{g})^K = \hat{g}^R\partial_x\hat{g}^K + \hat{g}^K\partial_x\hat{g}^A = \hat{g}^R\partial_x\left(\hat{g}^R\hat{h} - \hat{h}\hat{g}^A\right) = \partial_x\hat{h} - g^R\partial_x\hat{h}\hat{g}^A, \tag{F.2}$$

where we have used that the derivative of the retarded and the advanced Green functions vanish in a bulk material, the parametrization of the Keldysh Green function from Eq. (3.106), and the normalization condition from Eq. (4.31). Inserting this back into the Usadel equation, the left-hand side becomes

$$D\partial_x^2\left(\hat{h} - \hat{g}^R\hat{h}\hat{g}^A\right). \tag{F.3}$$

Since we want to calculate the spin mode in the material, we perform the trace operation $\mathrm{Tr}\{\hat{\tau}_3\hat{\sigma}_3...\}/4$, and find that the first term of Eq. (F.3) becomes $D\partial_x^2 h^z$. The second term is somewhat more complicated, because of the extra retarded and advanced Green functions. First, we use the relation for the advanced Green function in Eq. (3.109),

$$\begin{aligned}\hat{g}^A &= -\hat{\tau}_3\left(\mathcal{I}_g E\hat{\tau}_3 + \mathcal{I}_f\Delta\hat{J}_3\right)^\dagger\hat{\tau}_3 \\ &= -\hat{\tau}_3\left(\mathcal{I}_g^* E\hat{\tau}_3 + \mathcal{I}_f^*\Delta\left[-\hat{J}_3\right]\right)\hat{\tau}_3 \\ &= -\mathcal{I}_g^* E\hat{\tau}_3 - \mathcal{I}_f^*\Delta\hat{J}_3.\end{aligned} \tag{F.4}$$

In the last equation, we have used that $\hat{\tau}_3^2 = \hat{1}$ and that $\hat{\tau}_3$ anticommutes with any antidiagonal matrix, such as $\hat{J}_3$. The second term inside the parenthesis in Eq. (F.3) becomes

$$\frac{1}{4}\mathrm{Tr}\Big\{\hat{\tau}_3\hat{\sigma}_3\hat{g}^R\hat{h}\hat{g}^A\Big\} = -\frac{1}{4}\mathrm{Tr}\Big\{\hat{\tau}_3\hat{\sigma}_3\left(\mathcal{I}_g E\hat{\tau}_3 + \mathcal{I}_f\Delta\hat{J}_3\right)\hat{h}\left(\mathcal{I}_g^* E\hat{\tau}_3 + \mathcal{I}_f^*\Delta\hat{J}_3\right)\Big\}. \quad \text{(F.5)}$$

The four terms in this equation evaluate to

$$-\frac{E^2|\mathcal{I}_g|^2}{4}\mathrm{Tr}\Big\{\hat{\tau}_3\hat{\sigma}_3\hat{\tau}_3\hat{h}\hat{\tau}_3\Big\} = -E^2|\mathcal{I}_g|^2\hat{h}^z \quad \text{(F.6)}$$

$$-\frac{\Delta^2|\mathcal{I}_f|^2}{4}\mathrm{Tr}\Big\{\hat{\tau}_3\hat{\sigma}_3\hat{J}_3\hat{h}\hat{J}_3\Big\} = |\mathcal{I}_f|^2\Delta^2 h^z \quad \text{(F.7)}$$

$$-\frac{\Delta E\mathcal{I}_g\mathcal{I}_f^*}{4}\mathrm{Tr}\Big\{\hat{\tau}_3\hat{\sigma}_3\hat{\tau}_3\hat{h}\hat{J}_3\Big\} = 0 \quad \text{(F.8)}$$

$$-\frac{\Delta E\mathcal{I}_g^*\mathcal{I}_f}{4}\mathrm{Tr}\Big\{\hat{\tau}_3\hat{\sigma}_3\hat{J}_3\hat{h}\tau_3\Big\} = 0. \quad \text{(F.9)}$$

In the second equation, we have used that $\hat{J}_3\hat{h}\hat{J}_3 = -\mathrm{diag}(h_4, h_3, h_2, h_1)$, and in the third and fourth equations we used that terms containing one antidiagonal matrix and several diagonal matrices will be antidiagonal, making the trace vanish. Eq. (F.3) thus evaluates to

$$D\partial_x^2\Big(\hat{h} - \hat{g}^R\hat{h}\hat{g}^A\Big) = D\partial_x^2 h^z\left(1 + |\mathcal{I}_g|^2E^2 - |\mathcal{I}_f|^2\Delta^2\right) \quad \text{(F.10)}$$

We proceed by considering the right-hand side of the Usadel equation in Eq. (F.1). The kinetic and superconducting terms are diagonal in Keldysh space so that taking the Keldysh component of the commutator is equivalent to just replacing the Green function with its Keldysh component,

$$[E\hat{\tau}_3 + \Delta\hat{J}_3, \check{g}]^K = [E\hat{\tau}_3 + \Delta\hat{J}_3, \hat{g}^K] \quad \text{(F.11)}$$

Using this, we evaluate the spin-trace of the kinetic term, first noting that we have

$$[\hat{\tau}_3, \hat{g}^R] = \mathcal{I}_f[\hat{\tau}_3, \Delta\hat{J}_3] = \mathcal{I}_f\Delta\hat{J}_1 \quad \text{(F.12)}$$

and

$$[\hat{\tau}_3, \hat{g}^A] = \mathcal{I}_f^*[\hat{\tau}_3, \Delta\hat{J}_3] = \mathcal{I}_f^*\Delta\hat{J}_1, \quad \text{(F.13)}$$

with $\hat{J}_1$ the antidiagonal identity matrix. We thus get for the kinetic term,

$$\begin{aligned}
-\frac{\mathrm{i}}{4}\mathrm{Tr}\big\{\hat{\tau}_3\hat{\sigma}_3[E\hat{\tau}_3, \hat{g}^K]\big\} &= -\frac{\mathrm{i}E}{4}\mathrm{Tr}\Big\{[\hat{\tau}_3, \hat{g}^R\hat{h} - \hat{h}g^A]\Big\} \\
&= -\frac{\mathrm{i}E}{4}\mathrm{Tr}\Big\{\hat{\tau}_3\hat{\sigma}_3[\hat{\tau}_3, \hat{g}^R]\hat{h} - \hat{h}[\hat{\tau}_3, \hat{g}^A]\Big\} \\
&= \frac{E\Delta}{4}\mathrm{Tr}\Big\{\hat{\tau}_3\hat{\sigma}_3\left(\mathcal{I}_f\hat{J}_3\hat{h} - \mathcal{I}_f^*\hat{h}\hat{J}_3\right)\Big\} = 0
\end{aligned} \quad \text{(F.14)}$$

where we in the second line have used the commutator identity

$$[A, BC] = [A, B]C + B[A, C], \tag{F.15}$$

as well as the fact that the diagonal distribution matrix commutes with $\hat{\tau}_3$. In the last line, we used that the trace of any antidiagonal four-dimensional matrix is zero[1]. This result means that the kinetic term in the Usadel equation does not affect the spin mode of the system, which makes sense physically.

To calculate the superconducting term, we first calculate some more commutators,

$$[\hat{D}^T(E), \hat{g}^R] = \mathcal{I}_g E[\hat{D}^T(E), \hat{\tau}_3] = -2\mathcal{I}_g E D(E)\hat{J}_1 \tag{F.16}$$

$$[\hat{D}^T(E), \hat{g}^A] = -\mathcal{I}_g^* E[\hat{D}^T(E), \hat{\tau}_3] = 2\mathcal{I}_g^* E D(E)\hat{J}_1 \tag{F.17}$$

$$[\hat{D}^T(E), \hat{h}] = -D(E)\,\mathrm{antidiag}(h_1 - h_4, h_2 - h_3, h_2 - h_3, h_1 - h_4) \tag{F.18}$$

$$\hat{J}_3[\hat{D}^T(E), \hat{h}] = -D(E)\,\mathrm{diag}(h_2 - h_3, h_2 - h_3, -h_1 + h_4, -h_1 + h_4) \tag{F.19}$$

In total, we want to calculate

$$\begin{aligned} -\frac{\mathrm{i}}{4}\mathrm{Tr}\Big\{\hat{\tau}_3\hat{\sigma}_3\big[\hat{D}^T(E), \hat{g}^K\big]\Big\} &= -\frac{\mathrm{i}}{4}\mathrm{Tr}\Big\{\hat{\tau}_3\hat{\sigma}_3\Big(\big[\hat{D}^T(E), \hat{g}^R\hat{h}\big] - \big[\hat{D}^T(E), \hat{h}\hat{g}^A\big]\Big)\Big\} \\ &= -\frac{\mathrm{i}}{4}\mathrm{Tr}\Big\{\hat{\tau}_3\hat{\sigma}_3\Big(\big[\hat{D}^T(E), \hat{g}^R\big]\hat{h} + \hat{g}^R\big[\hat{D}^T(E), \hat{h}\big]\Big)\Big\} \\ &\quad - \frac{\mathrm{i}}{4}\mathrm{Tr}\Big\{\hat{\tau}_3\hat{\sigma}_3\Big(-\big[\hat{D}^T(E), \hat{h}\big]\hat{g}^A - \hat{h}[\hat{D}^T(E), \hat{g}^A]\Big)\Big\}. \end{aligned} \tag{F.20}$$

We consider the first and fourth terms in the last equation,

$$\begin{aligned} &-\frac{\mathrm{i}}{4}\mathrm{Tr}\Big\{\hat{\tau}_3\hat{\sigma}_3\Big(\big[\hat{D}^T(E), \hat{g}^R\big]\hat{h} - \hat{h}\big[\hat{D}^T(E), \hat{g}^A\big]\Big)\Big\} \\ =&-\frac{\mathrm{i}}{4}\mathrm{Tr}\Big\{\hat{\tau}_3\hat{\sigma}_3\Big(\big[\hat{D}^T(E), \hat{g}^R\big]\hat{h} - \big[\hat{D}^T(E), \hat{g}^A\big]\hat{h}\Big)\Big\} \\ =&\mathrm{i}\Re\{\mathcal{I}_g\}ED(E)\mathrm{Tr}\Big\{\hat{\tau}_3\hat{\sigma}_3\hat{J}_1\hat{h}\Big\} = 0, \end{aligned} \tag{F.21}$$

where we in the second line have commuted $\hat{h}$ through the diagonal matrices $\hat{\tau}_3$ and $\hat{\sigma}_3$, and used the cyclic permutation identity of the trace. In the last line, we have again used that the trace of an antidiagonal four-dimensional matrix is zero.

[1]The more general result is of course that the trace of a matrix in an even number of dimensions vanishes.

The second and third term of Eq. (F.20) becomes

$$\begin{aligned}
&-\frac{\mathrm{i}}{4}\mathrm{Tr}\Big\{\hat{\tau}_3\hat{\sigma}_3\left(\hat{g}^R[\hat{D}^T(E),\hat{h}]-[\hat{D}^T(E),\hat{h}]\hat{g}^A\right)\Big\}\\
=&\frac{-\mathrm{i}}{4}\mathrm{Tr}\Big\{\hat{\tau}_3\hat{\sigma}_3\left(\mathcal{I}_f\Delta\hat{J}_3[\hat{D}^T(E),\hat{h}]-[\hat{D}^T(E),\hat{h}]\mathcal{I}_f^*\Delta\hat{J}_3\right)\Big\}\\
=&\frac{\Delta\Im\{\mathcal{I}_f\}}{2}\mathrm{Tr}\Big\{\hat{\tau}_3\hat{\sigma}_3\left(\hat{J}_3[\hat{D}^T(E),\hat{h}]\right)\Big\}\\
=&-D(E)\Delta\frac{\Im\{\mathcal{I}_f\}}{2}\mathrm{Tr}\{\mathrm{diag}(h_2-h_3,-h_2+h_3,h_1-h_4,-h_1+h_4)\}=0,
\end{aligned}\tag{F.22}$$

where we in the third line have used again that the trace of an antidiagonal matrix vanishes as well as that $\hat{J}_3$ anticommutes with $\hat{\tau}_3$ and $\hat{\sigma}_3$, and in the last line we used Eq. (F.19). Thus, we have shown that the superconducting term as well will give no contribution to the equation of motion for the spin mode.

We proceed to calculate the spin-flip term,

$$\begin{aligned}
-\frac{\mathrm{i}}{4}\mathrm{Tr}\Big\{\hat{\tau}_3\hat{\sigma}_3\left[\check{\sigma}_{\mathrm{sf}},\check{g}\right]^K\Big\}&=-\frac{\mathrm{i}}{4}\mathrm{Tr}\big\{\hat{\tau}_3\hat{\sigma}_3\left[\hat{\sigma}_{\mathrm{sf}}^{\mathrm{R}}\hat{g}^K+\hat{\sigma}_{\mathrm{sf}}^{\mathrm{K}}\hat{g}^A-\hat{g}^R\hat{\sigma}_{\mathrm{sf}}^{\mathrm{A}}-\hat{g}^K\hat{\sigma}_{\mathrm{sf}}^{\mathrm{A}}\right]\big\}\\
&=\frac{h^z}{\tau_{\mathrm{sf}}}\left(2\Re\{\mathcal{I}_g\}^2E^2-\Delta^2\left[|\mathcal{I}_f|^2+\Re\{\mathcal{I}_f^2\}\right]\right),
\end{aligned}\tag{F.23}$$

where the calculation has been performed using mathematical software. Similarly, for the spin-orbit term we find

$$\begin{aligned}
-\frac{\mathrm{i}}{4}\mathrm{Tr}\Big\{\hat{\tau}_3\hat{\sigma}_3\left[\hat{\boldsymbol{\sigma}}_{\mathrm{so}},\check{g}\right]^K\Big\}&=-\frac{\mathrm{i}}{4}\mathrm{Tr}\big\{\hat{\tau}_3\hat{\sigma}_3\left[\hat{\boldsymbol{\sigma}}_{\mathrm{so}}^{\mathrm{R}}\hat{g}^K+\hat{\boldsymbol{\sigma}}_{\mathrm{so}}^{\mathrm{K}}\hat{g}^A-\hat{g}^R\hat{\boldsymbol{\sigma}}_{\mathrm{so}}^{\mathrm{A}}-\hat{g}^K\hat{\boldsymbol{\sigma}}_{\mathrm{so}}^{\mathrm{A}}\right]\big\}\\
&=\frac{h^z}{\tau_{\mathrm{so}}}\left(2\Re\{\mathcal{I}_g\}^2E^2+\Delta^2\left[|\mathcal{I}_f|^2+\Re\{\mathcal{I}_f^2\}\right]\right).
\end{aligned}\tag{F.24}$$

In total, the equation of motion for the spin mode reads

$$\begin{aligned}
D\partial_x^2h^z\left(1+|\mathcal{I}_g|^2E^2-|\mathcal{I}_f|^2\Delta^2\right)&=\frac{2h^z}{\tau_{\mathrm{sf}}}\left(\Re\{\mathcal{I}_g\}^2E^2-\Delta^2\left[|\mathcal{I}_f|^2+\Re\{\mathcal{I}_f^2\}\right]\right)\\
&\quad+\frac{2h^z}{\tau_{\mathrm{so}}}\left(\Re\{\mathcal{I}_g\}^2E^2+\Delta^2\left[|\mathcal{I}_f|^2+\Re\{\mathcal{I}_f^2\}\right]\right),
\end{aligned}\tag{F.25}$$

which can be isolated for the derivative as

$$\begin{aligned}
\partial_x^2h^z=&\frac{h^z}{D\tau_{\mathrm{sf}}}\frac{2\Re\{\mathcal{I}_g\}^2E^2-\Delta^2\left[|\mathcal{I}_f|^2+\Re\{\mathcal{I}_f^2\}\right]}{1+E^2|\mathcal{I}_g|^2-|\mathcal{I}_f|^2\Delta^2}\\
&+\frac{h^z}{D\tau_{\mathrm{so}}}\frac{2\Re\{\mathcal{I}_g\}^2E^2+\Delta^2\left[|\mathcal{I}_f|^2+\Re\{\mathcal{I}_f^2\}\right]}{1+E^2|\mathcal{I}_g|^2-|\mathcal{I}_f|^2\Delta^2}.
\end{aligned}\tag{F.26}$$

We now consider the two terms in detail, starting with the spin-flip term. We begin by noting that the normalization of $\hat{g}^R$ means that

$$\left(\hat{g}^R\right)^2 = \mathcal{I}_g^2 E^2 \hat{\tau}_3^2 + E\Delta\mathcal{I}_g\mathcal{I}_f\left(\hat{\tau}_3\hat{J}_3 + \hat{\tau}_3\hat{J}_3\right) + \Delta^2\mathcal{I}_f^2\hat{J}_3 = \mathcal{I}_g^2E^2 - \mathcal{I}_f^2\Delta^2 = 1. \quad \text{(F.27)}$$

Taking the real part of this, we find

$$\Re\{\mathcal{I}_g^2\}E^2 - \Re\{\mathcal{I}_f^2\}\Delta^2 = 1. \quad \text{(F.28)}$$

Inserting this into the spin-flip term, we find that the numerator becomes

$$\begin{aligned}
&2\Re\{\mathcal{I}_g\}^2E^2 - \Delta^2\left(|\mathcal{I}_f|^2 + \Re\{\mathcal{I}_f^2\}\right) && \text{(F.29)}\\
=&2\Re\{\mathcal{I}_g\}^2E^2 - \Delta^2|\mathcal{I}_f|^2 + 1 - \Re\{\mathcal{I}_g^2\}E^2 && \text{(F.30)}\\
=&1 - \Delta^2|\mathcal{I}_f|^2 + E^2\left(2\Re\{\mathcal{I}_g\}^2 - \Re\{\mathcal{I}_g^2\}\right) && \text{(F.31)}\\
=&1 - \Delta^2|\mathcal{I}_f|^2 + E^2\left(2\Re\{\mathcal{I}_g\}^2 - \Re\{\mathcal{I}_g\}^2 + \Im\{\mathcal{I}_g\}^2\right) && \text{(F.32)}\\
=&1 - \Delta^2|\mathcal{I}_f|^2 + E^2|\mathcal{I}_g|^2, && \text{(F.33)}
\end{aligned}$$

which cancels the denominator. Moving on to the spin-orbit term in Eq. (F.26), we can rewrite the numerator as

$$\begin{aligned}
&2\Re\{\mathcal{I}_g\}^2E^2 + \Delta^2\left(|\mathcal{I}_f|^2 + \Re\{\mathcal{I}_f^2\}\right) && \text{(F.34)}\\
=&2\Re\{\mathcal{I}_g\}^2E^2 - \Delta^2\left(|\mathcal{I}_f|^2 + \Re\{\mathcal{I}_f^2\}\right) + 2\Delta^2\left(|\mathcal{I}_f|^2 + \Re\{\mathcal{I}_f^2\}\right) && \text{(F.35)}\\
=&\left[1 - \Delta^2|\mathcal{I}_f|^2 + E^2|\mathcal{I}_g|^2\right] + 4\Delta^2\Re\{\mathcal{I}_f\}^2 && \text{(F.36)}
\end{aligned}$$

where we have used Eq. (F.28) in the last line. Using this, we rewrite Eq. (F.26), and obtain the final expression for the equation of motion for the spin mode,

$$\partial_x^2 h^z = \frac{h^z}{D\tau_{\text{sf}}} + \frac{h^z}{D\tau_{\text{so}}}\left(1 + \frac{4\Delta^2\Re\{\mathcal{I}_f\}^2}{1 + E^2|\mathcal{I}_g|^2 - |\mathcal{I}_f|^2\Delta^2}\right). \quad \text{(F.37)}$$

Bibliography

[1] T. E. of Encyclopaedia Britannica. "Ferromagnetism," Encyclopaedia Britannica. (20th Jul. 1998), [Online]. Available: https://www.britannica.com/science/ferromagnetism (visited on 10/05/2022).

[2] C. Timm, *Theory of Magnetism*, 4th Nov. 2015.

[3] M. N. Baibich, J. M. Broto, A. Fert, F. N. Van Dau, F. Petroff, P. Etienne, G. Creuzet, A. Friederich and J. Chazelas, "Giant Magnetoresistance of (001)Fe/(001)Cr Magnetic Superlattices," *Physical Review Letters*, vol. 61, p. 2472, 21st Nov. 1988, DOI: 10.1103/PhysRevLett.61.2472.

[4] G. Binasch, P. Grünberg, F. Saurenbach and W. Zinn, "Enhanced magnetoresistance in layered magnetic structures with antiferromagnetic interlayer exchange," *Physical Review B*, vol. 39, p. 4828, 1st Mar. 1989, DOI: 10.1103/PhysRevB.39.4828.

[5] "The Nobel Prize in Physics 2007," NobelPrize.org. (9th Oct. 2007), [Online]. Available: https://www.nobelprize.org/prizes/physics/2007/summary/ (visited on 16/06/2022).

[6] J. Linder and J. W. A. Robinson, "Superconducting spintronics," *Nature Physics*, vol. 11, p. 307, Apr. 2015, DOI: 10.1038/nphys3242.

[7] I. Žutić, J. Fabian and S. Das Sarma, "Spintronics: Fundamentals and applications," *Reviews of Modern Physics*, vol. 76, p. 323, 23rd Apr. 2004, DOI: 10.1103/RevModPhys.76.323.

[8] L. N. Cooper, "Bound Electron Pairs in a Degenerate Fermi Gas," *Physical Review*, vol. 104, p. 1189, 15th Nov. 1956, DOI: 10.1103/PhysRev.104.1189.

[9] C. Whyte. "How Maglev Works," Energy.gov. (14th Jun. 2016), [Online]. Available: https://www.energy.gov/articles/how-maglev-works (visited on 16/06/2022).

[10] D. Ginsberg. "Superconductivity," Encyclopaedia Britannica. (15th Feb. 2007), [Online]. Available: https://www.britannica.com/science/superconductivity (visited on 10/05/2022).

[11] M. Eschrig, "Spin-polarized supercurrents for spintronics," *Physics Today*, vol. 64, p. 43, 2011, DOI: 10.1063/1.3541944.

[12] V. L. Berezinskii, "New model of anisotropic phase of the superfluid He3," *JETP Letters*, vol. 20, p. 287, Nov. 1974[*Pis'ma v Zhurnal Ehksperimental'noj i Teoreticheskoj Fiziki*, vol. 20, p. 287, 1974].

[13] J. Linder and A. V. Balatsky, "Odd-frequency superconductivity," *Reviews of Modern Physics*, vol. 91, p. 045005, 24th Dec. 2019, DOI: 10.1103/RevModPhys.91.045005.

[14] L. G. Johnsen and J. Linder, "Spin injection and spin relaxation in odd-frequency superconductors," *Physical Review B*, vol. 104, p. 144513, 28th Oct. 2021, DOI: 10.1103/PhysRevB.104.144513.

[15] R. Seoane Souto, D. Kuzmanovski and A. V. Balatsky, "Signatures of odd-frequency pairing in the Josephson junction current noise," *Physical Review Research*, vol. 2, p. 043193, 6th Nov. 2020, DOI: 10.1103/PhysRevResearch.2.043193.

[16] A. Di Bernardo, Z. Salman, X. Wang, M. Amado, M. Egilmez, M. Flokstra, A. Suter, S. Lee, J. Zhao, T. Prokscha, E. Morenzoni, M. Blamire, J. Linder and J. Robinson, "Intrinsic Paramagnetic Meissner Effect Due to s -Wave Odd-Frequency Superconductivity," *Physical Review X*, vol. 5, p. 041021, 6th Nov. 2015, DOI: 10.1103/PhysRevX.5.041021.

[17] S. Diesch, P. Machon, M. Wolz, C. Sürgers, D. Beckmann, W. Belzig and E. Scheer, "Creation of equal-spin triplet superconductivity at the Al/EuS interface," *Nature Communications*, vol. 9, p. 5248, Dec. 2018, DOI: 10.1038/s41467-018-07597-w.

[18] T. Rachataruangsit and S. Yoksan, "Spin orbit scattering effect on long-range odd frequency triplet pairing in ferromagnet/superconductor bilayers," *Physica C: Superconductivity and its Applications*, vol. 467, p. 156, Dec. 2007, DOI: 10.1016/j.physc.2007.10.004.

[19] R. Heid, "On the thermodynamic stability of odd-frequency superconductors," *Zeitschrift für Physik B Condensed Matter*, vol. 99, p. 15, Mar. 1995, DOI: 10.1007/s002570050003.

[20] P. Coleman, E. Miranda and A. Tsvelik, "Possible realization of odd-frequency pairing in heavy fermion compounds," *Physical Review Letters*, vol. 70, p. 2960, 10th May 1993, DOI: 10.1103/PhysRevLett.70.2960.

[21] D. Solenov, I. Martin and D. Mozyrsky, "Thermodynamical stability of odd-frequency superconducting state," *Physical Review B*, vol. 79, p. 132502, 6th Apr. 2009, DOI: 10.1103/PhysRevB.79.132502.

[22] M. Eschrig, A. Cottet, W. Belzig and J. Linder, "General boundary conditions for quasiclassical theory of superconductivity in the diffusive limit: Application to strongly spin-polarized systems," *New Journal of Physics*, vol. 17, p. 083037, 18th Aug. 2015, DOI: 10.1088/1367-2630/17/8/083037.

[23] M. Eschrig, "Spin-polarized supercurrents for spintronics: A review of current progress," *Reports on Progress in Physics*, vol. 78, p. 104501, 1st Oct. 2015, DOI: 10.1088/0034-4885/78/10/104501.

[24] K.-R. Jeon, C. Ciccarelli, A. J. Ferguson, H. Kurebayashi, L. F. Cohen, X. Montiel, M. Eschrig, J. W. A. Robinson and M. G. Blamire, "Enhanced spin pumping into superconductors provides evidence for superconducting pure spin currents," *Nature Materials*, vol. 17, p. 499, Jun. 2018, DOI: 10.1038/s41563-018-0058-9.

[25] J. P. Morten, "Spin and Charge Transport in Dirty Superconductors," M.S. thesis, Norwegian University of Science and Technology, 2003.

[26] M. Amundsen, "Quasiclassical Theory Beyond 1D: Supercurrents and Topological Excitations," M.S. thesis, Norwegian University of Science and Technology, May 2016.

[27] J. Rammer, *Quantum Field Theory of Non-Equilibrium States*, First. Cambridge Univ. Press, 2011, ISBN: 978-0-521-18800-5.

[28] D. J. Griffiths, *Introduction to Electrodynamics*, 4th ed. Cambridge University Press, 2018, ISBN: 978-1-108-42041-9.

[29] N. Bohr, J. R. Nielsen and L. Rosenfeld, *Early Work (1905-1911)*. North-Holland, 1986, ISBN: 978-0-7204-1801-9.

[30] D. van Delft and P. Kes, "The discovery of superconductivity," *Physics Today*, vol. 63, p. 38, Sep. 2010, DOI: 10.1063/1.3490499.

[31] H. K. Onnes, *Research notebooks 56, 57*, 1911.

[32] W. Meissner and R. Ochsenfeld, "Ein neuer Effekt bei Eintritt der Supraleitfähigkeit," *Naturwissenschaften*, vol. 21, p. 787, 1st Nov. 1933, DOI: 10.1007/BF01504252.

[33] M. Tinkham, *Introduction to Superconductivity*, 2nd ed. Dover Publications, 2015, ISBN: 978-0-486-43503-9.

[34] K. H. Bennemann and J. B. Ketterson, Eds., *Superconductivity*. Springer Berlin Heidelberg, 2008, ISBN: 978-3-540-73252-5, DOI: 10.1007/978-3-540-73253-2.

[35] J. Bardeen, L. N. Cooper and J. R. Schrieffer, "Theory of Superconductivity," *Physical Review*, vol. 108, p. 1175, 1st Dec. 1957, DOI: 10.1103/PhysRev.108.1175.

[36] F. Gross, B. S. Chandrasekhar, D. Einzel, K. Andres, P. J. Hirschfeld, H. R. Ott, J. Beuers, Z. Fisk and J. L. Smith, "Anomalous temperature dependence of the magnetic field penetration depth in superconducting UBe13," *Zeitschrift für Physik B Condensed Matter*, vol. 64, p. 175, Jun. 1986, DOI: 10.1007/BF01303700.

[37] C. Kittel, *Introduction to Solid State Physics*, 8th ed. Wiley, 2005, ISBN: 978-0-471-41526-8.

[38] F. B. Silsbee, "Current distribution in supraconductors," *Scientific Papers of the Bureau of Standards*, vol. 22, p. 293, Mar. 1927, DOI: 10.6028/nbsscipaper.242.

[39] V. Ginzburg, "Ferromagnetic superconductors," *Soviet Physics-JETP*, vol. 4, p. 153, 1957 [*Zhurnal Ehksperimental'noj i Teoreticheskoj Fiziki* , vol. 31, p. 202, 1956].

[40] B. T. Matthias, H. Suhl and E. Corenzwit, "Ferromagnetic Superconductors," *Physical Review Letters*, vol. 1, p. 449, 15th Dec. 1958, DOI: 10.1103/PhysRevLett.1.449.

[41] P. Fulde and R. A. Ferrell, "Superconductivity in a Strong Spin-Exchange Field," *Physical Review*, vol. 135, A550, 3A 3rd Aug. 1964, DOI: 10.1103/PhysRev.135.A550.

[42] A. I. Larkin and Y. N. Ovchinnikov, "Nonuniform State of Superconductors," *Soviet Physics-JETP*, vol. 20, p. 762, 1965 [*Zhurnal Ehksperimental'noj i Teoreticheskoj Fiziki*, vol. 47, p. 1136, 1964].

[43] R. Balian and N. R. Werthamer, "Superconductivity with Pairs in a Relative p Wave," *Physical Review*, vol. 131, p. 1553, 15th Aug. 1963, DOI: 10.1103/PhysRev.131.1553.

[44] A. Andreev, "The Thermal Conductivity of the Intermediate State in Superconductors," *Soviet Physics-JETP*, vol. 19, p. 1228, 1964 [*Zhurnal Ehksperimental'noj i Teoreticheskoj Fiziki*, vol 46, p. 1823, 1964].

[45] J. A. Ouassou, "Manipulating superconductivity in magnetic nanostructures in and out of equilibrium," Ph.D. dissertation, Norwegian University of Science and Technology, Mar. 2019.

[46] P. G. D. Gennes and E. Guyon, "Superconductivity in "normal" metals," *Physics Letters*, vol. 3, p. 168, 1963, DOI: 10.1016/0031-9163(63)90401-3.

[47] N. R. Werthamer, "Theory of the Superconducting Transition Temperature and Energy Gap Function of Superposed Metal Films," *Physical Review*, vol. 132, p. 2440, 15th Dec. 1963, DOI: 10.1103/PhysRev.132.2440.

[48] B. Pannetier and H. Courtois, "Andreev Reflection and Proximity effect," *Journal of Low Temperature Physics*, vol. 118, p. 599, 2000, DOI: 10.1023/A:1004635226825.

[49] F. S. Bergeret, A. F. Volkov and K. B. Efetov, "Long-Range Proximity Effects in Superconductor-Ferromagnet Structures," *Physical Review Letters*, vol. 86, p. 4096, 30th Apr. 2001, DOI: 10.1103/PhysRevLett.86.4096.

[50] F. S. Bergeret, A. F. Volkov and K. B. Efetov, "Odd Triplet Superconductivity and Related Phenomena in Superconductor-Ferromagnet Structures," *Reviews of Modern Physics*, vol. 77, p. 1321, 28th Nov. 2005, DOI: 10.1103/RevModPhys.77.1321.

[51] A. Balatsky and E. Abrahams, "New class of singlet superconductors which break the time reversal and parity," *Physical Review B*, vol. 45, p. 13125, 1st Jun. 1992, DOI: 10.1103/PhysRevB.45.13125.

[52] F. S. Bergeret and I. V. Tokatly, "Spin-orbit coupling as a source of long-range triplet proximity effect in superconductor-ferromagnet hybrid structures," *Physical Review B*, vol. 89, p. 134517, 23rd Apr. 2014, DOI: 10.1103/PhysRevB.89.134517.

[53] Y. Tanaka and A. A. Golubov, "Theory of the Proximity Effect in Junctions with Unconventional Superconductors," *Physical Review Letters*, vol. 98, p. 037003, 16th Jan. 2007, DOI: 10.1103/PhysRevLett.98.037003.

[54] Y. Asano, A. A. Golubov, Y. V. Fominov and Y. Tanaka, "Unconventional Surface Impedance of a Normal-Metal Film Covering a Spin-Triplet Superconductor Due to Odd-Frequency Cooper Pairs," *Physical Review Letters*, vol. 107, p. 087001, 16th Aug. 2011, DOI: 10.1103/PhysRevLett.107.087001.

[55] A. Altland and B. Simons, *Condensed Matter Field Theory*, 2nd ed. Cambridge University Press, 2010, ISBN: 978-0-521-76975-4.

[56] J. J. Sakurai and J. Napolitano, *Modern Quantum Mechanics*, 3rd ed. Cambridge University Press, 2021, ISBN: 978-1-108-47322-4.

[57] A. Zee, *Quantum Field Theory in a Nutshell*, 2nd ed. Princeton University Press, 2010, ISBN: 978-0-691-14034-6.

[58] H. G. Giil, "Non-equilibrium Quasiclassical Theory and Spin Accumulation with a polarized barrier," Specialization thesis, Norwegian University of Science and Technology, 2021.

[59] Y. Nambu, "Quasi-Particles and Gauge Invariance in the Theory of Superconductivity," *Physical Review*, vol. 117, p. 648, 1st Feb. 1960, DOI: 10.1103/PhysRev.117.648.

[60] F. London, *Superfluids*. Wiley, 1950, vol. 1.

[61] A. Schmid and G. Schön, "Linearized kinetic equations and relaxation processes of a superconductor near T c," *Journal of Low Temperature Physics*, vol. 20, p. 207, Jul. 1975, DOI: 10.1007/BF00115264.

[62] M. E. Peskin and D. V. Schroeder, *An Introduction to Quantum Field Theory*. CRC Press, Taylor & Francis Group, 2019, ISBN: 978-0-367-32056-0.

[63] L. V. Keldysh, "Diagram Technique for Nonequilibrium Processes," *Soviet Physics-JETP*, vol. 20, p. 1018, 1965 [*Zhurnal Ehksperimental'noj i Teoreticheskoj Fiziki*, vol. 47, 1515-1527, 1964].

[64] M. Amundsen and J. Linder, "General solution of 2D and 3D superconducting quasiclassical systems: Coalescing vortices and nanoisland geometries," *Scientific Reports*, vol. 6, p. 22765, Sep. 2016, DOI: 10.1038/srep22765.

[65] G. D. Mahan, *Many-Particle Physics*, 3rd ed. Springer Science + Business Media, 2000, ISBN: 978-1-4757-5714-9.

[66] J. Linder, *Quasiclassical theory (personal notes)*, 2021.

[67] M. Koshino and T. Ando, "Transport in Bilayer Graphene: Calculations within a self-consistent Born approximation," *Physical Review B*, vol. 73, p. 245403, 5th Jun. 2006, DOI: 10.1103/PhysRevB.73.245403.

[68] H. Goldstein, C. P. Poole and J. L. Safko, *Classical Mechanics*, 3rd ed. Pearson, 2014, ISBN: 978-1-292-02655-8.

[69] M. Amundsen and J. Linder, "Quasiclassical theory for interfaces with spin-orbit coupling," *Physical Review B*, vol. 100, p. 064502, 1st Aug. 2019, DOI: 10.1103/PhysRevB.100.064502.

[70] J. A. Sauls, "Theory of disordered superconductors with applications to nonlinear current response," *Progress of Theoretical and Experimental Physics*, vol. 2022, p. 033I03, 30th Mar. 2022, DOI: 10.1093/ptep/ptac034.

[71] J. Rammer and H. Smith, "Quantum field-theoretical methods in transport theory of metals," *Reviews of Modern Physics*, vol. 58, p. 323, 1st Apr. 1986, DOI: 10.1103/RevModPhys.58.323.

[72] K. D. Usadel, "Generalized Diffusion Equation for Superconducting Alloys," *Physical Review Letters*, vol. 25, p. 507, 24th Aug. 1970, DOI: 10.1103/PhysRevLett.25.507.

[73] S. H. Jacobsen, J. A. Ouassou and J. Linder, "Critical temperature and tunneling spectroscopy of superconductor-ferromagnet hybrids with intrinsic Rashba-Dresselhaus spin-orbit coupling," *Physical Review B*, vol. 92, p. 024510, 24th Jul. 2015, DOI: 10.1103/PhysRevB.92.024510.

[74] M. Y. Kuprianov and V. F. Lukichev, "Influence of boundary transparency on the critical current of "dirty" SS'S structures," *Soviet Physics-JETP*, vol. 67, p. 1163, 1988 [*Zhurnal Ehksperimental'noj i Teoreticheskoj Fiziki*, vol. 94, p. 139, 1988].

[75] E. N. Economou, *Green's Functions in Quantum Physics*, 3rd ed. Springer, 2006, ISBN: 978-3-540-28838-1.

[76] J. O. Fjærestad, *Introduction to Green functions and many-body perturbation theory*, 2013.

[77] C. Espedal, T. Yokoyama and J. Linder, "Anisotropic Paramagnetic Meissner Effect by Spin-Orbit Coupling," *Physical Review Letters*, vol. 116, p. 127002, 25th Mar. 2016, DOI: 10.1103/PhysRevLett.116.127002.

[78] J. A. Ouassou, T. D. Vethaak and J. Linder, "Voltage-induced thin-film superconductivity in high magnetic fields," *Physical Review B*, vol. 98, p. 144509, 11th Oct. 2018, DOI: 10.1103/PhysRevB.98.144509.

[79] G. Labahn and M. Mutrie, *Reduction of Elliptic Integrals to Legendre Normal Form*, 10th Jan. 1997.

[80] F. Herman and R. Hlubina, "Thermodynamic properties of Dynes superconductors," *Physical Review B*, vol. 97, p. 014517, 22nd Jan. 2018, DOI: 10.1103/PhysRevB.97.014517.

[81] R. C. Dynes, V. Narayanamurti and J. P. Garno, "Direct Measurement of Quasiparticle-Lifetime Broadening in a Strong-Coupled Superconductor," *Physical Review Letters*, vol. 41, p. 1509, 20th Nov. 1978, DOI: 10.1103/PhysRevLett.41.1509.

[82] E. A. Demler, G. B. Arnold and M. R. Beasley, "Superconducting proximity effects in magnetic metals," *Physical Review B*, vol. 55, p. 15174, 1st Jun. 1997, DOI: 10.1103/PhysRevB.55.15174.

[83] Y. V. Fominov, Y. Tanaka, Y. Asano and M. Eschrig, "Odd-frequency superconducting states with different types of Meissner response: Problem of coexistence," *Physical Review B*, vol. 91, p. 144514, 30th Apr. 2015, DOI: 10.1103/PhysRevB.91.144514.

[84] T. Yokoyama, Y. Tanaka and N. Nagaosa, "Anomalous Meissner Effect in a Normal-Metal–Superconductor Junction with a Spin-Active Interface," *Physical Review Letters*, vol. 106, p. 246601, 13th Jun. 2011, DOI: 10.1103/PhysRevLett.106.246601.

[85] M. Alidoust, K. Halterman and J. Linder, "Meissner effect probing of odd-frequency triplet pairing in superconducting spin valves," *Physical Review B*, vol. 89, p. 054508, 18th Feb. 2014, DOI: 10.1103/PhysRevB.89.054508.

[86] D. L. Cox and A. Zawadowski, "Exotic Kondo effects in metals: Magnetic ions in a crystalline electric field and tunnelling centres," *Advances in Physics*, vol. 47, p. 599, Sep. 1998, DOI: 10.1080/000187398243500.

[87] S. Higashitani, "Mechanism of Paramagnetic Meissner Effect in High Temperature Superconductors," *Journal of the Physical Society of Japan*, vol. 66, p. 2556, 15th Sep. 1997, DOI: 10.1143/JPSJ.66.2556.

[88] J. A. Ouassou, A. Pal, M. Blamire, M. Eschrig and J. Linder, "Triplet Cooper pairs induced in diffusive s-wave superconductors interfaced with strongly spin-polarized magnetic insulators or half-metallic ferromagnets," *Scientific Reports*, vol. 7, p. 1932, Dec. 2017, DOI: 10.1038/s41598-017-01330-1.

[89] Y. Zhu, A. Pal, M. G. Blamire and Z. H. Barber, "Superconducting exchange coupling between ferromagnets," *Nature Materials*, vol. 16, p. 195, Feb. 2017, DOI: 10.1038/nmat4753.

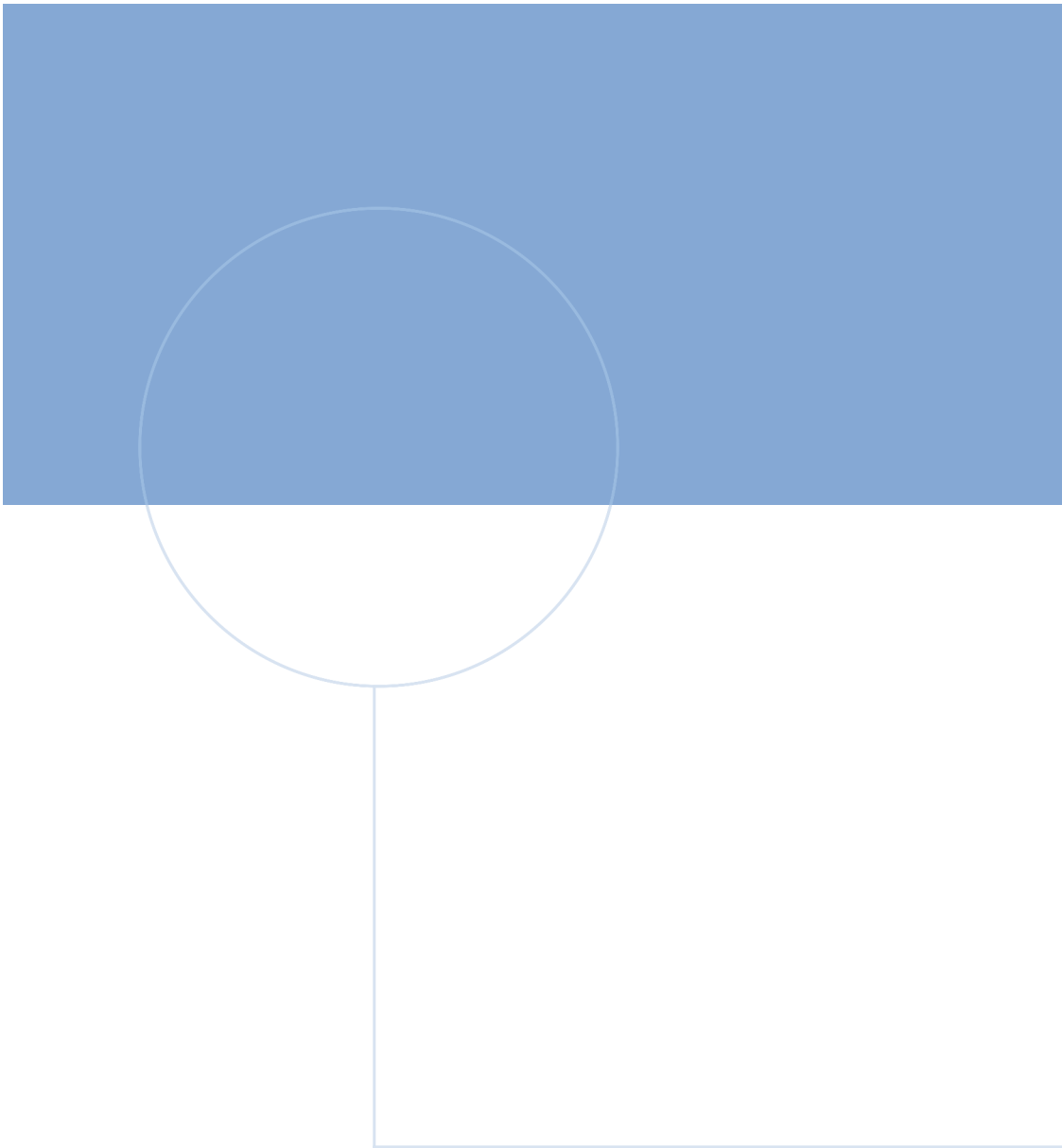

NTNU

Norwegian University of
Science and Technology